USING GEOCHEMICAL INDICATORS TO DISTINGUISH HIGH BIOGEOCHEMICAL ACTIVITY IN THE SUBSURFACE

by

Amy M. Kenwell

A thesis submitted to the Faculty and the Board of Trustees of the Colorado School of Mines in partial fulfillment of the requirements for the degree of Master of Science (Hydrology).

Golden, Colorado

Date _____

Signed: _____
Amy M. Kenwell

Signed: _____
Dr. Alexis K. Navarre-Sitchler
Thesis Advisor

Golden, Colorado

Date _____

Signed: _____
Dr. Terri S. Hogue
Professor and Program Director
Hydrologic Science and Engineering

Signed: _____
Dr. Paul Santi
Professor and Head
Geology and Geological Engineering

ABSTRACT

A better understanding of how microbial communities interact with their surroundings in physically and chemically heterogeneous subsurface environments will lead to improved quantification of biogeochemical reactions and associated nutrient cycling. This study develops a methodology to predict elevated rates of biogeochemical activity (microbial "hotspots") in subsurface environments by correlating microbial community structure with the spatial distribution of geochemical indicators in subsurface sediments. Statistical hierarchical cluster analyses (HCA) of simulated precipitation leachate, HCl and hydroxylamine extractable iron, total organic carbon (TOC), and microbial community structure were used to identify sample characteristics indicative of biogeochemical hotspots within fluvially-derived aquifer sediments. The method has previously been applied to alluvial materials collected at a former uranium mill site near Rifle, Colorado and this study introduces a new field site of relatively undisturbed floodplain deposits (soils and sediments) collected along the East River near Crested Butte, Colorado. At the East River 46 soil/sediment samples were collected across and perpendicular to 3 active meanders and an oxbow meander. Results indicate a strong relationship between TOC and microbial DNA whereas the influence of metals as terminal electron acceptors is specific to the dominant terminal electron accepting process. Linear regression of log-transformed TOC and bulk microbial DNA for 34 East River shallow meander and 14 alluvial Rifle samples produces a preliminary empirical relationship. Applying the method to identify hotspots in both contaminated and natural floodplain deposits and their associated alluvial aquifers demonstrates the broad applicability of a geochemical indicator based approach.

TABLE OF CONTENTS

ABSTRACT iii

LIST OF FIGURES vii

LIST OF TABLES x

ACKNOWLEDGMENTS xi

CHAPTER 1 INTRODUCTION 1

1.1 Background 1

1.2 Site Description 5

1.3 Previous Work 6

CHAPTER 2 METHODS 7

2.1 Sample Collection and Preparation 7

2.2 Total Organic Carbon (TOC) 8

2.3 Iron and Manganese Extractions 9

2.4 Synthetic Precipitation Leaching 10

2.5 DNA Extraction and Quantitative PCR Analysis 10

2.6 Statistical Methods 12

CHAPTER 3 RESULTS AND DISCUSSION 13

3.1 Total Organic Carbon (TOC) 13

3.2 Iron and Manganese Extractions 14

3.3 Synthetic Precipitation Leaching 17

3.4 DNA Extraction and Quantitative PCR Analysis 19

3.5 Relationships between Geochemical Parameters and Bulk Microbial DNA .. 21

3.5.1 Test for Normality 22

3.5.2 Pairwise Correlations 23

3.5.3 Linear Regression of Bulk DNA and TOC 25

3.5.4 Statistical Hierarchical Clustering Analysis 27
CHAPTER 4 CONCLUSIONS 29
REFERENCES 31
APPENDIX A FIGURES 38
APPENDIX B ADDITIONAL SOIL CHARACTERIZATION 57
B1 Methods 57
B1.1 Bulk Density and Moisture Content 57
B1.2 Size Characterization 57
B1.3 X-ray fluorescence (XRF) Spectrometry 58
B1.4 Fourier Transform Infrared Spectroscopy (FTIR) 58
B1.5 Ordinary Spatial Kriging of Total Organic Carbon and HCl Extractable Iron Data 59
B2 Results and Discussion 60
B2.1 Bulk Density and Moisture Content 60
B2.2 Size Characterization 60
B2.3 X-ray fluorescence (XRF) Spectrometry 61
B2.4 Fourier Transform Infrared Spectroscopy (FTIR) 63
B2.5 Ordinary Spatial Kriging of Total Organic Carbon and HCl Extractable Iron Data 63
B3 References for Appendix B 65
APPENDIX C WATER CHARACTERIZATION 77
C1 Introduction 77
C2 Methods 77
C2.1 Sample Collection and Laboratory Testing 77
C2.2 Ultraviolet Absorbance 78
C2.3 Excitation-Emission Matrices 78

C2.4 DNA Extraction and Quantitative PCR Analysis 79
C3 Results and Discussion 79
C3.1 Sample Collection and Laboratory Testing 79
C3.2 Ultraviolet Absorbance 81
C3.3 Excitation-Emission Matrices 82
C3.4 DNA Extraction and Quantitative PCR Analysis 83
C4 References for Appendix C 84
APPENDIX D ADDITIONAL PLOTS AND TABLES 100

LIST OF FIGURES

Figure 1. (a) Location map of East River field site near Crested Butte, Colorado and (b) locations of specific river meanders A, C, D and O. 38

Figure 2. Sample locations on meanders A and C (a), D (b) and O (c)..... 39

Figure 3. Distribution of TOC on meanders A, C, D and O 40

Figure 4. Average extractable iron and manganese extracted from the 0.5N HCl and 0.25N hydroxylamine in 0.5N HCl extractions 41

Figure 5. Distribution of average 0.5NHCl and 0.25N hydroxylamine in 0.5N HCl extractable iron on meanders A, C, D and O 42

Figure 6. Distribution of average 0.5NHCl and 0.25N hydroxylamine in 0.5N HCl extractable manganese on meanders A, C, D and O 43

Figure 7. Average extractable manganese plotted versus average extractable iron with each meander shown in a different symbol. 44

Figure 8. Iron and manganese leached during an 18 hour test with a pH 4.2 solution of 60:40 sulfuric:nitric acid. 45

Figure 9. Leachable manganese plotted versus leachable Fe with each meander shown in a different symbol. 46

Figure 10. Distribution of leachable iron, manganese and aluminum across and down the center of meanders. 47

Figure 11. (a) Percentage of bacterial DNA (16S) represented by *nirK* and *nirS* denitrifying bacteria by meander and (b) bulk microbial DNA in ng of DNA per g of dry sediment by meander.. 48

Figure 12. Percentage of bacterial DNA (16S) represented by *nirK* (black squares) and *nirS* (green circles) denitrifying bacteria as a function of bulk microbial DNA in ng of DNA per g of dry sediment by meander. 49

Figure 13. Percentage of bacterial DNA (16S) represented by *nirK* (black squares) and *nirS* (green circles) denitrifying bacteria as moisture content varied..... 50

Figure 14. Pairwise correlations between soil parameters for all East River data.. 51

Figure 15. Plots of metals against DNA by meander. 52

Figure 16. Bulk microbial DNA as a function of total organic carbon for (a) alluvial Rifle and all East River samples, (b) alluvial Rifle and shallow East River samples, with each meander distinguished by shape.. 53

Figure 17. Linear regression of log-transformed and normalized TOC and bulk microbial DNA. 54

Figure 18. Dendrogram of statistical hierarchical clustering results using standardized average extractable iron and standardized log-transformed TOC, DNA, leached iron and leached manganese. 55

Figure 19. Sample-specific results of statistical hierarchical clustering analysis using standardized average extractable iron and standardized log-transformed TOC, DNA, leached iron and leached manganese. 56

Figure B1. Bulk density of sediment in g per cubic centimeter and natural moisture content percentage by meander 66

Figure B2. Bulk density of sediment as a function of natural moisture content 67

Figure B3. Natural moisture content as a function of total organic carbon 68

Figure B4. Grain size distributions of sediment by meander by dry sieving 69

Figure B5. Major elemental content of soils from X-ray fluorescence (XRF) spectrometry . 70

Figure B6. Trace elemental content of soils from X-ray fluorescence (XRF) spectrometry .. 71

Figure B7. Redox elemental content of soils from X-ray fluorescence (XRF) spectrometry 72

Figure B8. Major, trace and bulk elemental content of Mancos Shale outcrop from X-ray fluorescence (XRF) spectrometry 73

Figure B9. Absorbance peaks from Fourier Transform Infrared Spectroscopy (FTIR) 74

Figure B10. Ordinary kriging results for TOC in weight % carbon 75

Figure B11. Ordinary kriging results for HCl extractable iron in g/kg 76

Figure C1. Anion concentrations in surface water, hyporheic water and groundwater 86

Figure C2. Cation concentrations in surface water, hyporheic water and groundwater 87

Figure C3. Select cations (iron, manganese and aluminum) plotted against dissolved oxygen for river water, hyporheic water and groundwater 88

Figure C4. Ultraviolet (UV) absorbance for river water, hyporheic water and groundwater. 89

Figure C 5. Excitation-Emission Matrices for water samples 90

Figure C 6. Excitation-Emission Matrices for water samples with the same range 93

Figure C7. Bulk microbial DNA in river, hyporheic and groundwater samples 96

Figure C8. Percent of bacterial (16S) DNA represented by *nirK* and *nirS* denitrifying bacteria 97

Figure C9. Percentage of bacterial (16S) DNA represented by *nirK* and *nirS* denitrifying bacteria as a function of pH 98

Figure C10. Percentage of bacterial (16S) DNA represented by *nirK* and *nirS* denitrifying bacteria as a function of water temperature 99

Figure D1. Iron extracted from soils with 0.5N HCl and 0.25N hydroxylamine in 0.5N HCl (HA). 118

Figure D2. Manganese extracted from soils with 0.5N HCl and 0.25N hydroxylamine in 0.5N HCl (HA)..... 118

Figure D3. Q-Q plots for HCl extractable Fe and log-transformed HCl extractable Fe..... 119

Figure D4. Q-Q plots for HA extractable Fe and log-transformed HA extractable Fe..... 119

Figure D5. Q-Q plots for HCl extractable Mn and log-transformed HCl extractable Mn.... 119

Figure D6. Q-Q plots for HA extractable Mn and log-transformed HA extractable Mn 120

Figure D7. Q-Q plots for TOC and log-transformed TOC 120

Figure D8. Q-Q plots for leach Fe and log-transformed leach Fe..... 120

Figure D9. Q-Q plots for leach Mn and log-transformed leach Mn 121

Figure D10. Q-Q plots for DNA and log-transformed DNA 121

Figure D11. Multivariate Q-Q plot with logTOC, logDNA, HCl extractable Fe, HA extractable Fe, HCl extractable Mn, HA extractable Mn, log-leach Fe and log-leach Mn 122

Figure D12. Multivariate Q-Q plot with logTOC, logDNA, HCl extractable Fe, HCl extractable Mn, log-leach Fe and log-leach Mn..... 122

Figure D13. Multivariate Q-Q plot with logTOC, logDNA, log-leach Fe and log-leach Mn. 123

Figure D14. Q-Q plots for moisture content and log-transformed moisture content 123

Figure D15. Q-Q plots for bulk density and log-transformed bulk density 123

LIST OF TABLES

Table 1. Relationship between metals and log-transformed bulk microbial DNA 24

Table 2. TOC-DNA relationship for variable datasets 26

Table 3. Average standardized parameter values of statistical hierarchical clusters 28

Table C1. Average field water measurements 80

Table D1. East River total organic carbon analysis (weight %) 100

Table D2. East River HCl extractable iron (mg/kg), hydroxylamine extractable iron (mg/kg) and relative percent difference (%) 101

Table D3. East River HCl extractable manganese (mg/kg), hydroxylamine extractable manganese (mg/kg) and relative percent difference (%) 104

Table D4. East River leachable iron (mg/kg) and leachable manganese (mg/kg) from a simulated precipitation leach test at pH 4.2 using 60:40 H2SO4:HNO3 106

Table D5. East River bulk microbial DNA (ng/g) in soils and percentage of 16S DNA represented by nirK and nirS denitrifying genes 108

Table D6. East River major elemental concentration (weight %) in soil samples from XRF analysis 110

Table D7. East River trace elemental concentration (weight %) in soil samples from XRF analysis 112

Table D8. East River redox elemental concentration (weight %) in soil samples from XRF analysis 114

Table D 9. East River major, trace and redox elemental concentration (weight %) in Mancos Shale outcrop from XRF analysis 116

Table D 10. East River bulk microbial DNA (ng/g) in water and percentage of 16S DNA represented by *nirK* and *nirS* denitrifying genes 117

ACKNOWLEDGMENTS

I would like to thank my committee (Alexis Sitchler, John Spear, Reed Maxwell and Amanda Hering) for supporting me while doing this research. In particular my advisor, Alexis Sitchler for making sure I always had the information and supplies I needed to keep going.

I also want to thank Kenneth Williams from Lawrence Berkeley National Laboratory and Rosemary Carroll from the Desert Research Institute. Their work at the East River site made my project possible and their input while planning the project was also very valuable.

Thank you to all of the people who trained me on the many laboratory methods I needed to learn. Taking the time to help me get started was really appreciated: Zack Jones, Chris Trivedi, Dina Drennan, Rodrigo Prugue, Estefani Bustos, Lee Landkamer, Chris Matthews, and Tara Pandey.

Finally, thanks to those who helped me with my field and lab work. You made my job so much easier: Christine Pribulick, Joe Beisman, Karena Gill, Rania Eldam, Brian Jackson, and Rachel Hallnan.

This work was made possible through funding from the U.S. Department of Energy's Sustainable Systems Scientific Focus Area 2.0 and the Natural Sciences and Engineering Research Council of Canada. Official endorsement of this work by these agencies should not be inferred.

CHAPTER 1 INTRODUCTION

Biological dependence on physical and chemical characteristics of subsurface materials is an active area of study that will broaden understanding of natural systems. This work is part of the Department of Energy's Sustainable Systems Scientific Focus Area 2.0.

1.1 Background

Heterogeneous distributions of chemical and physical parameters in the subsurface exert control on important hydrologic, geochemical and microbial processes but connectivity between these systems is poorly understood (Chen & MacQuarrie, 2004; Hedin et al., 1998; Boano et al., 2014). Variations in the chemistry of organic matter, nitrogen, iron and other metals can be found in natural systems at scales down to a centimeter and smaller (Schilling & Jacobson, 2012; Englert et al., 2009; Murphy et al., 1997; Boano et al., 2014). These variations may be a driving force for distribution of microbial communities and activity in the subsurface due to shifts in availability of terminal electron acceptors and electron donors required for microbial metabolism (Sena et al., 2011; García-Balboa et al., 2011; Hakala et al., 2009). Thus, prediction of the distribution of microbial communities and microbial activity may be possible by defining geochemical and hydrological indicators of biogeochemical activity. If such an approach is valid, simple geochemical tests to evaluate levels of microbial activity can enhance our ability to identify important areas for detailed microbial characterization in natural systems.

Hydrologic variations in natural systems can be considerable, even at meter scale or less (Jackson & Caldwell, 1993). Floodplain environments are often very heterogeneous because of regular spatial and temporal variations in depositional environment. Migrating meanders cause lateral accretion of sediments with grain sizes ranging from coarse sandy point bars to fine overbank deposits (Schilling & Jacobson, 2012; Pinay et al., 2000). Strong changes in hydraulic conductivity related to the grain size distributions influence flow patterns and cause preferential flow paths (Li et al., 2010; Li et al., 2011; Atchley et al., 2013). Heterogeneity in sediment moisture content is a controlling factor in nutrient cycling (Takatert et al., 1999; Pinay et al., 2007), and in some cases is more important than the influence of sediment lithology (Pinay et al., 2000). In a floodplain environment, ridge and swale topography leads to swales with high

moisture content, fine-grained lithology, and shallow groundwater tables (Schilling and Jacobson, 2012). Therefore, heterogeneities in both lithology and moisture content in floodplain environments are important for nutrient cycling, particularly in the formation of hotspots of high biogeochemical activity within floodplains (Schilling & Jacobson, 2012; Pinay et al., 2007).

Heterogeneous microbial populations are an expected result of hydrological distributions (Murphy et al., 1997) of moisture content (Pinay et al., 2007) because of its control on geochemical conditions (Schilling & Jacobson, 2012; Murphy et al., 1997). As oxygen concentrations decrease due to increased water saturation (Takatert et al., 1999), terminal electron acceptors used by microbes for metabolism follow a sequence of energetic favorability from O_2 to NO_3^- to Mn^{4+} to Fe^{3+} to SO_4^{2-} and finally CO_2. Each of these microbial metabolic pathways is preferential for a specific microbial community, the spatial separation of which can be very strong in lakes (Sweerts et al., 1991) and aquifers (Chapelle & Lovley, 1992) but tends to be less distinct in fluvial systems due to substantial groundwater-surface water mixing which causes fluctuations in redox conditions (Morrice et al., 2000). These changes can be particularly important in floodplain hyporheic zones, where aerobic surface water mixes with anaerobic groundwater over a small vertical scale (Boano et al., 2014) producing strong gradients in microbial communities (Hill et al., 2000; Hedin et al., 1998; McDowell et al., 1992). The most abundant terminal electron acceptor for microbial metabolism in subsurface environments is often iron (García-Balboa et al., 2011; reviewed by Lovley et al., 1991), but studies have found that mixing of shallow oxidized water and deep reduced water in the hyporheic zone is particularly favorable for denitrification (Morrice et al., 2000; Hedin et al., 1998). Transition zones between anaerobic and aerobic environments can also stimulate microbial reactions and dominate microbial activity in natural geochemical systems (Prommer et al., 2006). The availability of electron donors and acceptors also controls the composition of microbial populations because they are reactants for the microbial metabolic reactions (Hakala et al., 2009; Hill et al., 2000; Hedin et al., 1998; Molz et al., 1986). On the other hand, microbial populations themselves can control distributions of hydrologic and geochemical properties through accumulation of biomass, clogging of pore networks, and fates of organic compounds and nutrients (Li et al., 2010; Englert et al., 2009; Sena et al., 2011).

Physical and chemical heterogeneity and associated rapid changes in redox conditions and microbial populations are particularly challenging aspects of subsurface modeling (Atchley et al., 2013; Li et al., 2011; Boano et al., 2014; Beisman et al., in press), in part because microbial processes are controlled by small-scale interactions while hydrologic processes act at much larger scales (Boano et al., 2014). Current models are unable to accurately upscale pore-scale microbial models to a macroscopic scale (Tartakovsky et al., 2009; King et al., 2010; Tartakovsky et al., 2013) because of steep chemical and microbial community gradients (Boano et al., 2014; Pinay et al., 2000; Hill et al., 2000). Another issue may be the use of solute concentrations from streams instead of subsurface geochemical knowledge for model boundary conditions and parameter estimation (Gooseff et al., 2005; Bencala & Walters, 1983; Scott et al., 2003). Solute concentrations amalgamate inputs from upstream sediment weathering and are unable to represent mechanisms of biogeochemical nutrient transformations (Boano et al., 2014). Field studies that characterize floodplains and elucidate biogeochemical relationships are needed in order to parameterize and constrain watershed-scale models (Fleckenstein et al., 2010; Boano et al., 2014; Englert et al., 2009). Though complex relationships between microbial species and their habitats are not yet understood, they are important for evaluating and modeling solute transport and other geochemical and hydrological processes in floodplains because of the microbial role in nutrient cycling and organic matter distribution (Takatert et al., 1999; Pinay et al., 2000; Li et al., 2011; Murphy et al., 1997).

Floodplain scale studies of relationships between physical and chemical heterogeneity and microbial activity in subsurface materials are limited (Hedin et al., 1998, Pinay et al., 2000). Studies show that even minor changes in concentration or type of available electron acceptors can inhibit microbial functions but the biogeochemical mechanisms that drive these observations are still poorly understood (Molz et al., 1986; Englert et al., 2009; Chen & MacQuarrie, 2004). Of particular interest are operationally defined biogeochemical hotspots or small-scale heterogeneities where microbial activity is high relative to the bulk or average microbial activity of the larger scale system. Because these hotspots can disproportionately influence nutrient cycling in natural systems, understanding these features is necessary for an accurate conceptual model (Hedin et al., 1998). One method of identifying potential hotspot locations is to look for correlations between microbial activity and other subsurface characteristics. Similar correlations have already been found between physical and chemical heterogeneities in natural systems

(Schilling & Jacobson, 2012; Boano et al., 2014). Floodplain topography is associated with groundwater quality and there is potential to use LiDAR and surface geophysics for large-scale characterization based on this relationship (Schilling and Jacobson, 2012). If a similar correlation exists between chemical and microbial characteristics and processes, there is potential for field and watershed scale microbial characterization and identification of microbial hotspots through easily measured geochemical parameters.

This study analyzes soil and sediment samples from an active floodplain of the East River, Colorado to evaluate correlations between physical and chemical properties of subsurface materials and microbial activity as measured by bulk DNA. Such correlations can provide a basis for simplification of future numerical simulation of biogeochemical processes in this system (Atchley et al., 2013), one that is representative of other hyporheic environments that control systems such as nitrogen transport, carbon storage and nutrient transformations (reviewed by Boano et al., 2014). The primary goals of this study are to:

1) quantify hydrologic properties of soil and sediment on floodplains
2) classify chemical composition and release to characterize geochemical reactions
3) specify microbial communities to establish a hypothesis of microbiological reactions, and
4) identify correlations between physical, chemical and microbial characteristics.

Characterizing hydrologic, chemical and microbial attributes of a floodplain system will provide data to investigate geochemical indicators characteristic of microbial hotspots to develop a method for identifying zones of increased biogeochemical activity and test the hypothesis that *hydrologic and chemical parameters correlate to activity of microbial communities*. Biogeochemical hotspots are predicted to be characterized by soils and sediment with high organic carbon and high bioavailable metals which provide terminal electron acceptors and electron donors required for microbial metabolism (Hakala et al., 2009). Specifically, organic carbon is the primary electron donor and a source of energy for microbial populations in natural systems (Campbell et al., 2012). However, dissolved organic matter can also act as a ligand to limit adsorption of reduced iron to oxidized iron surfaces, a mechanism that can prevent microbes from reaching and reducing remaining iron (Parker et al., 2013; Hakala et al., 2009). Iron plays a crucial role in geochemistry of soils as a terminal electron acceptor for dissimilatory

reduction reactions (Li et al., 2011; Hakala et al., 2009; García-Balboa et al., 2011). Oxidized manganese concentrations in soils and relative nitrate and sulfate concentrations in hyporheic water samples can also help predict dominant terminal electron acceptors in a system.

Co-dependence between distributions of geochemical properties of soils and development of microbial community structure is of interest for both large-scale climate models and smaller scale studies with high microbial activity such as bioremediation experiments and organic contaminants (Englert et al., 2009; Sena et al., 2011; Murphy et al., 1997; Prommer et al., 2006). If consistent relationships are found between subsurface properties and microbial properties, microbial characteristics may be predictable based on only chemical and physical analyses. Such correlation models can be critical to balance field activities with a project budget (Li et al., 2011). Identifying relationships between hydrologic, chemical and microbiological processes can also lead to more efficient site characterization. For many historical studies with only the latter datasets, knowing these relationships could even define proxy microbial patterns without requiring additional data collection.

1.2 Site Description

The East River floodplain is downstream of the Rocky Mountain Biological Laboratory (RMBL) in Gothic, CO (Figure 1). This watershed exhibits characteristic fluvial progression and serves as a representative example of many headwater catchments within the upper Colorado River basin. The East River is an ideal location to study floodplain dynamics because of its relatively undisturbed nature, high organic carbon contribution from the underlying Mancos Formation (Morrison et al., 2012) and varying meander characteristics such as meander length, symmetry and radius of curvature (Leopold et al., 1992).

Four meanders from the study site were chosen for sampling (Figure 1). Meander A has a narrow neck and short vegetation with no surface water channels. Meander C is a much longer meander with many potential hyporheic flowpaths and some inner channels and trees. Meander D is large but contains dry areas with trees as well as regions that are seasonally saturated with wetlands and internal streams. Meander O is a fairly cutoff oxbow meander whose riverbed is seasonally inundated though not contributing to the main flow of the river. Additional soil

sampling stations include an upstream station and several locations within a dry riverbed in a cutoff section of the river at meander O.

The first letter of each sample name (A, C, D or O) refers to which meander the sample was collected from (Figure 2). The second letter refers to its position, with samples “a” through “e” across the neck of the meander, where “a” is on the downstream side. Samples collected down the meander axis toward the toe of the meander are labeled “c1” through “c5”, with “c5” being nearest the toe. Some samples have a “D” or an “R” at the end of the sample name to refer to a deeper or riverbed sample, respectively. For example, sample Cc4D is from meander C, the center of the meander (c), the fourth position toward the toe (4), and it is the deeper sample at this location (D).

1.3 Previous Work

A study specifically investigating the microbial population-geochemical habitat relationship began in April 2013 when eight monitoring wells were installed on the outer edge of the Old Rifle Integrated Field Research Challenge Site (IFRC). From these sediment cores, samples were collected every 5 ft as well as when core sediment had notable color or texture changes with depth. Some of these samples were placed in sealed bags and archived at -80^{o}C. 27 samples were collected in centrifuge tubes and stored at -20^{o}C until analysis; 8 of these were determined to be floodplain alluvium. An additional six samples were taken out of long term storage a year later. Sediment was analyzed for elemental concentrations using X-ray fluorescence (XRF) and clay mineralogy with X-ray diffraction (XRD). Total organic carbon (TOC) and bioavailable iron and manganese concentrations were also measured. The results of these tests contributed to a statistical hierarchical cluster analysis. Initial clustering revealed that operationally defined hotspots were characterized by high organic carbon, bioavailable iron and dark sediment colors but not necessarily low hydraulic conductivity. Further details can be found in Prugue (2014). Confirmation of the geochemical indicator method at a second field site will ensure that relationships apply to both active and inactive floodplains and are independent of anthropogenic influence.

CHAPTER 2 METHODS

The methods used in this study help characterize physical, chemical and microbial properties of the floodplain sediments.

2.1 Sample Collection and Preparation

Soil and sediment samples were collected from three East River meanders (A, C and D) on June 24th and June 25th 2014 (Figure 2). The field site was revisited on September 27th 2014 and samples were collected from meander O (Figure 2). Surface vegetation was removed using a shovel and a 16 cm bulk density sampler was then hand-augured to collect a soil/sediment sample. An additional grab sample was collected beneath the bulk density hole using a shovel. Where possible, a second bulk density sample was collected beneath the first (Cc4D, DaD, DdD and DeD). Samples OdT and OdB refer to stations at the top and bottom of the river bank, respectively. For three sample stations (Aa, Ab and Ac) a hand-corer was used to extract 20 – 50 cm of soil core. From core Aa, subsamples were taken from the top and bottom of the core. For Ab and Ac, a single core sample was analyzed along with a grab sample.

Samples were collected across the neck and down the body of each meander (Figure 2). Across samples were distributed along the necks of meanders where hyporheic through-flow could be expected. They were spaced approximately evenly with one sample station at each bank and three inside the meander. Down samples were evenly spaced beginning at the toe of the meander and progressing down the meander axis. Areas with heavy vegetation (mainly trees) were not sampled because the shallow sampling would most likely reflect substantial influences from local vegetation and would not be representative of larger scale trends. Therefore, there are no down samples on the more vegetated Meander D. A grab sample from the riverbed (Cc5R) and an oxidized iron rich sample from a waterway running across the inside of meander D (DI) were also taken. In the oxbow meander (O), three samples were collected from the cutoff riverbed: one in a stagnant pool (OxU), one at the toe of the down transect (Oc5R) and one in an outcrop of Mancos shale (OxM). An additional sample (Yule) was collected at the Rocky Mountain Biological Lab (RMBL) near the upstream autosampling river station. The sample effort constituted 46 soil and sediment samples in total.

Once collected, samples were placed in coolers and transported on dry ice to Colorado School of Mines where they were stored at -20°C until analysis. Grab samples were thawed in an anaerobic chamber. Once thawed, a subsample was collected in a 50 ml centrifuge tube and left in the anaerobic chamber for chemical extractions while remaining sample was removed and exposed to oxygen. Core samples and sample splits for bulk density analysis were not thawed in an anaerobic chamber but transferring a subsample to an anaerobic chamber soon after thawing minimized exposure to oxygen. A subsample of approximately 5 g (wet mass) was freeze-dried using a FreeZone 6 Liter Benchtop Freeze Dry System (Labconco, Kansas City, MO) and approximately 25 g (wet mass) was oven dried at 110^{o}C. Any remaining sample was refrozen. Oven-dried samples were hand mortared and passed through a 0.991 cm sieve for XRF and leach test analyses. Samples AbC, Ac1, Ac4, Cc5R, Oa, Ob, Oc, OxU and OxM required a ball mill with steel and/or aluminum components to reduce enough sample to the proper size. Thus, these samples may have metal contamination from the ball mill procedure.

2.2 Total Organic Carbon (TOC)

Total organic carbon (TOC) analysis was performed using a CM 5014 Coulometer (UIC, Joliet, IL, USA). This device consists of two modules: a total carbon (TC) combustion furnace and a total inorganic carbon (TIC) acidification system. At the beginning of each run, a cathode-anode cell was calibrated to approximately a 3200 nm wavelength and a blank sample was analyzed. 10 to 12 mg of a calcium carbonate standard was tested approximately every ten samples. Samples were analyzed in duplicate during different runs to prevent calibration error.

In the TC module approximately 12 mg of sample was heated to 935^{o}C to convert all carbon in the sample to CO_2 gas. The CO_2 gas was carried by 99.5% purity oxygen into a coulometer where the concentration of CO_2 was analyzed using spectrophotometric methods (Myrbo, 2004). The CO_2 concentration was analyzed every 5 minutes for a minimum of three analyses. If the mass of carbon did not stabilize to a 2% difference then the procedure continued for an additional five minutes.

Inorganic carbon in 30 mg of sediment was dissolved and released as CO_2 gas by reacting each sample with 2% sulfuric acid at a boiling temperature. The mass of carbon was analyzed in the same coulometer procedure as the TC module but CO_2 was carried to the coulometer with

atmospheric air scrubbed of CO_2 with potassium hydroxide. In samples with low carbon concentrations the analysis was manually stopped after 30 minutes.

2.3 Iron and Manganese Extractions

An iron and manganese extraction method was developed by testing 6 variations of previously published extraction methods. The mass of soil, volume and strength of extractant, length of extraction, bottle type and temperature of extraction were varied and results compared. These variations were based on methods from Chao and Zhou (1983), Lovley et al. (1987), Wang et al. (1987), Roden and Zachara (1996), McCarty et al. (1998), Li et al. (2012), García-Balboa et al. (2011), Li et al. (2006), de Santiago et al. (2007), Campbell et al. (2012), Parker et al. (2013), Chen et al. (2013), Vinson et al. (2007) and personal communication with K. Campbell (2014).

HCl-extractable iron and manganese were recovered by combining 3 g of wet sediment with 150 mL of 0.5 N HCl in an HDPE bottle within an anaerobic chamber. In another bottle, 150 mL of 0.25 N hydroxylamine hydrochloride (HA) in 0.5 N HCl was combined with the same amount of wet sediment. Bottles were sealed, removed from the anaerobic chamber and placed on a shaker table at room temperature for 24 hours +/- 15 minutes. They were then returned to the anaerobic chamber and sampled using a 0.45 μm filter and acidified with nitric acid. The concentrations of iron and manganese in the extractant solution were determined with ICP-AES (Department of Chemistry and Chemical Engineering, Colorado School of Mines, Golden, CO).

The mass was higher than most of the documented material to remove the effect of heterogeneity in natural soils. The volume of extractant was also increased to maintain a 1:50 ratio of sample mass to extractant fluid to prevent oversaturation. Many methods also had shorter extraction times but this proved to make a substantial difference in the amount of extractable metals. The bottle type and temperature did not have an apparent effect. The acidity of the solutions after combination with sediment was also tested to rule out carbonate neutralization and the pH was well below 2.

Operationally defined hydroxylamine (HA)-reducible iron and manganese were determined by subtracting the mass of iron and manganese extracted with HCl from the mass of iron and manganese extracted with an HA-HCl solution (Lovley et al., 1987). This analysis may

be more effective for manganese extraction than iron (Li et al., 2006). The HCl extraction targeted acid-extractable Fe(II) found in amorphous iron-oxides though it could also remove iron from carbonates and some poorly-crystalline iron-oxides (Campbell et al., 2012). The HA-HCl extraction additionally removed Fe(III) oxyhydroxides that were reduced by the HA during the extraction procedure. It is assumed that these Fe(III) oxyhydroxides represent iron that could be microbially reducible (Campbell et al., 2012; Li et al., 2011). The results from the HA-HCl extraction may represent minimum Fe(III) concentrations as only 40% of the amorphous Fe(III) oxyhydroxides in natural sediments were reduced by the HA extraction in one experiment (Lovley et al., 1987). However, the hydroxylamine method of determining Fe(III) was still more effective than oxalate or ferrozine methods (García-Balboa et al., 2011).

2.4 Synthetic Precipitation Leaching

Synthetic precipitation leach tests were conducted to determine metal mobility. This method was adapted from EPA method 1312 for solid phase non-volatile extractions in wastewater (1994). The synthetic precipitation consisted of 60:40 H_2SO_4:HNO_3 in Milliq water adjusted to a pH of 4.2 +/- 0.05. This extraction fluid was combined with dry sediment passed through a 0.991 cm sieve in a 20:1 ratio of extractant to sediment. The combined sample was then placed on a shaker table for 18 hours +/- 15 minutes for leaching to occur. The extract was subsequently sampled using a 0.45 µm filter and acidified with nitric acid prior to analysis by ICP-AES (Department of Chemistry and Chemical Engineering, Colorado School of Mines, Golden, CO). A blank test of each extraction solution was also conducted.

2.5 DNA Extraction and Quantitative PCR Analysis

DNA was extracted from sediment samples using the PowerSoil DNA Isolation Kit (MO BIO Laboratories, Inc., Carlsbad, CA, USA). Extractions were performed according to the manufacturer's directions except that a 1 minute bead beating replaced the 10 minute vortexing step as was done in Pepe-Ranney et al. (2012). Extracted DNA was stored at -20^{o}C.

Quantitative PCR was performed in triplicate on a Roche LightCycler 480 system (Roche Diagnostics, Indianapolis, IN, USA). Working curves for sediment and groundwater DNA were created by amplifying environmental samples with primers, combining the triplicates, and bead

purifying them with Agencourt AMPure XP (Beckman Coulter, Indianapolis, IN, USA). These were quantified using a Qubit 2.0 Fluorometer and Qubit dsDNA High Sensitivity Assay Kit (Life Technologies, Grand Island, NY, USA). Bulk microbial DNA in raw samples was determined using the same system. The results of the Qubit analyses were converted to copies using the URI Genomics and Sequencing Center converter (Staroscik, 2004). The purified amplicons were serially diluted ten-fold with nuclease-free water to form a standard curve template. Quality assurance was performed by analyzing some amplicons using agarose gel electrophoresis and ethidium bromide staining. Negatives and positive controls were also analyzed.

16S Primers: Universal primers were used to amplify bacterial 16S rRNA genes. Each well in the 96 well optical plate contained 2 µl of sample DNA, 12.5 µl of PerfeCTa SYBR Green Super Mix (Promega Corporation, Madison, WI, USA), 1 µl each of forward primer EUB338F (5'ACTCCTACGGGAGGCAGCAG) and reverse primer EUB518R (5'ATTACCGCGGCTGCTGG) and 8.5 µl of nuclease-free water. The PCR reactions were run on the LightCycler with pre-incubation at 95^{o}C for 15 min followed by a PCR protocol of 40 cycles at 95^{o}C for 60 s, 53^{o}C for 30 s and 72^{o}C for 60 s. This was followed by a melting curve protocol of 95^{o}C for 5 s, 65^{o}C for 60 s and a continuous drop from 98^{o}C with final cooling at 40^{o}C for 10 s (Fierer et al., 2005).

nirK Primers: Denitrifying *nirK* genes were amplified as above except with primers *nirK*876F (5'ATYGGCGGVCAYGGCGA) and *nirK*1040R (5'GCCTCGATCAGRTTRTGGTT). Samples were denatured at 95^{o}C for 5 min prior to a 6 cycle touchdown at 95^{o}C for 15 s, 63^{o}C for 30 s and 72^{o}C for 30 s. The PCR amplification was 15 s at 95^{o}C, 30 s at 58^{o}C and 30 s at 72^{o}C for 40 cycles. The melt curve was one cycle of 95^{o}C for 15 s, 55^{o}C for 1 s and a continuous drop from 99^{o}C followed by 40^{o}C for 1 s (Henry et al., 2004).

nirS Primers: Denitrifiers with *nirS* genes were also investigated. The primers for these genes were *nirS*cd3aF (5'GTSAACGTSAAGGARACSGG) and *nirS*3cdR (5'GASTTCGGRTGSGTCTTGA). The LightCycler protocol for *nirS* was the same as for *nirK* (Throbäck et al., 2004). Both *nirK* and *nirS* primers represent the denitrification step where nitrite is reduced to nitric oxide (Priemé et al., 2002).

dsr Primers: Sulfate reducing genes were tested for using *dsr* primers. Each PCR reaction included 2 µl of sample DNA, 10 µl of PerfeCTa SYBR Green Super Mix, 2 µl of each primer and 6 µl of nuclease-free water. The primers applied were *dsr*1F+ (5'ACSCACTGGAAGCACGGCGG) and *dsr*-R (5'GTGGMRCCGTGCAKRTTGG) as in Kondo et al. (2004). The PCR protocol began with an initial denaturation at 95 ^{o}C for 10 min followed by 40 cycles of PCR amplification of 95^{o}C for 30 s, 58^{o}C for 30 s, 72^{o}C for 40 s, and a continuous drop from 80^{o}C. The melting curve protocol was 1s at 55^{o}C and a continuous drop from 95 ^{o}C. Final cooling took place at 40 ^{o}C for 1 s.

2.6 Statistical Methods

Datasets were tested for normality using quantile-quantile (Q-Q) plots in open-source R software using the function qqnorm, which compares theoretical and sample quantiles of each dataset. This was completed using both raw data and log transformed data. Multivariate Q-Q plots were also constructed using the deviation matrices of select parameters as well as the covariance matrices.

Pairwise scatter plots including histograms and correlations were created using the pairs20x R function for select parameters. Linear regression was applied to a subset of TOC and bulk DNA data using Minitab software (Minitab Inc., State College, PA, USA). This analysis found a regression equation for the log-transformed data using DNA as the dependent parameter.

Statistical hierarchical cluster analysis (HCA) was performed using Minitab software. A Ward clustering scheme (Ward, 1963) was chosen with Euclidean distances in parameter space and the number of clusters was based on substantial distances between dendrogram splits. HCA was performed on standardized data transformed into approximately normal distributions as necessary.

CHAPTER 3 RESULTS AND DISCUSSION

After applying the methods described in the previous section, trends appeared both within parameter results and between multiple characteristics.

3.1 Total Organic Carbon (TOC)

Total organic carbon (TOC) percentages in the East River averaged 3.9% with a minimum TOC concentration of 0.5% and maximum of 18% (Figure 3; Table C1). With 2.4%, 3.0 % and 2.9% average TOC, respectively, meanders A, C and O had similar concentrations of TOC and less than half the average 7.7% TOC in meander D. Where multiple depths were sampled, TOC was lower in deeper samples except at sample location De on the upstream bank of meander D. TOC varied spatially within all meanders. In meander A, TOC decreased from the upstream to downstream edge of the meander neck. However, the opposite pattern was observed in meanders C and D where TOC decreased from the downstream to upstream edge of the neck. In meander O, TOC across the cutoff neck did not vary substantially. TOC in coarse-grained deposits downstream of meanders C and D (Figure 3) were not considered when evaluating the spatial patterns. These TOC values were lower than meander averages (1.2% and 1.7%, respectively for sample locations Ca and Da).

TOC in samples from the toes of meanders inland along the meander axes had a more consistent spatial trend than the samples from across the meander necks. TOC increased from the toe to the center of meanders A, C and O with the exception of sample Cc3 and samples at the boundary between the meander and the river which were higher in organic carbon than the inland samples for active meanders. These high TOC values may be attributed to recent overbank deposition of organic rich sediments. For inactive meander O, the lowest organic carbon on the progressively inland transect was closest to the dry riverbed, likely due to lack of ongoing deposition. Samples from the riverbed of the oxbow meander as well as the flowing river on meander C also had very low TOC values (1% or less). In addition, meanders A and C had slightly lower organic carbon in the c4 samples (Figure 3), which is where the slowest hyporheic flow and longest flowpaths in the meander are predicted to occur (Revelli et al., 2008). This could reflect increased microbial activity consuming the organic carbon when the fluid residence time is longer. Meander D is a wide, treed meander but at the time of sampling water was

running across the neck and this meander may be in the process of being cut off. The water saturated nature of the sampling area and the predominance of wetland vegetation may explain the very high TOC percentages found in these samples.

3.2 Iron and Manganese Extractions

The East River samples showed very little variation between HCl extractable iron and manganese and hydroxylamine-HCl (HA) extractable iron and manganese (Tables D2 and D3, Figures D1 and D2 in Appendix D). Relative percent differences in concentration between the two extractions were generally below 20% for iron and below 25% for manganese. Given the heterogeneous nature of the soils and that wet weight was used in this experiment, it is reasonable to conclude that substantial HA reducible iron does not exist in these samples and that most of the iron in readily accessible forms is Fe(II) or was not reducible with the HA extraction. Previous studies have recognized that more Fe(III) was reduced in experiments than extracted with hydroxylamine and may represent crystalline Fe(III) that is not HA reducible but could still be used for microbial metabolism (Roden & Zachara, 1996; Lovley et al., 1987). Correlation between the total percent iron reduced and the percent extracted with HA (Roden & Zachara, 1996) suggests that extractable iron could still be representative of the relative amount of microbially reducible iron concentrations between samples. Therefore, the remaining discussion and analysis of extractable metals in the soils is based on the average of hydroxylamine-HCl and HCl-extractable iron and manganese (Figure 4).

For all samples, average extractable iron ranged from 900 mg/kg to 7700 mg/kg with an average of 4700 mg/kg and a standard deviation of 1500 mg/kg (Figure 4). Average concentrations for each meander were similar and ranged from 4400 mg/kg to 5200 mg/kg for meanders A and C, respectively. Concentrations within each meander also exhibited low variability with standard deviations of approximately 1300 mg/kg for meanders A, C and O. The exception was meander D, which had an average extractable iron concentration of 5100 mg/kg and a standard deviation of 1900 mg/kg. Additionally, extractable iron concentrations in core samples from meander A were approximately 50% lower than other samples in that meander. For example, the core samples at sample stations Ab and Ac1 had extractable iron concentrations of 2800 mg/kg and 3200 mg/kg while the grab samples at these locations contained 5900 mg/kg

and 5500 mg/kg of average extractable iron, respectively. Combined with the large standard deviation in meander D which included several deep samples, this could mean that extractable iron concentrations vary with depth as has been previously recognized in shallow alluvial systems (Vinson et al., 2007). Additionally, the core samples were not kept sealed until inside the anaerobic chamber because the sample tubes were too large for the door to the chamber and they were therefore exposed to more oxygen during sub-sampling than the grab samples.

Extractable iron concentrations followed different spatial trends for each meander (Figure 5). Meander A had fairly constant extractable iron concentrations throughout the meander with a standard deviation of only 390 mg/kg for the grab samples. Extractable iron in meander C was highest in the center of the meander and generally decreased towards the toe. Meander O also displayed this trend of decreasing iron towards the meander toe though concentrations were highest at the eroding bank of station Oe rather than the center of the cutoff meander neck. In contrast, meander D's extractable iron was lowest in the center of the meander where organic carbon was very high. The high concentrations of electron donors may have led to increased microbial reduction of Fe(III) to Fe(II). This meander was also fairly saturated with several moisture contents above 100% and the mobile Fe(II) could have been transported away by water.

Extractable manganese varied more between samples than extractable iron, with a minimum average concentration of 12 mg/kg and maximum of 290 mg/kg in samples Db and Oe, respectively (Figure 6). The average concentration for all samples was 150 mg/kg with a standard deviation of 75 mg/kg. The highest variability within individual meanders was in meander O with a standard deviation of 64 mg/kg followed by meander D with a standard deviation of 62 mg/kg. Extractable manganese in meander A was between 170 mg/kg and 230 mg/kg except at sample locations AaT, AaB and AbC. Similar to the spatial trend of extractable iron, extractable manganese in meander C decreased towards the toe but was less consistent across the neck than extractable iron concentrations. Meander O had the opposite pattern, with extractable manganese increasing towards the toe except sample Oc3. Meander D had higher extractable manganese concentrations near the upstream riverbank, though average extractable manganese in meander D was much lower than in other meanders (54 mg/kg rather than approximately 180 mg/kg). In general, samples from locations seasonally inundated by river water (AaT, AaB, Cc5R, OxM and OxU) had lower concentrations of extractable metals than

those that remain unsaturated for most of the year. This trend was stronger for iron than manganese; seasonally inundated sample locations had extractable iron concentrations more than one standard deviation less than the overall average but extractable manganese concentrations were within one standard deviation of the average with the exception of AaB.

Evaluation of data from individual meanders shows positive linear correlation between extractable manganese and iron (Figure 7). Correlation in meanders A and O were strong or moderate with R^2 values of 0.71 and 0.41, respectively. The correlation for meander C was weaker (R^2=0.19) and for meander D it was very weak (R^2 = 0.11). The intercept of the trendline for meander D was also much lower than the rest of the meanders. Other studies have concluded that the relationship between hydroxylamine reducible Fe(III) and what was microbially reduced depended on the mineralogy (Parker et al., 2013; McCarty et al., 1998). Thus, mineralogy of the samples can introduce differences in the availability of iron in comparison to manganese. For example, hydrous ferric oxide and ferrihydrite are more susceptible to microbial reduction than hematite (Parker et al., 2013). East River XRF results (Appendix B) showed that the chemical composition of the soils was fairly consistent, suggesting the soils were mineralogically homogenized. Therefore, the trends of extractable iron and manganese can be compared across the site even if the extractions are not removing the exact minerals expected. More caution should be taken while comparing East River extraction results to other studies which could vary in both mineralogy and extraction technique. East River sediments had much less extractable iron than spodosols (Wang et al., 1987) and acid mine drainage which contained up to 100,000 mg/kg HCl extractable iron (McCarty et al., 1998). The East River also had more HCl extractable iron than East China sea sediments (Chen et al., 2013) and agricultural crops which could have as little as 40 mg/kg HCl extractable iron (deSantiago et al., 2008). In comparison to other alluvial (Li et al., 2006; Campbell et al., 2012; Vinson et al., 2007), intertidal (Hyacinthe et al., 2006) and estuarine (Lovley et al., 1987) sediments, the East River had approximately average HCl extractable iron with concentrations of approximately 4700 mg/kg. There is less data on HCl extractable manganese, but in comparison to approximately 300 mg/kg in river surficial sediment (Li et al., 2006) and concentrations of nearly 1,000 mg/kg in shallow alluvium (Vinson et al., 2007) the East River had relatively low HCl extractable manganese concentrations averaging 150 mg/kg.

3.3 Synthetic Precipitation Leaching

Also of interest are metals leachable by precipitation events because metals can be essential nutrients or contaminants depending on their concentrations. Results from a synthetic precipitation leach test represent metals and metal concentrations that may be highly mobile and therefore readily available for microbial processes. Unlike the HA-HCl extractions, this analysis does not provide information about concentrations of different redox states. Across the site, leachable iron concentrations varied from 0.17 to 13 mg/kg with an average of 3.1 mg/kg (Figure 8, Table C4). Leachable manganese concentrations averaged 0.69 mg/kg with a range from 0.08 mg/kg to 1.8 mg/kg (Figure 8, Table C4). These concentrations are approximately three orders of magnitude less than HCl-extractable iron and manganese because simulated precipitation leaching targets only highly mobile metals.

As with extractable metals, meander-specific trends of leachable metals indicate that terminal electron acceptors are dependent on the small-scale meander environments. For leachable metals, iron is fairly consistent between meanders A, C and O with averages of 1.5 mg/kg, 2.2 mg/kg and 2.7 mg/kg, respectively, while leachable manganese varies between sample locations with a standard deviation of 0.44 mg/kg in comparison with the average leachable manganese of 0.69 mg/kg. Meander A had iron concentrations with a range of only 1.6 mg/kg but the manganese concentrations were quite variable with samples AaT, Ac5 and Ae having particularly high manganese concentrations of 1.6 mg/kg, 1.2 mg/kg and 1.7 mg/kg, respectively, in comparison to the average concentration in meander A of 0.75 mg/kg. These samples were located on the three sampled riverbanks of meander A. The consistent iron in meander A was also evident in the XRF results (Appendix B) but there was no indication of higher manganese in this meander. Meander C concentrations did not vary substantially for leachable iron or manganese with standard deviations of 0.98 mg/kg and 0.20 mg/kg, respectively. Samples DaD, De and DeD riverbank samples had approximately less than 3 mg/kg of leachable iron in comparison with average meander D leachable iron concentrations of 6.8 mg/kg. Leachable manganese generally decreased from the upstream to downstream side of the meander. Meander O leachable iron concentrations were lower (less than 2 mg/kg) in the dry oxbow (OxM, OxU, Oc5R) and on the downstream beach (Oa) than in the rest of the meander. Leachable manganese was also less than 0.5 mg/kg in these samples along with sample OdB.

Comparing leachable iron to leachable manganese, each meander had a distinct trend (Figure 9). Meander A samples showed variation only in leachable manganese, leachable iron concentrations were similar across the meander. Meander C results had a small range for both leachable iron and manganese, with a weak positive correlation between leachable iron and manganese that improved if deep sample Cc4D was not included. Leachable iron in meander D generally increased with leachable manganese except in samples De and DeD, which had low leachable iron but high manganese concentrations relative to the rest of the dataset. It is possible that at this edge of meander D, as well as the edges of meander A, oxygenated river water enters the meanders as hyporheic flow and causes oxidation of manganese to Mn(IV), which is less mobile than Mn(II). The less mobile Mn(IV) may deposit and stay in the upstream bank. Meander O leachable iron generally increased with leachable manganese concentration except three samples from the edge of the river or dry riverbed (Oc5R, Oa and OdB), which had very low manganese concentrations and may have already been leached by real rainfall or river water. Leachable iron concentrations were generally higher in meander D than all other meanders while leachable manganese had some relatively high concentrations in each meander except meander C. These results suggest that some areas may be manganese reducing but the correlation between manganese and iron in most locations suggests that manganese and iron reduction may both be occurring so manganese reduction may not be the dominant reducing mechanism for the floodplain. In addition, the high organic carbon and leachable metals in meander D may classify this meander as a microbial hotspot. High concentrations of electron donors and terminal electron acceptors make an ideal habitat where microbial populations can thrive. Meander D may therefore have a disproportionately high influence on the nutrient cycling and geochemistry of the system.

There may also be some correlation between leachable metals and influence of Mancos Shale (Figure 10). Manganese concentrations were below average on rocky downstream samples De and Oe as well as sample OdB which was on a muddy bank. In contrast, manganese concentrations were high on the banks of meander A, which had fine grained sediments. Samples DaD and Oc5R, both Mancos-dominated because of low organic carbon, tended to have lower leachable metals overall. The upstream Yule sample also had generally lower metal concentrations except for iron, aluminum and manganese, which were relatively high. These metals, along with nickel, were low in the rockier Oa sample, probably reflecting association

between iron oxides and many trace metals (McCarty et al., 1998). Sample Cc5R and AbC (core) were relatively high in sodium and potassium while elevated concentrations of zinc and nickel were found in sample DdD. This suggests that though XRF data (Appendix B) found relatively consistent elemental content, the easily leachable fraction often has variability and potentially hotspots of some metals.

3.4 DNA Extraction and Quantitative PCR Analysis

Here we use bulk microbial DNA as a proxy for total microbial activity in a given sample. To understand the microbial communities that make up the microbial population, functional genes, which encode for specific enzymes such as *nirK* and *nirS* for denitrification and *dsr* for sulfate reduction, were quantified through quantitative PCR (qPCR). This approach identifies microbial populations according to biological functions rather than taxonomy (Throbäck et al., 2004). The *nirK* and *nirS* nitrite reductase genes identify the microbial population capable of reducing nitrite to nitric oxide (Braker et al., 1998; Throbäck et al., 2004) while the *dsr* dissimilatory sulfite reductase gene identifies microbial communities which can reduce sulfite to sulfide, the final step in sulfate reduction (Geets et al., 2006; Kondo et al., 2004).

Bulk microbial DNA varied from 79 to 25000 ng/g (ng of DNA per g of dry sediment) with an average of 6400 ng/g (Figure 11, Table C5). Some of these results approached the high and low ends of the detection limit for the instrument. The average was fairly consistent between meanders with a standard deviation of 730 ng/g between meander averages. The bulk amount of DNA was highest near the center of meanders, which did not correlate to identification of denitrifying bacteria with *nir* genes. *Nir* genes are reported as a percentage of universal 16S bacterial DNA to quantify what percentage of the bacterial population are denitrifying. The percentages of *nir* genes compared to 16S genes were highest near the edges of meanders including the cutoff neck of meander O. This is consistent with the conclusion that denitrification is important in the hyporheic zone because the meander edges are where the river water is potentially entering the banks and becoming hyporheic flow as it mixes with groundwater (Morrice et al., 2000). Many of the samples with lowest bulk DNA had the highest percentages of *nir* genes. As bulk DNA increased (greater than approximately 3000 ng/g) the *nirK* and *nirS*

percentages of 16S genes were almost exclusively below 0.01 % (Figure 12). Therefore, the microbial communities dominating in areas with highest microbial activity (evaluated as highest bulk DNA) were not denitrifiers identified with *nirK* and *nirS* gene strands.

Additional testing of 4 samples (Cc3, Cc5, Db and Cc3S) with the *dsr* sulfate reducing gene did not reveal any appropriately amplifying samples. Test samples were chosen because they had more than 15 ng/µl bulk DNA for sediment and almost 2 ng/µl bulk DNA for water, concentrations high enough that they should amplify if *dsr* genes were present but not so high as to introduce sample-specific inhibition by nucleic acids, humic and fulvic acids or heavy metals (Hargreaves et al., 2013; Schriewer et al., 2011). In addition, test sample Db was a high carbon, high moisture content sample which would be one of the most likely to have sulfate reducing conditions because sulfate reducers are most abundant in anaerobic environments (Kondo et al., 2004). Testing all samples for appropriate amplification would be an inefficient use of time and finances. Therefore, based on gel electrophoresis results from the four test samples, there was no evidence of sulfate reducers in near-surface soils at the East River but there could potentially be sulfate reducers in other samples or sulfate reducers with different genes. Given the low abundance of nitrogen reducers and undetectable sulfate reduction gene, the dominant terminal electron acceptors in the East River study site are most likely to be those with energetic favorability between denitrification and sulfate reduction, commonly oxidized forms of manganese and iron (Morrice et al., 2000), which is what is often expected in the subsurface (García-Balboa et al., 2011; reviewed by Lovley et al., 1991). There was evidence of reduced iron in the system in a core from sample Aa that changed color from dark brown/black to red in refrigerated sample storage as iron oxidized. This may, however, not be reflective of widespread high concentrations of reduced iron as the core was taken from saturated sediment beneath the river whereas most samples were from deposits outside the riverbed and thus likely unsaturated and in more oxidizing conditions.

In samples from the East River, the percentage of 16S DNA comprised of *nirK* and *nirS* genes was highest when moisture content was approximately 50% (Figure 13). Though little is known about the habitats of denitrifying bacteria with *nirK* and *nirS* genes, moisture content is considered one of the regulating influences (Priemé et al., 2002; Bergaust et al., 2010). Very water saturated soils have less available oxygen which makes nitrate the first dominant terminal

electron acceptor. Therefore, in wetter soils, it is more likely for enough nitrate to have been reduced that the system may be beyond a nitrogen reducing state. In contrast, dry areas may be too aerobic for preferential denitrification because oxygen is a more energetically favorable terminal electron acceptor for microbial metabolism (Morrice et al., 2000; Sweets et al., 1991). Nitrate will not serve as the dominant terminal electron acceptor until the oxygen supply has been reduced. Changes in saturation through seasonally fluctuating moisture contents tend to be ideal locations for denitrification because of seasonal re-introduction of oxygen (Bergaust et al., 2010). Moisture content is a dominant control on denitrification rate as measured by static core acetylene inhibition assay, with moisture content of 50-80% being ideal for denitrification in floodplain soils (Pinay et al, 2007). The East River had highest *nir* percentages near 50% moisture content. Given the evidence of moisture content regulating redox conditions, 50% moisture content may be indicative of ideal redox conditions for reduction of nitrite to nitrous oxide in the East River soils (Takatert et al., 1999). Moisture content's influence on redox conditions and microbial community may be particularly important in Meander D, which had high moisture content (often above 60%), high total carbon and high total DNA but relatively low amounts of *nir* genes, particularly in samples where carbon and metals were highest. If moisture content is high enough that nitrate has already been reduced in meander D then this meander may be in an iron reducing state. Overall, meanders contain a diversity of hydrologic and chemical characteristics and floodplain systems may have a similarly heterogeneous distribution of dominant terminal electron acceptors.

3.5 Relationships between Geochemical Parameters and Bulk Microbial DNA

Statistical analyses were performed to explore quantitative relationships between geochemical and biological characteristics of the samples; in particular between the geochemical parameters and bulk microbial DNA. Each parameter exhibits normal distribution for the data set containing all samples. A pairwise correlation analysis was used to examine correlations for each pair of parameters (Figure 14). Statistical hierarchical clustering analysis identified how the overall dataset was distributed spatially.

3.5.1 Test for Normality

This study tests many parameters which are reported in different units and can therefore have very different magnitudes. For example, DNA in ng/g has much higher values than TOC in percent carbon by mass. As a result, DNA also has a much larger variance which can skew statistical tests such as statistical clustering. To overcome this, data should be standardized by subtracting the mean and dividing by the standard deviation. In addition, many of the algorithms used by Minitab software for statistical hierarchical clustering with Euclidean distances assume an approximately normal distribution for each dataset (Cormack, 1971; Milligan, 1980).

Quantile-quantile (Q-Q) plots can be used to visually assess whether data follows the normal distribution or needs to be transformed prior to standardization (Figures D3 through D15). The extractable iron (both HCl and HA) data were approximately normally distributed according to their Q-Q plots. Extractable manganese was not as well approximated by a normal distribution but the fit worsened for log-transformed values. TOC, leachable iron and leachable manganese were approximately normally distributed for log-transformed values. Microbial DNA followed a growth curve and normality was better approximated for log-transformed values but the quantiles were not as strongly correlated to a normal distribution as the other parameters. A multivariate Q-Q plot was created for log-transformed TOC, DNA, leachable iron and leachable manganese as well as untransformed HCl and HA extractable iron and manganese. Multivariate Q-Q plots compare n variables with an n-dimensional normal distribution with a vector of means and a covariance matrix consisting of variances on the diagonals and covariances on the off-diagonals (Brown, 1998). Geometrically, the multivariate normal probability density function consists of ellipsoids on a set of axes defined by the eigenvectors of the covariance matrix. The multivariate normality for the entire East River dataset was weak though it was improved when HA extractable metals were removed as this was only duplicating the variation already accounted for by HCl extractable metals. When all extractable metals were removed from the multivariate Q-Q plot, the data was approximately multivariate normal. Q-Q plots of original and transformed data can be found in Appendix D.

3.5.2 Pairwise Correlations

Pairwise correlations are an efficient method for analyzing correlations between each pair of variables in a dataset with several parameters. For 8 parameters, a single R command (pairs20x) computes 28 scatterplots and correlations to see what parameters are strongly, weakly or uncorrelated. Though this study is primarily looking at each parameter's relationship to DNA, recognizing strong relationships to other parameters can provide insights about the cause of the DNA relationship. Identifying the strongest pairs quickly also determined which parameters should be investigated more thoroughly for their correlation to microbial DNA.

Pairwise correlations between parameters using the full datasets and standardized and transformed according to the results of Section 3.5.1 show that some parameters were more strongly correlated than others (Figure 14). As discussed in Section 3.2, HCl Fe-HA Fe and HCl Mn-HA Mn were very strongly correlated (0.93 and 0.96, respectively) and essentially represented the same parameters in the datasets (Fe(II) and Mn(II)). Otherwise, the correlation between log-transformed TOC and log-transformed leachable iron was the strongest identified in the dataset (0.67). Log-transformed TOC was strongly correlated to log-transformed DNA (0.66) while the correlation between log-transformed leachable iron and log-transformed DNA was weaker (0.45). Correlation between leachable iron and DNA may be based on a relationship between iron and TOC but could still be significant. Leachable manganese had a weaker but still reasonable correlation to both TOC and DNA (0.56 and 0.28), as did extractable iron (0.46 and 0.34). Extractable manganese correlated with extractable iron (0.35) but was otherwise uncorrelated to the remaining parameters.

Because of the heterogeneous nature of soil data, we consider correlations to be strong when R^2 values are greater than 0.4. All linear correlations between DNA and metals at the East River site were positive except the correlation between DNA and extractable iron for meander D. Linear correlations between log-transformed microbial DNA and metals had R^2 values of 0.23, 0.19 and 0.25, respectively for log-transformed leachable iron, log-transformed leachable manganese, and untransformed average extractable iron (Figure 15, Table 1). These full dataset trends were weak; therefore the correlations for individual meanders were explored. Correlations using only shallow meander samples were also calculated to see whether samples such as

riverbed, deep and oxbow samples obscured a correlation. The trend between using only shallow meander samples and using all samples was inconsistent. DNA in meander A did not correlate strongly with leachable metals but meander A's entire dataset had an R^2 value of 0.51 for DNA correlated to average extractable iron. DNA was moderately positively correlated with leachable iron (R^2=0.38) for meander C's entire dataset but a stronger correlation was found between DNA and extractable iron in meander C (R^2=0.75). Meander D was most strongly correlated to leachable iron with an R^2 of 0.49 for shallow samples. Meander O correlated strongly with all three metals but had the strongest relationship with leachable manganese, with an R^2 of 0.92 for all samples. The R^2 value for shallow meander O samples for leachable iron was 0.82 and for all meander O samples and extractable iron it was 0.49.

Table 1. Relationship between metals and log-transformed bulk microbial DNA

Meander	All Meander Samples	Shallow Meander Samples
log-Leachable Fe-All	0.23	0.25
A	0.07	0.15
C	0.38	0.33
D	0.38	0.49
O	0.50	0.82
log-Leachable Mn – All	0.19	0.14
A	0.06	0.01
C	0.05	0.00
D	0.10	0.01
O	0.51	0.92
HCl Extractable Fe-All	0.25	0.11
A	0.51	0.33
C	0.75	0.67
D	0.00	0.22
O	0.49	0.30

The correlation between leachable manganese and microbial activity in meander O suggests that manganese-reducing bacteria may be present at this location. Given the lower connectivity of meander O to the river, hyporheic and surface flow is likely ephemeral. Thus, redox conditions may be more variable throughout the year in meander O than in other meanders, leading to times when conditions are favorable for manganese reduction in meander O but not in other meanders. However, in a manganese reducing environment it would be expected to see bioavailable (or HA-reducible) iron and manganese. The similarity between HCl and

hydroxylamine-HCl extractions suggests that HA-reducible iron and manganese are absent or very low at this location. The same discrepancy applies when hypothesizing that meanders A, C and D are primarily iron reducing. Also, despite strong pairwise correlation between leachable iron and bulk microbial DNA, correlations for individual meanders was generally relatively weak. The relationship of leachable iron to DNA may result from a correlation between leachable iron and total organic carbon.

Overall, correlation between meander O's DNA and leachable manganese, and correlations between meanders A and C's DNA and extractable iron and meander D's DNA and leachable iron suggest that there is a possibility for these metals to be used in predicting microbial activity. However, identifying which metal to test for would be the first step and, based on the extraction results and qPCR analysis, this prediction may not be straightforward. The process would be particularly complicated by a hydrologically heterogeneous system like a floodplain where flowpaths even between the edges and inside of the meanders can be quite variable. Methods of identifying the dominant redox couple of an environment could establish metals as geochemical indicators of microbial activity but metals are likely not a consistent screening tool that can be easily applied to heterogeneous environments.

3.5.3 Linear Regression of Bulk DNA and TOC

Log-transformed bulk microbial DNA from the East River is positively linearly correlated to log-transformed TOC with an R^2 for all East River data of 0.60 (Figure 16). Linear correlations between the log-transformed data were usually improved by removing samples that were not related to active meander deposition and erosion processes such as dry oxbow samples, riverbed samples and deep samples (Table 2). Individual meander C and the overall East River correlations did not improve with removal of these types of samples. Additional data from deeper samples may follow a different trend but this study was primarily looking for 2-dimensional trends. Note that for meander A, core samples at stations B and C were incomplete and it was inconclusive whether grab or core samples were deeper so all were included in these statistical analyses. Individually, TOC from meander A had a much weaker correlation to microbial DNA than TOC from other meanders with an R^2 of only 0.55 for shallow samples. TOC from meanders C and D had very similar correlations with DNA when only shallow

samples were included (R^2=0.86 for both) while meander O's TOC and DNA were particularly well correlated with an R^2 of 0.95.

Table 2. TOC-DNA relationship for variable datasets

Sample Set	Log-Transformed R^2
East River Samples	0.60
Shallow East River	0.54
East River and Rifle Samples	0.85
Shallow East River and Rifle	0.87
Meander A	0.34
Meander C	0.90
Meander D	0.80
Meander O	0.95
Rifle	0.14
Meander A Shallow	0.55
Meander C Shallow	0.86
Meander D Shallow	0.86
Meander O Shallow	0.97

East River samples have generally high TOC in comparison with inactive alluvium settings (Campbell et al., 2012) and river surficial sediment (Li et al., 2006) with a minimum TOC of 0.5%. Bulk microbial DNA was often approaching the upper detection limit of the instrument with an average concentration of 6300 ng/g. Combining East River results with a low TOC and DNA dataset from a previous study in Rifle, Colorado (Prugue, 2014) with maximum 0.4% TOC and 218 ng/g DNA, respectively, creates a broader range for the relationship. The correlation of joint log-transformed datasets had an R^2 of 0.85 (Table 2). A dataset of alluvial Rifle and shallow meander East River samples had the best fit with an R^2 of 0.87. Rifle samples alone had a very weak correlation (R^2=0.14) but overall correlation improved from an R^2 of 0.60 to an R^2 of 0.85 when Rifle results were included. This may be because there were few samples from the Rifle site (14) and they all had low concentrations of both TOC and DNA. Detection limits may influence the accuracy of results but when combined with higher-concentration East River data they fit the overall trend relationship by adding lower end-members. Increased variability may also be caused by differing depths between Rifle samples. Improved fit with both datasets suggests that the TOC-DNA relationship is consistent across floodplain field sites with different characteristics.

A linear regression of the 34 shallow East River and 14 alluvial Rifle samples resulted in the following equation with an R^2 of 0.87 (Figure 17):

$$logDNA = 2.894 + 1.605logTOC$$

This equation is the first step towards creating an empirical method of using TOC as a proxy for bulk microbial DNA. Obviously inclusion of more datasets would be needed to test this model and additional data from other types of geologic settings should be included to investigate whether a similar relationship applies to non-floodplain deposits.

3.5.4 Statistical Hierarchical Clustering Analysis

Statistical clustering was also performed on multiple datasets. Extractable manganese had no effect on the clustering results and was not included because it would be a random noise variable that would add error rather than contributing to the clustering (Milligan, 1980). In addition, average extractable iron was used because including both HA and HCl extractable iron would essentially be duplicating that data. Removing the leachable iron and/or manganese made a substantial difference whereas removing all extraction data resulted in similar clusters to when all data was included. Final clustering was based on standardized data for average extractable iron and log-transformed TOC, DNA, leachable iron and leachable manganese.

The resulting four clusters were distributed by the variables according to Table 3, the dendrogram in Figure 18 and the spatial distribution of clusters in Figure 19. Four clusters were chosen based on the distances between cluster separations. A parameter distance of less than 9 was chosen to represent a single cluster. Cluster 1 contained many of the samples representing the bulk average characterization of the site as it did not have highest or lowest cluster average for any of the parameters and more variability in leachable and extractable iron than all other clusters (Table 3). Cluster 2 was characterized by metals with the highest standardized cluster averages of extractable iron (0.093), leachable iron (1.0) and leachable manganese (0.42). This cluster also had the highest average DNA (0.63). Cluster 3 had the highest carbon and also high DNA (cluster averages of 1.3 and 0.51, respectively). These samples were rich in organic carbon but had low leachable manganese with an average of -1.0. Cluster 4 had the lowest average values of TOC, DNA, extractable iron, and leachable iron (-1.3, -1.4, -0.56 and -0.80, respectively). There was also a lot of variability with standard deviations above 0.5 for all

parameters except extractable iron so it was possibly the iron extractions that clustered these samples together.

Table 3. Average standardized parameter values of statistical hierarchical clusters

Variable	Cluster 1	Cluster 2	Cluster 3	Cluster 4
logTOC	-0.12±0.48	0.55±0.44	1.3±0.84	-1.3±0.55
logDNA	0.23±0.33	0.63±0.31	0.51±0.68	-1.4±0.95
HClFe	-0.42±0.41	0.093±0.17	-0.48±0.16	-0.56±0.25
logLFe	-0.30±0.86	1.0±0.57	-0.63±0.52	-0.80±0.68
logLMn	0.099±0.52	0.42±1.03	-1.0±1.28	-0.18±0.91

Cluster 1 was dominantly found on meander A, though there were a few samples from each of the other meanders, often near one of the banks (Figure 19). Samples in cluster 2 were mostly on meanders C and O though there were a few samples from this cluster on each meander. Almost all samples in cluster 3 were from meander D. This suggests that the geochemistry of specific meanders was distinct enough for many of the samples to cluster together. Samples in cluster 4 were either rocky shoreline or from the riverbed itself suggesting that these samples were dominated by Mancos material rather than a combination of soils and weathered Mancos rocks. The low organic carbon in these samples influences what geochemical and microbial reactions can occur. In addition, iron in the Mancos-formation is more likely to be crystalline which could explain the low extractable and leachable iron in these samples. In addition, almost all of cluster 4's samples (8 of the 11) were removed from the dataset to improve the correlations between parameters and DNA (these were the ones removed to create the "shallow East River" subset). Only four samples removed from that dataset didn't cluster into cluster 4. This introduces the potential to use clustering to decide which samples should be used in creating the empirical relationship.

CHAPTER 4 CONCLUSIONS

This study presents data from an investigation of the importance of hydrological and geochemical heterogeneity in microbial activity and community structure. Certain geochemical properties can be used as indicators of high microbial activity. The strong relationship between electron donors and bulk microbial DNA has been confirmed in both an inactive floodplain and on active and ephemerally active floodplain meanders.

East River soil samples had TOC percentages greater than 1% with a few exceptions along the riverbanks. There was average HCl and HA extractable iron and manganese averaging 4700 mg/kg and 150 mg/kg, respectively, though no HA-reducible metals which would be available for microbial metabolism. Leach tests revealed meander-scale trends between iron and manganese with a weak whole-dataset relationship. Meander A had almost no variability of iron but a wide range of manganese while most samples in meanders D and O showed an increase of manganese with iron and meander C had little variability in either. Bulk microbial DNA was high in most East River samples, averaging 6300 ng/g and approaching detection limits which suggests a very biologically active system. No evidence of sulfate reducers was found but the denitrifying bacteria did not dominate where microbial activity was highest, suggesting that dominant terminal electron acceptors across the site are iron and manganese. The high organic carbon, leachable iron and microbial DNA on meander D may classify this meander as a biogeochemical hotspot with a controlling influence on the nutrient cycling of the system.

The relationship between microbial activity and metals was not consistent for the entire dataset. When separated by meander, strong correlations were found between microbial DNA and either manganese or iron but there was insufficient data on each individual meander to do a linear regression. In particular, meander O correlated with leachable manganese while meanders A and C were more strongly correlated with extractable iron and meander D with leachable iron. This data may reflect dominant terminal electron acceptors but qPCR and extraction results did not agree; therefore terminal electron acceptors would not make a consistent geochemical indicator except perhaps in a well-characterized homogeneous system.

There was a strong relationship between the dominant electron donor (organic carbon) and microbial activity measured as bulk microbial DNA. This relationship grew stronger with

inclusion of data from both the high-carbon East River site and the low-carbon Rifle site. There was sufficient data to do a linear regression which produced an equation with an R^2 value of 0.86. This establishes TOC as a consistent geochemical indicator for determination of microbial activity on floodplains.

Cluster analyses resulted in substantial spatial trends with certain clusters dominating on some meanders and other clusters consisting of riverbank samples. This suggests that trends of microbial DNA, TOC and metals in meander soils are spatially determinable and with further study could be used for large-scale prediction. In particular, samples which do not contribute to active meander processes tended to cluster out.

REFERENCES

Anibas, C., Buis, K., Verhoeven, R., Meire, P., Batelaan, O. (2011). A simple thermal mapping method for seasonal spatial patterns of groundwater-surface water interaction. *Journal of Hydrology, 397, 93-104.*

Atchley, A.L., Maxwell, R.M., Navarre-Sitchler, A.K. (2013). Using streamlines to simulate stochastic reactive transport in heterogeneous aquifers: Kinetic metal release and transport in CO_2 impacted drinking water aquifers. *Advances in Water Resources, 52, 93-106.*

Bencala, K.E., Walters, R.A. (1983). Simulation of solute transport in a mountain pool-and-riffle stream: A transient storage model. *Water Resources Research, 19(3), 718-724.*

Bergaust, L., Mao, Y., Bakken, L.R., Frostegård, Å. (2010). Denitrification response patterns during the transition to anoxic respiration and posttranscriptional effects of suboptimal pH on nitrogen oxide reductase in *Paracoccus denitrificans. Applied and Environmental Microbiology, 76(19), 6387-6396.*

Boano, F., Harvey, J.W., Marion, A., Packman, A.I., Revelli, R., Ridolfi, L., Wörman, A. (2014). Hyporheic flow and transport processes: Mechanisms, models, and biogeochemical implications. *AGU Publications: Reviews of Geophysics, 603-679*

Brown, C.E. (1998). Applied Multivariate Statistics in Geohydrology and Related Sciences. Springer: Berlin, Germany.

Campbell, K.M., Kukkadapu, R.K., Qafoku, N.P., Peacock, A.D., Lesher, E., Williams, K.H., Bargar, J.R., Wilkins, M.J., Figueroa, L., Ranville, J., Davis, J.A., Long, P.E. (2012). Geochemical, mineralogical and microbiological characteristics of sediment from a naturally reduced zone in a uranium-contaminated aquifer. *Applied Geochemistry, 27, 1499-1511.*

Chao, T.T., Zhou, L. (1983). Extraction techniques for selective dissolution of amorphous iron oxides from soils and sediments. *Soil Science Society of America Journal, 47, 225-232.*

Chapelle, F.H., Lovley, D.R. (1992). Competitive exclusion of sulfate reduction by Fe(III)-reducing bacteria: a mechanism for producing discrete zones of high-iron ground water. *Ground water, 30(1), p. 29-36.*

Chen, L., Zhu, M., Yang, G., Huang, X. (2013). Reductive reactivity of iron(III) oxides in the East China sea sediments: characterization by selective extraction and kinetic dissolution. *PLoS ONE, 8(11), e80367.*

Cormack, R.M. (1971). A review of classification. *Journal of the Royal Statistical Society. Series A, 134(3), 321-367.*

de Santiago, A., Díaz, I., del Carmen del Campillo, M., Torrent, J., Delgado, A. (2008). Predicting the incidence of iron deficiency chlorosis from hydroxylamine-extractable iron in soil. *Soil Science Society of America Journal, 72(5), 1493-1499.*

Englert, A., Hubbard, S.S., Williams, K.H., Li, L., Steefel, C.I. (2009). Feedbacks between hydrological heterogeneity and bioremediation induced biogeochemical transformations. *Environmental Science and Technology, 43, 5197-5204.*

EPA. (1994). Method 1312: Synthetic precipitation leaching procedure.

Fierer, N., Jackson, J.A., Vilgalys, R., Jackson, R.B. (2005). Assessment of soil microbial community structure by use of taxon-specific quantitative PCR assays. *Applied and Environmental Microbiology, 71(7), 4117-4120.*

Fleckenstein, J.H., Krause, S., Hannah, D.M., Boano, F. (2010). Groundwater-surface water interactions: New methods and models to improve understanding of processes and dynamics. *Advances in Water Resources, 33(11), 1291-1295.*

Fustec, E., Mariotti, A., Grillo, X., Sajus, J. (1991). Nitrate removal by denitrification in alluvial ground water: Role of a former channel. *Journal of Hydrology, 123, 337-354.*

García-Balboa, C., Vicente, M.S., Blázquez, M.L., González, F., Muñoz, J.A., Ballester, A. (2011). Iron speciation in dissimilatory Fe(III)-reducing cultures. *Geomicrobiology Journal, 28, 371-379.*

Geets, J., Borremans, B., Diels, L., Springael, D., Vangronsveld, J., van der Lelie, D., Vanbroekhoven, K. (2006). *DsrB* gene-based DGGE for community and diversity surveys of sulfate-reducing bacteria. *Journal of Microbiological methods, 66, 194-205.*

Gooseff, M.N., LaNier, J., Haggerty, R., Kokkeler, K. (2005). Determining in-channel (dead zone) transient storage by comparing solute transport in a bedrock channel-alluvial channel sequence, Oregon. *Water Resources Research, 41, W06014.*

Groffman, A.R., Crossey, L.J. (1999). Transient redox regimes in a shallow alluvial aquifer. *Chemical Geology, 161(4), 415-442.*

Hakala, J.A., Fimmen, R.L., Chin, Y., Agrawal, S.G., Ward, C.P. (2009). Assessment of the geochemical reactivity of Fe-DOM complexes in wetland sediment pore waters using a nitroaromatic probe compound. *Geochimica et Cosmochimica Acta, 73(5), 1382-1393.*

Hargreaves, S.K., Roberto, A.A., Hofmockel, K.S. (2013). Reaction- and sample-specific inhibition affect standardization of qPCR assays of soil bacterial communities. *Soil Biology & Biochemistry, 59, 89-97.*

Hedin, L.O., von Fischer, J.C., Ostrom, N.E., Kennedy, B.P., Brown, M.G., Robertson, G.P. (1998). Thermodynamic constraints on nitrogen transformations and other biogeochemical processes at soil-stream interfaces. *Ecology, 79(2), 684-703.*

Henry, S., Baudoin, E., López-Gutiérrez, J.C., Martin-Laurent, F., Brauman, A., Philippot, L. (2004). Quantification of denitrifying bacteria in soils by nirK gene targeted real-time PCR. *Journal of Microbiological Methods, 59(3), 327-335.*

Hill, A.R., Devito, K.J., Campagnolo, S., Sanmugadas, K. (2000). Subsurface denitrification in a forest riparian zone: Interactions between hydrology and supplies of nitrate and organic carbon. *Biogeochemistry, 51, 193-2000.*

King, E.L., Tuncay, K., Ortoleva, P., Meile, C. (2010). Modeling biogeochemical dynamics in porous media: Practical considerations of pore scale variability, reaction networks, and microbial population dynamics in a sandy aquifer. *Journal of Contaminant Hydrology, 112, 130-140.*

Kondo, R., Nedwell, D.B., Purdy, K.J., de Queiroz Silva, S. (2004). Detection and enumeration of sulphate-reducing bacteria in estuarine sediments by competitive PCR. *Geomicrobiology Journal, 21, 145-157.*

Leopold, L.B., Wolman, M.G., Miller, J.P. (1995). Fluvial Processes in Geomorphology. Dover Publications, Mineola: NY.

Li, F., Wang, X., Li, Y., Guo, S., Zhong, A. (2006). Selective extraction and separation of Fe, Mn oxides and organic materials in river surficial sediments. *Journal of Environmental Sciences, 18(6), 1233-1240.*

Li, L., Steefel, C.I., Kowalsky, M.B., Englert, A., Hubbard, S.S. (2010). Effects of physical and geochemical heterogeneities on mineral transformation and biomass accumulation during biostimulation experiments at Rifle, Colorado. *Journal of Contaminant Hydrology, 112, 45-63.*

Li, L., Gawande, N., Kowalsky, M.B., Steefel, C.I., Hubbard, S.S. (2011). Physicochemical heterogeneity controls on uranium bioreduction rates at the field scale. *Environmental Science & Technology, 45, 9959-9966.*

Li, X., Liu, T., Li, F., Zhang, W., Zhou, S., Li, Y. (2012). Reduction of structural Fe(III) in oxyhydroxides by *Shewanella decolorationis* S12 and characterization of the surface properties of iron minerals. *Journal of Soils and Sediments, 12, 217-227.*

Lovley, D.R., Phillips, E.J.P. (1987). Rapid assay for microbially reducible ferric iron in aquatic sediments. *Applied and Environmental Microbiology, 53(7), 1536-1540.*

McCarty, D.K., Moore, J.N., Marcus, W.A. (1998). Mineralogy and trace element association in an acid mine drainage iron oxide precipitate; comparison of selective extractions. *Applied Geochemistry, 13(2), 165-176.*

McDowell, W.H., Bowden, W.B., Asbury, C.E. (1992). Riparian nitrogen dynamics in two geomorphologically distinct tropical rain forest watersheds: subsurface solute patterns. *Biogeochemistry, 18, 53-72.*

Milligan, G.W. (1980). An examination of the effect of six types of error perturbation on fifteen clustering algorithms. *Psychometrika, 45(3), 325-342.*

Molz, F.J., Widdowson, M.A., Benefield, L.D. (1986). Simulation of microbial growth dynamics coupled to nutrient and oxygen transport in porous media. *Water Resources Research, 22(8), 1207-1216.*

Morrice, J.A., Dahm, C.N., Valett, H.M., Unnikrishna, P.V., Campana, M.E. (2000). Terminal electron accepting processes in the alluvial sediments of a headwater stream. *Journal of the North American Benthological Society, 19(4), 593-608.*

Morrison, S.J., Goodknight, C.S., Tigar, A.D., Bush, R.P., Gil, A. (2012). Naturally occurring contamination in the Mancos Shale. *Environmental Science and Technology, 46, 1379-1387.*

Murphy, E.M., Ginn, T.R., Chilakapati, A., Resch, C.T., Phillips, J.L., Wietsma, T.W., Spadoni, C.M. (1997). The influence of physical heterogeneity on microbial degradation and distribution in porous media. *Water Resources Research, 33(5), 1087-1103.*

Myrbo, A. (2004). Total carbon (TC) coulometry. *Limnological Research Center Core Facility, SOP series.*

Parker, C.W., Wolf, J.A., Auler, A.S., Barton, H.A., Senko, J.M. (2013). Microbial reducibility of Fe(III) phases associated with the genesis of iron ore caves in the iron quadrangle, Minas Gerais, Brazil. *Minerals, 3, 395-411.*

Pepe-Ranney, C., Berelson, W.M., Corsetti, F.A., Treants, M., Spear, J.R. (2012). Cyanobacterial construction of hot spring siliceous stromatolites in Yellowstone National Park. *Environmental Microbiology. 14(5), 1182-1197.*

Pinay, G., Black, V.J., Planty-Tabacchi, A.M., Gumiero, B., Décamps, H. (2000). Geomorphic control of denitrification in large river floodplain soils. *Biogeochemistry, 50, 163-182.*

Pinay, G., Gumiero, B., Tabacchi, E., Gimenez, O., Tabacchi-Planty, A.M., Hefting, M.M., Burt, T.P., Black, V.A., Nilsson, C., Iordache, V., Bureau, F., Vought, L., Petts, G.E.,

Décamps, H. (2007). Patterns of denitrification rates in European alluvial soils under various hydrological regimes. *Freshwater Biology, 52, 252-266.*

Priemé, A., Braker, G., Tiedje, J.M. (2002). Diversity of nitrite reductase (*nirK* and *nirS*) gene fragments in forested upland and wetland soils. *Applied and Environmental Microbiology, 68(4), 1893-1900.*

Prommer, H., Tuxen, N., Bjerg, P.L. (2006). Fringe-controlled natural attenuation of phenoxy acids in a landfill plume: Integration of field-scale processes by reactive transport modeling. *Environmental Science and Technology, 40, 4732-4738.*

Prugue, R. (2014). MS Thesis: Identification of reducing conditions and correlated hydrological and biogeochemical properties in a heterogeneous floodplain aquifer. Colorado School of Mines: Golden CO.

Revelli, R., Boano, F., Camporeale, C., Ridolfi, L. (2008). Intra-meander hyporheic flow in alluvial rivers. *Water Resources Research, 44, W12428.*

Robertson, A.L., Wood, P.J. (2010). Ecology of the hyporheic zone: origin, current knowledge and future directions. *Fundamentals of Applied Limnology, 176 (4), 279-289.*

Roden, E.E., Zachara, J.M. (1996). Microbial reduction of crystalline iron(III) oxides: influence of oxide surface area and potential for cell growth. *Environmental Science and Technology, 30(5), 1618-1628.*

Schilling, K.E., Jacobson, P. (2012). Spatial relations of topography, lithology and water quality in a large river floodplain. *River Research and Applications, 28, 1417-1427.*

Schriewer. A., Wehlmann, A., Wuertz, S. (2011). Improving qPCR efficiency in environmental samples by selective removal of humic acids with DAX-8. *Journal of Microbiological Methods, 85, 16-21.*

Scott, D.T., Gooseff, M.N., Bencala, K.E., Runkel, R.L. (2003). Automated calibration of a stream solute transport model: implications for interpretation of biogeochemical parameters. *Journal of the North American Benthological Society, 22(4), 492-510.*

Sena, C., Molinero, J., Ajima, S., Todaka, N. (2012). Modelling microbial degradation coupled to reactive transport in groundwater: A benchmark analysis. *Mathematical Geosciences, 44, 209-226.*

Staroscik, A. (2004). Calculator for determining the number of copies of a template. URI Genomics & Sequencing Center. <http://cels.uri.edu/gsc/cndna.html>.

Stotzky, G. (1967). Clay minerals and microbial ecology. *Transactions of the New York Academy of Sciences: Division of Environmental Sciences, 30 (1), 11-21.*

Sweerts, J.R., Bär-Gilissen, M., Cornelese, A.A., Cappenberg, T.E. (1991). Oxygen-consuming processes at the profundal and littoral sediment-water interface of a small meso-eutrophic lake (Lake Vechten, The Netherlands). *Limnology and Oceanography, 36(6), 1124-1133.*

Takatert, N., Sánchez-Pérez, J.M., Trémolières, M. (1999). Spatial and temporal variations of nutrient concentration in the groundwater of a floodplain: effect of hydrology, vegetation and substrate. *Hydrological Processes, 13, 1511-1526.*

Tartakovsky, A.M., Scheibe, T.D., Meakin, P. (2009). Pore-scale model for reactive transport and biomass growth. *Journal of Porous Media, 12(5), 417-434.*

Tartakovsky, G.D., Tartakovsky, A.M., Scheibe, T.D., Fang, Y., Mahadevan, R., Lovley, D.R. (2013). Pore-scale simulation of microbial growth using a genome-scale metabolic model: Implications for Darcy-scale reactive transport. *Advances in Water Resources, 59, 256-270.*

Throbäck, I.N., Enwall, K., Jarvis, A.S., Hallin, S. (2004). Reassessing PCR primers targeting nirS, nirK and nosZ genes for community surveys of denitrifying bacteria with DGGE. *FEMS Microbiology Ecology, 49, 401-417.*

Vinson, D.S., Block, S.E., Crossey, L.J., Dahm, C.N. (2007). Biogeochemistry at the zone of intermittent saturation: Field-based study of the shallow alluvial aquifer, Rio Grande, New Mexico. *Geosphere, 3(5), 366-380.*

Wang, C., Schuppli, P.A., Ross, G.J. (1987). A comparison of hydroxylamine and ammonium oxalate solutions as extractants for Al, Fe and Si from spodosols and spodosol-like soils in Canada. *Geoderma, 40, 345-355.*

Ward, J.H. Jr. (1963). Hierarchical grouping to optimize an objective function. *Journal of the American Statistical Association, 58(301), 236-244.*

APPENDIX A FIGURES

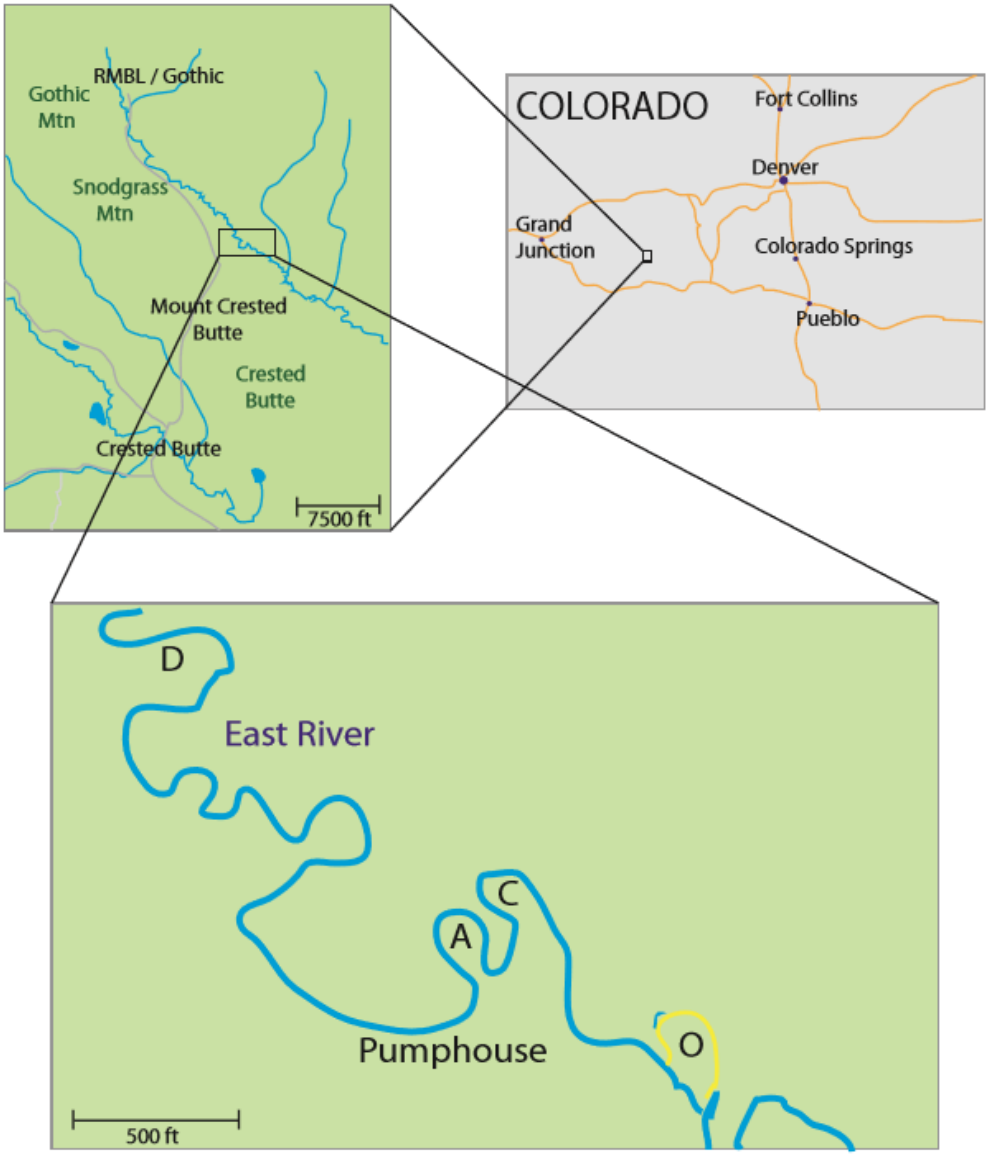

Figure 1. (a) Location map of East River field site near Crested Butte, Colorado and (b) locations of specific river meanders A, C, D and O.

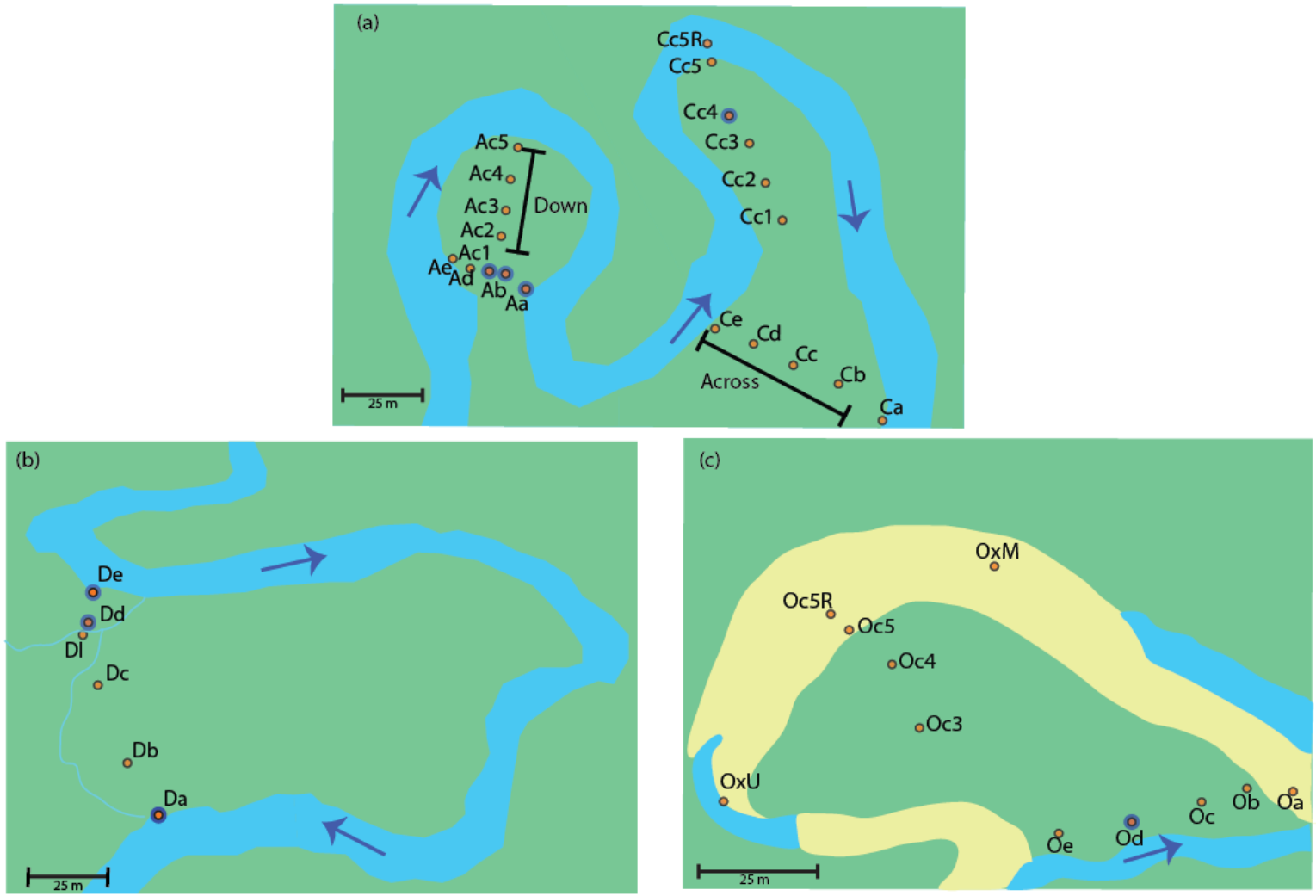

Figure 2. Sample locations on meanders A and C (a), D (b) and O (c). Deeper samples are indicated by purple circles. Flow direction of the East River is also indicated by arrows.

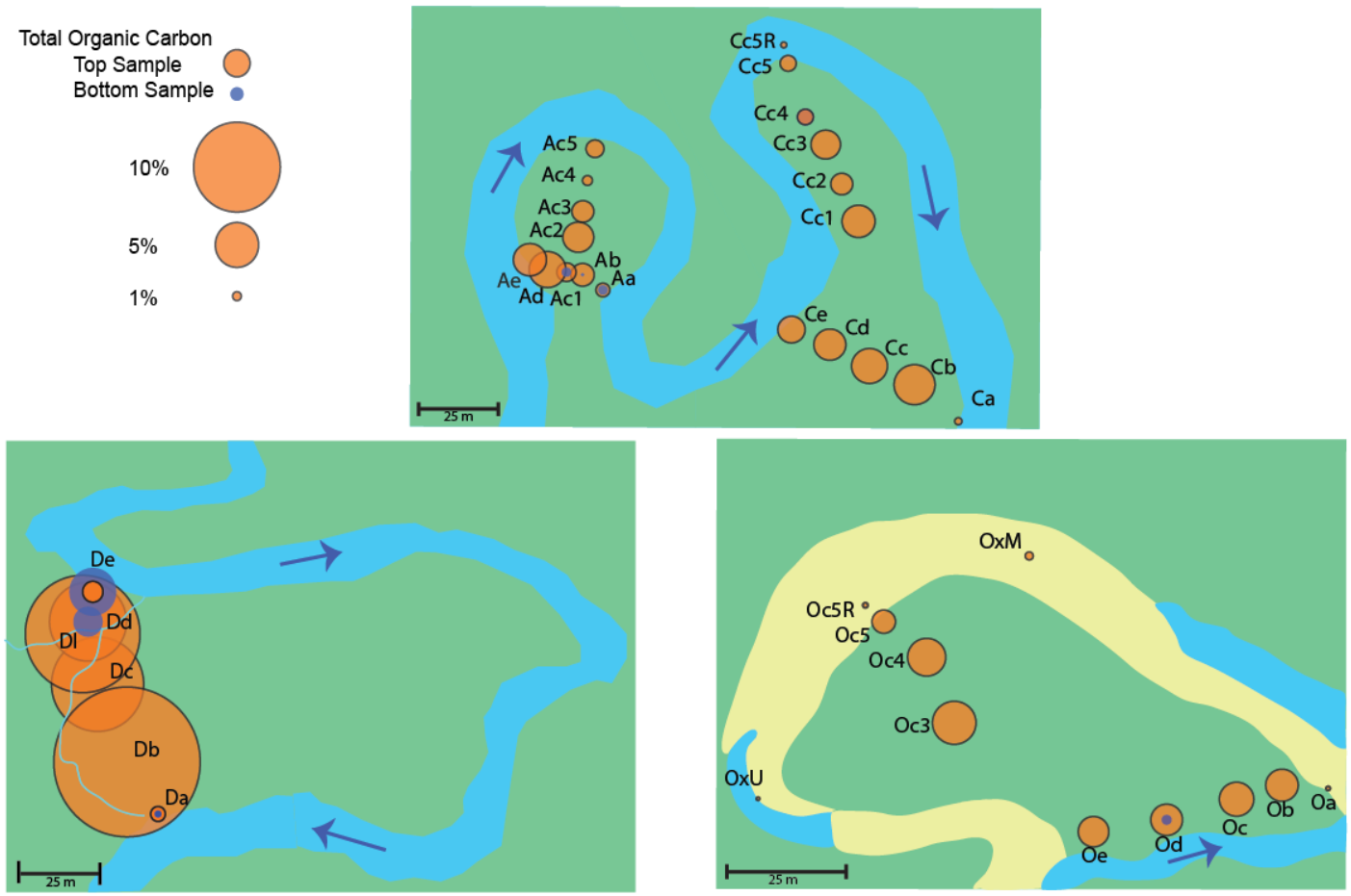

Figure 3. Distribution of TOC on meanders A, C, D and O shown with orange circles. Circle diameter is proportional to TOC percentage. Purple circles indicate deeper samples. TOC generally increased towards the center and at the neck of meanders A and C but there was no consistent relationship across the necks. The high organic content in meander D was likely a result of the wet, marshy neck of this meander. Like meanders A and C, the carbon increased toward the center of meander O but, in this case, it was lower along the cutoff meander neck. TOC within the dry mender bend was also relatively low.

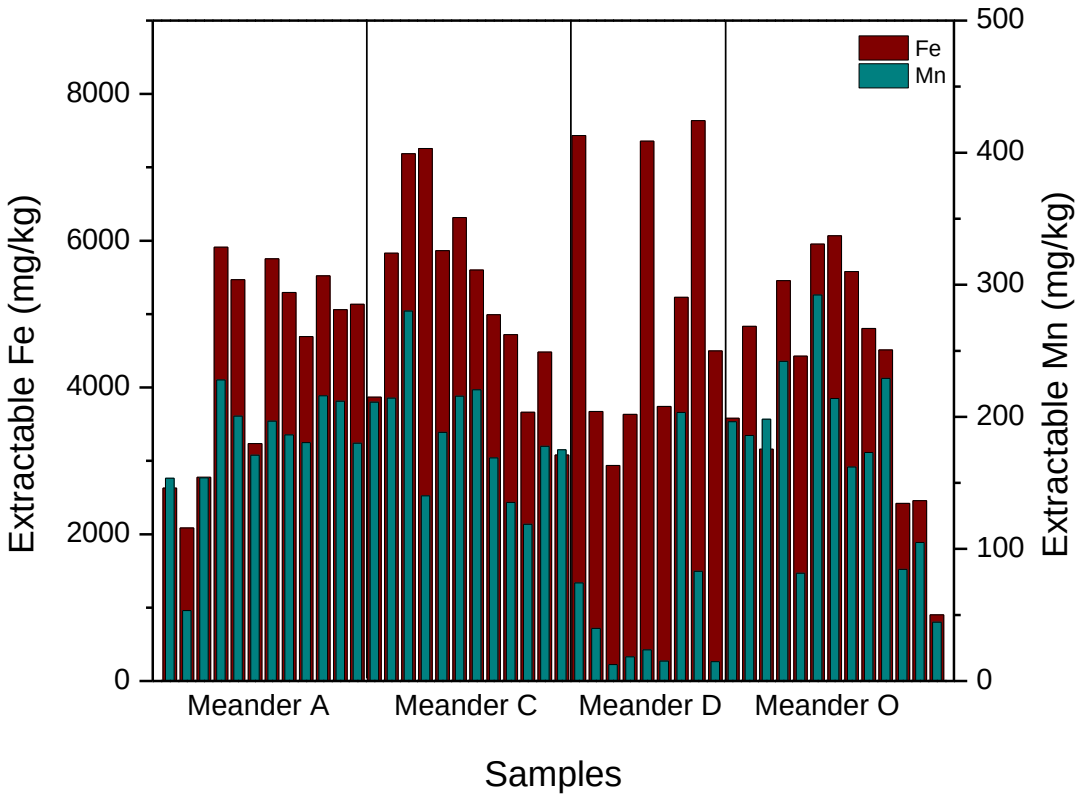

Figure 4. Average extractable iron and manganese extracted from the 0.5N HCl and 0.25N hydroxylamine in 0.5N HCl extractions.

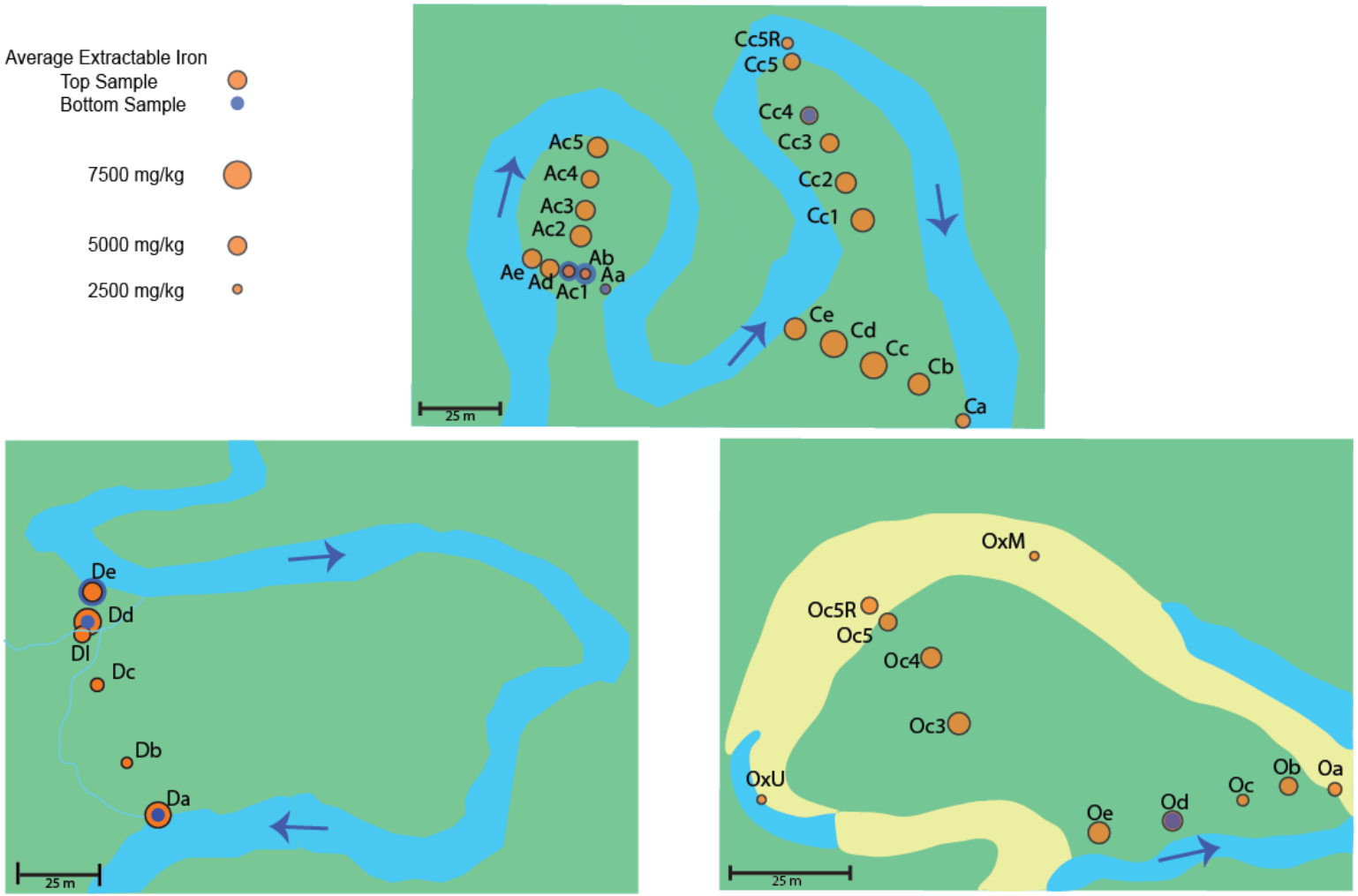

Figure 5. Distribution of average 0.5NHCl and 0.25N hydroxylamine in 0.5N HCl extractable iron on meanders A, C, D and O. Purple circles indicate deeper samples. Samples near the edges of the meanders or in the riverbed generally had less reducible iron than samples on the inner meanders.

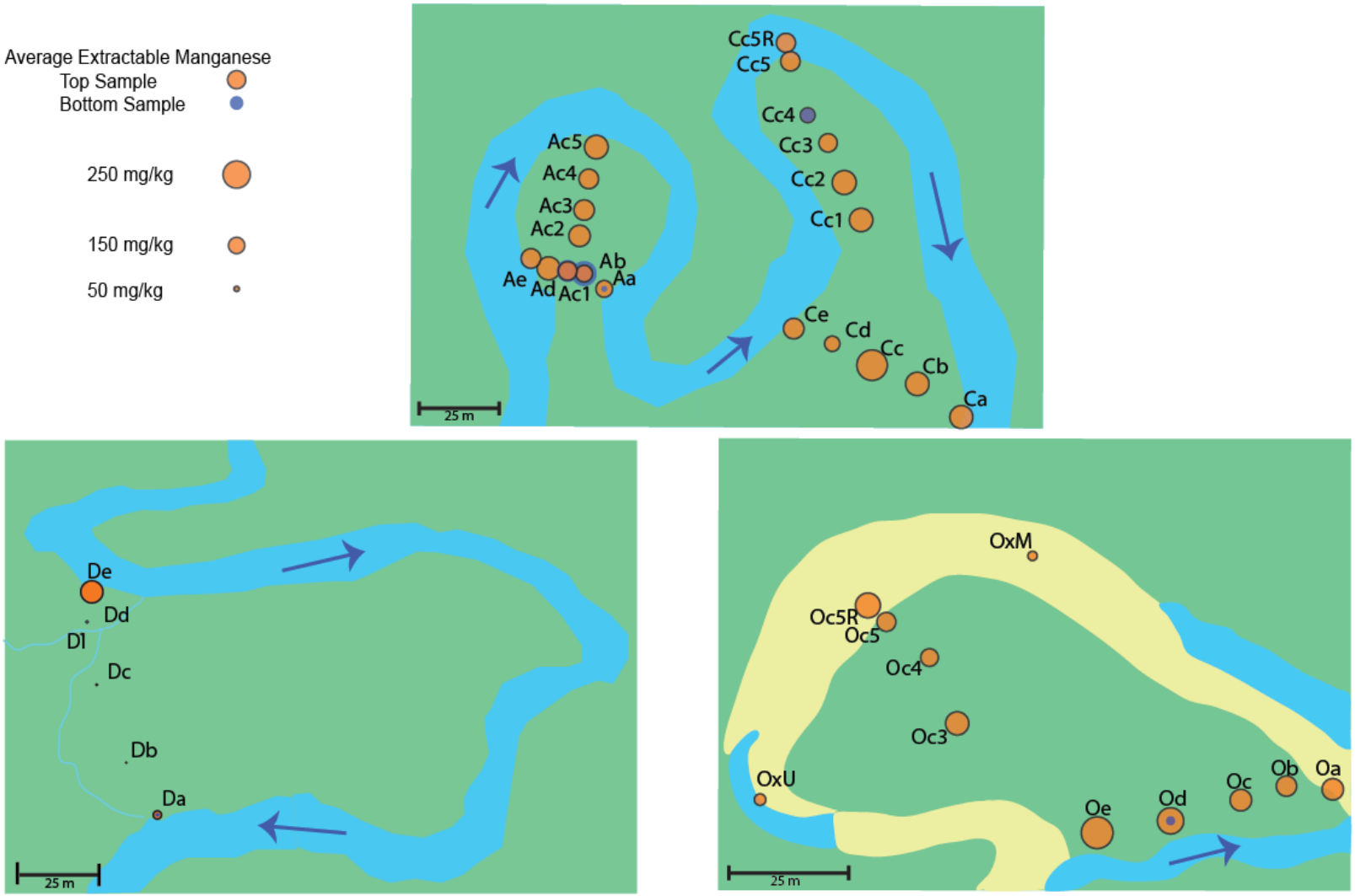

Figure 6. Distribution of average 0.5NHCl and 0.25N hydroxylamine in 0.5N HCl extractable manganese on meanders A, C, D and O. Purple circles indicate deeper samples.

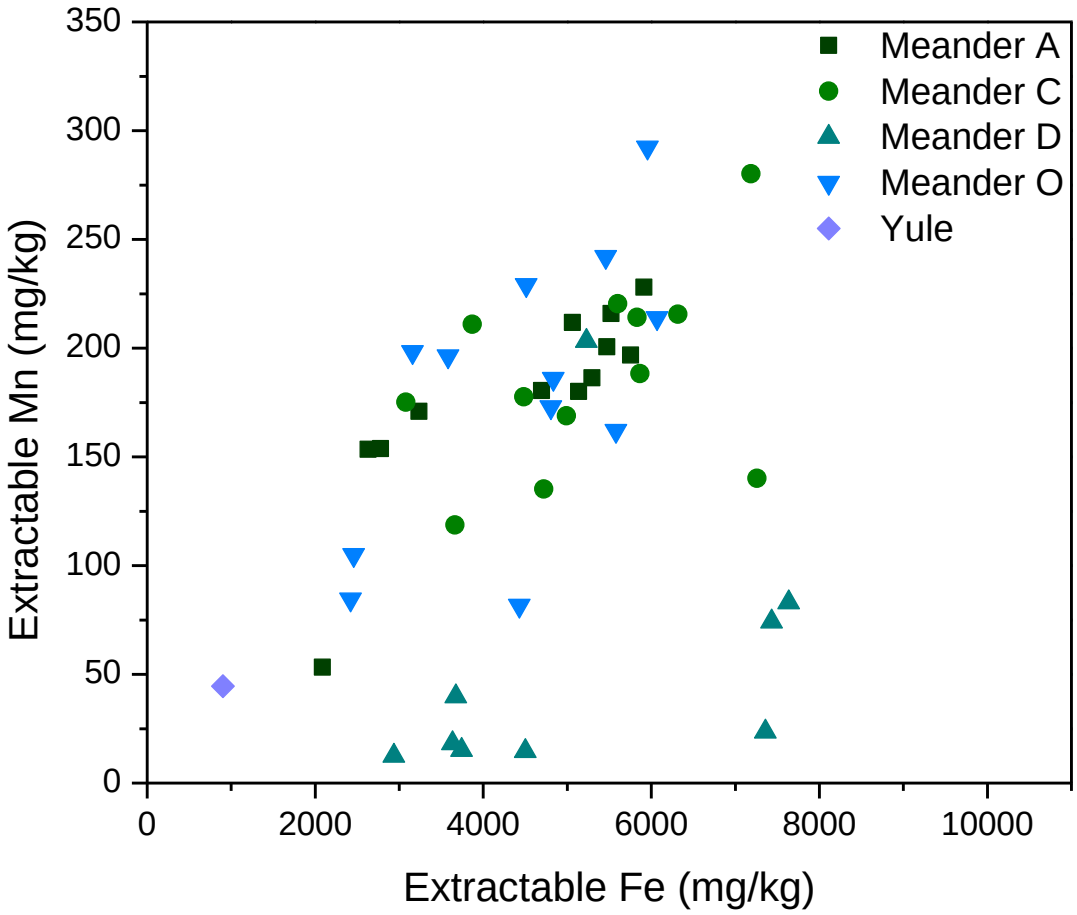

Figure 7. Average extractable manganese plotted versus average extractable iron with each meander shown in a different symbol. All meanders showed a general trend of increasing manganese concentrations with increasing iron concentrations.

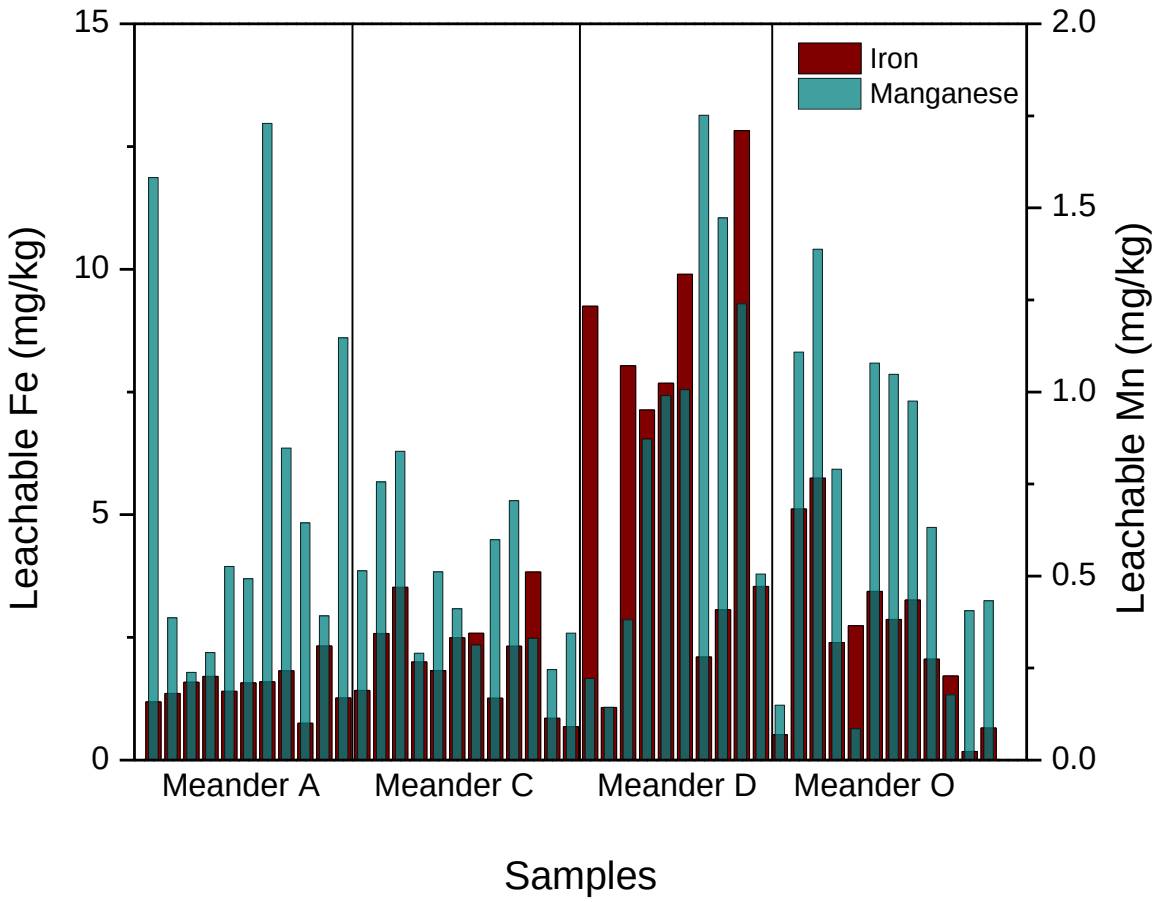

Figure 8. Iron and manganese leached during an 18 hour test with a pH 4.2 solution of 60:40 sulfuric:nitric acid.

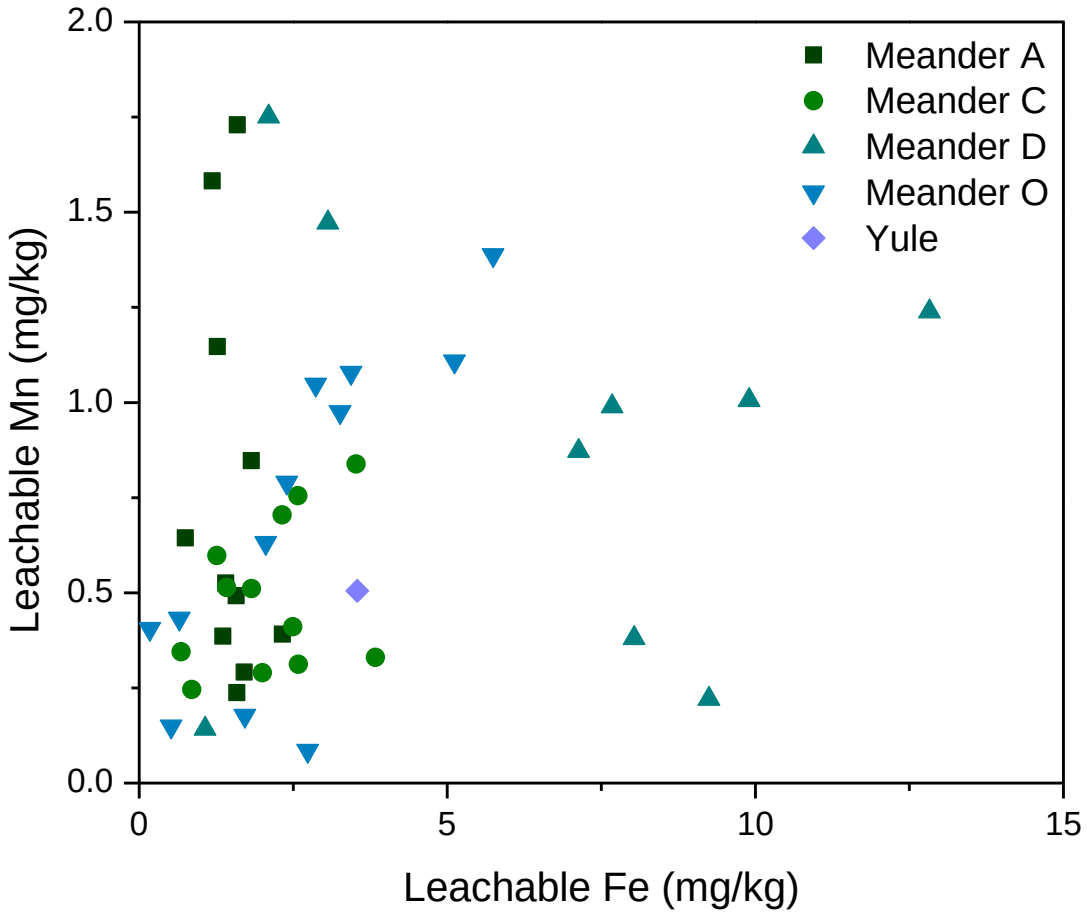

Figure 9. Leachable manganese plotted versus leachable Fe with each meander shown in a different symbol. Iron generally increased with manganese in meanders D and O while iron stayed fairly constant in meander A. Meander C metals had little variability.

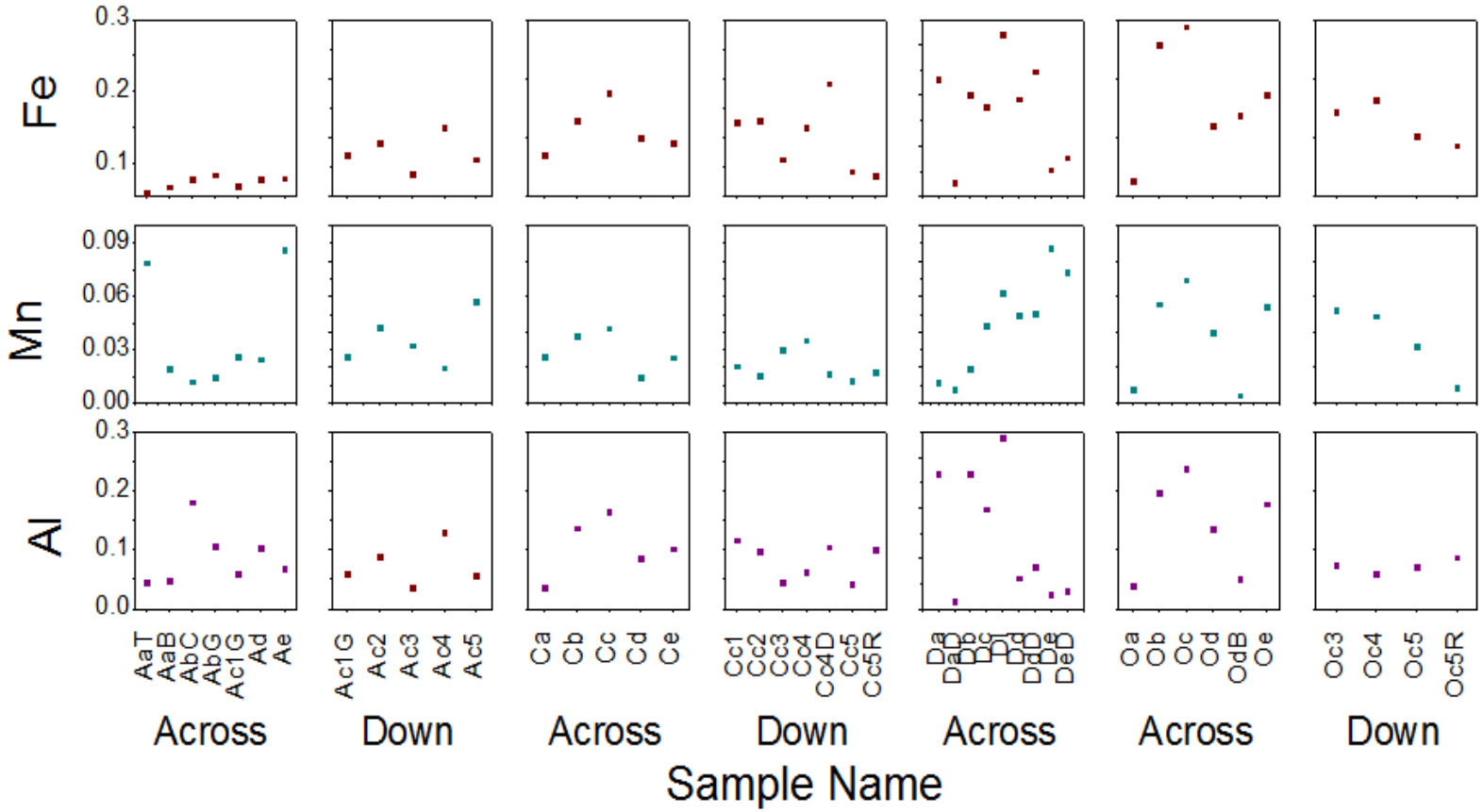

Figure 10. Distribution of leachable iron, manganese and aluminum across and down the center of meanders. Samples from rockier, Mancos-dominated materials tended to have less leachable metals.

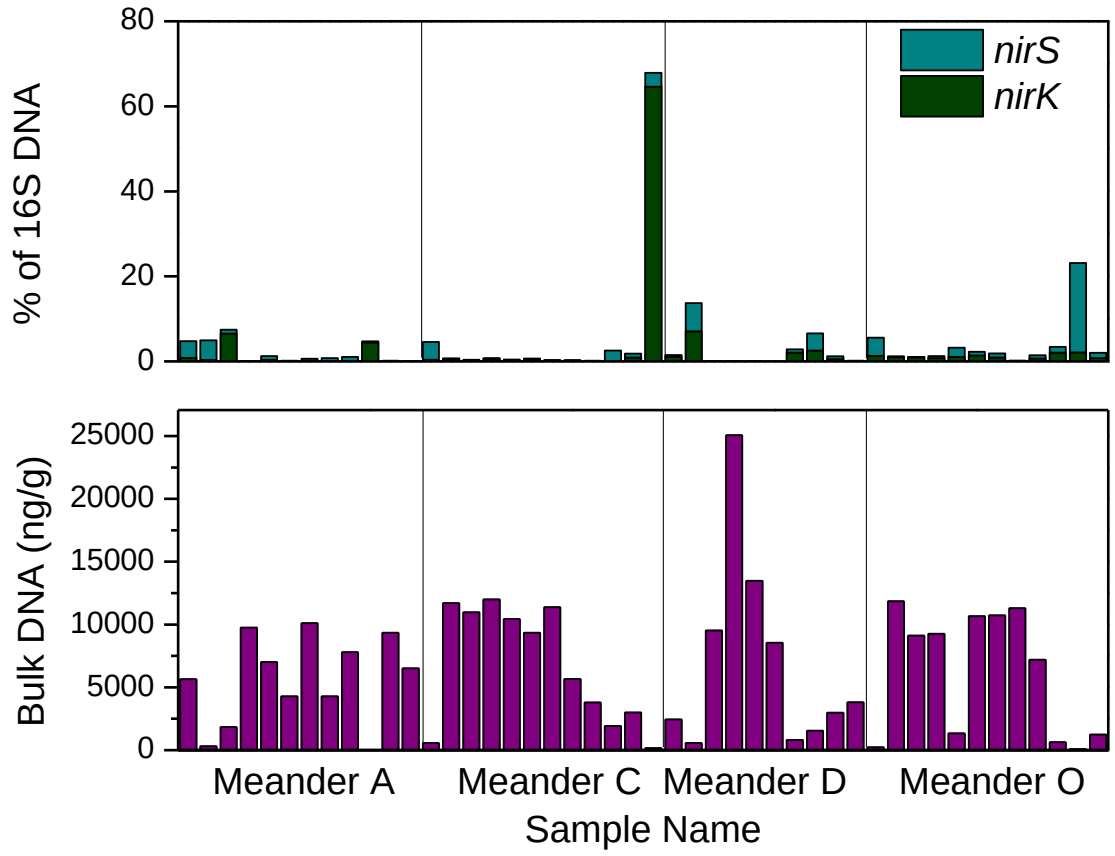

Figure 11. (a) Percentage of bacterial DNA (16S) represented by *nirK* and *nirS* denitrifying bacteria by meander and (b) bulk microbial DNA in ng of DNA per g of dry sediment by meander. The denitrifying bacteria did not dominate where microbial activity as measured by bulk DNA was highest.

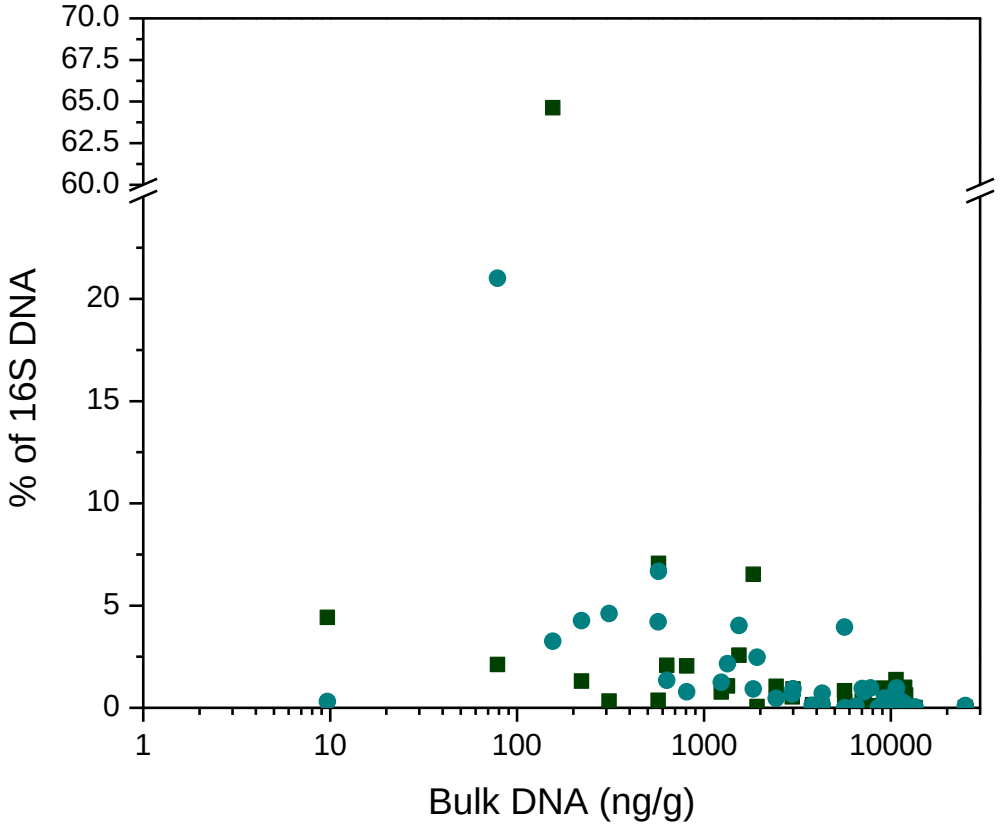

Figure 12. Percentage of bacterial DNA (16S) represented by *nirK* (black squares) and *nirS* (green circles) denitrifying bacteria as a function of bulk microbial DNA in ng of DNA per g of dry sediment by meander. The amount of denitrifying bacteria was not correlated to the amount of bulk microbial activity. The highest percentages of *nirK* and *nirS* were reported for samples Cc5R and OxU, respectively.

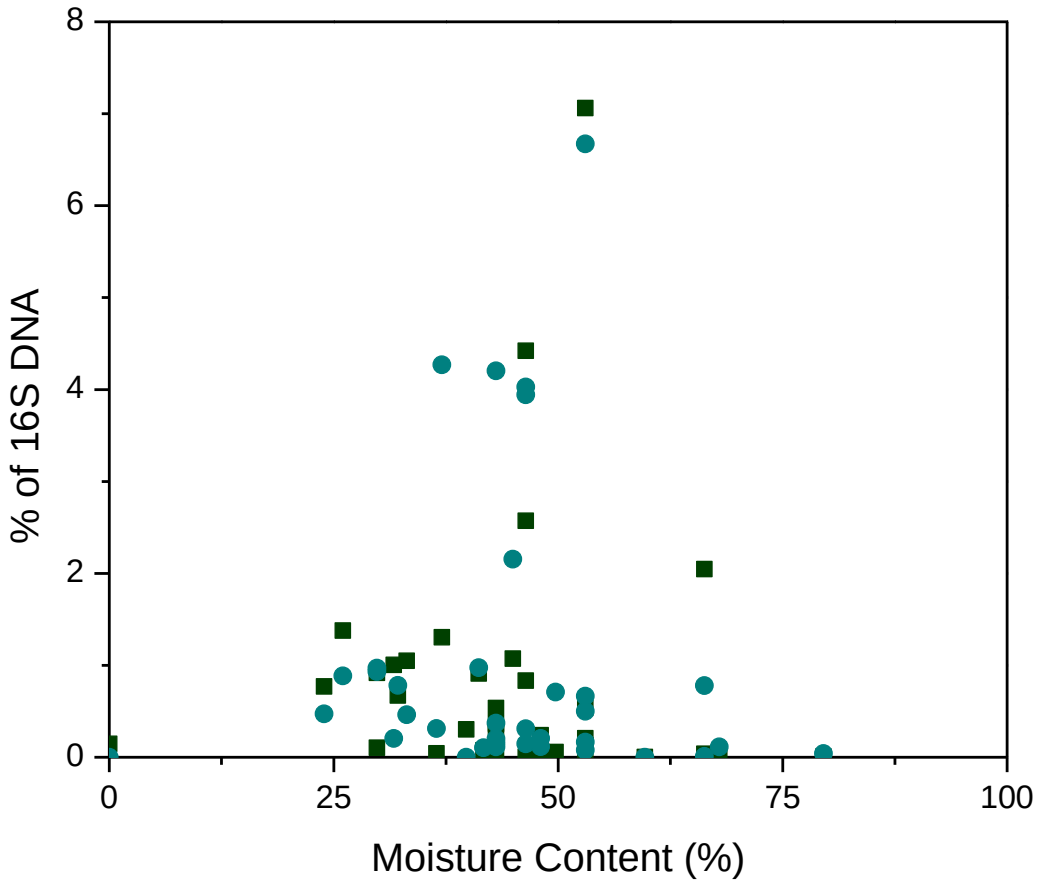

Figure 13. Percentage of bacterial DNA (16S) represented by *nirK* (black squares) and *nirS* (green circles) denitrifying bacteria as moisture content varied. Denitrifying bacteria appeared to prefer moisture content near 50%.

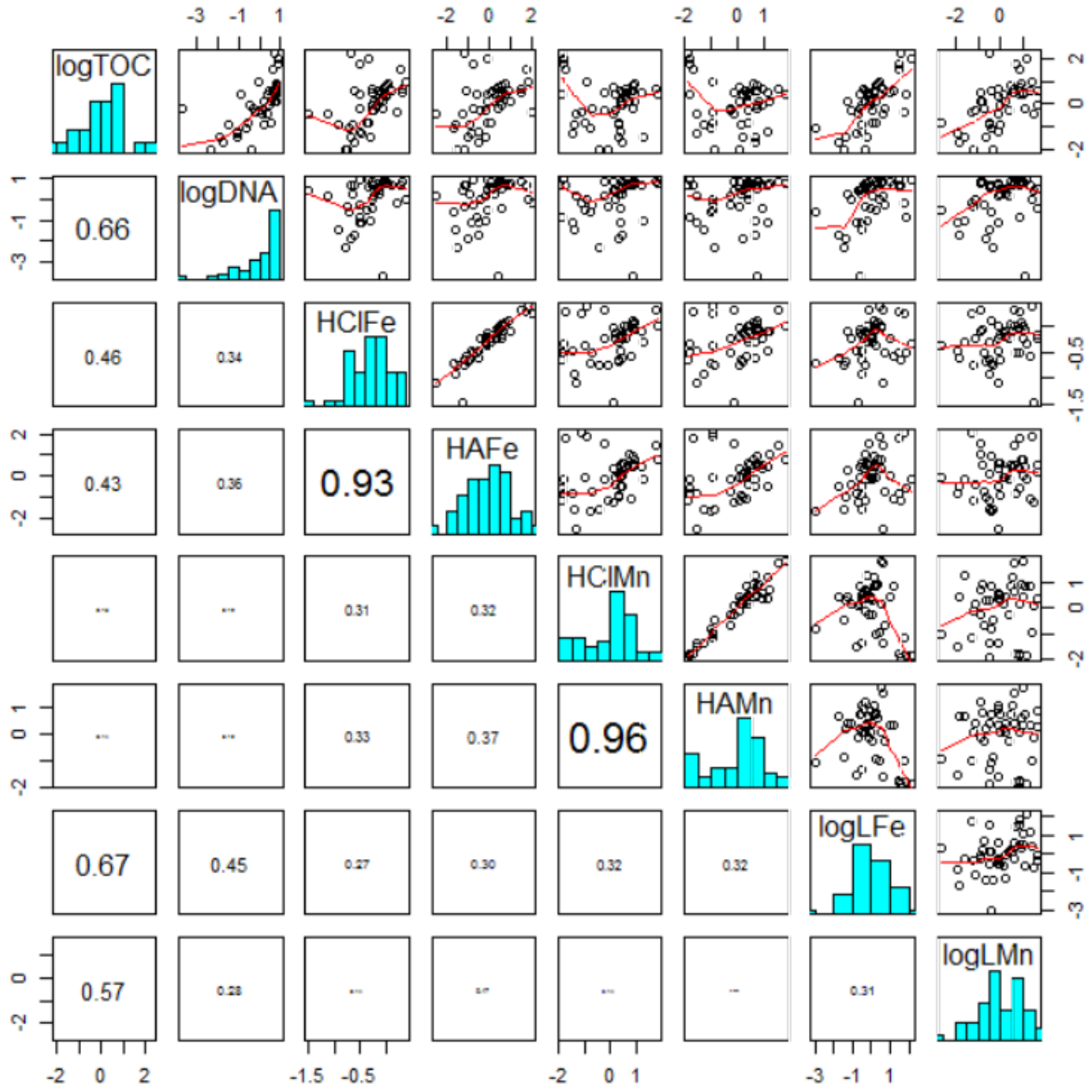

Figure 14. Pairwise correlations between soil parameters for all East River data. The upper triangle are pairwise scatter plots, the diagonal are histograms and the lower triangle are correlations with number size scaled according to strength of correlation.

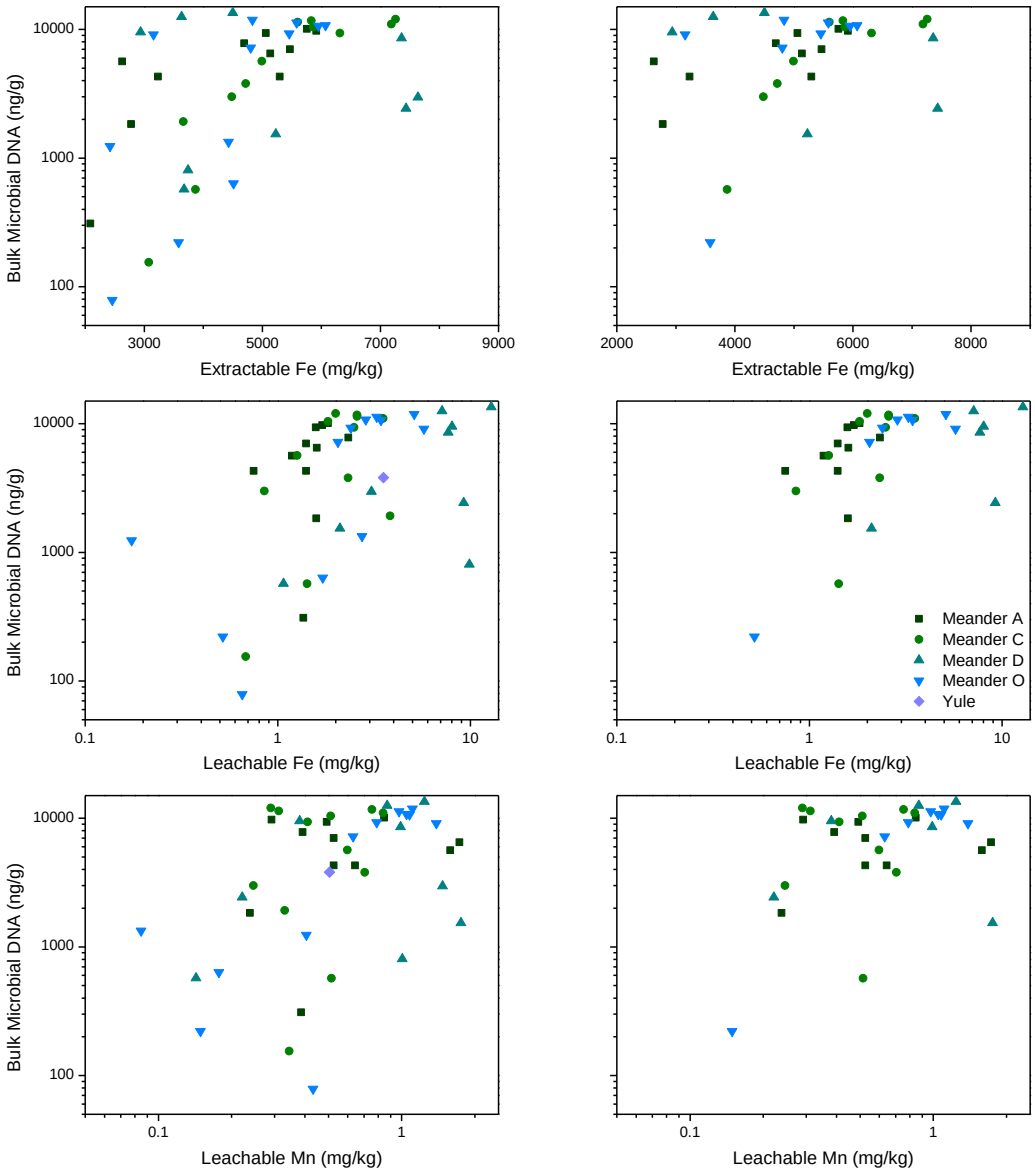

Figure 15. Plots of metals against DNA by meander. Plots on left include all East River samples, plots on right include only shallow meander samples.

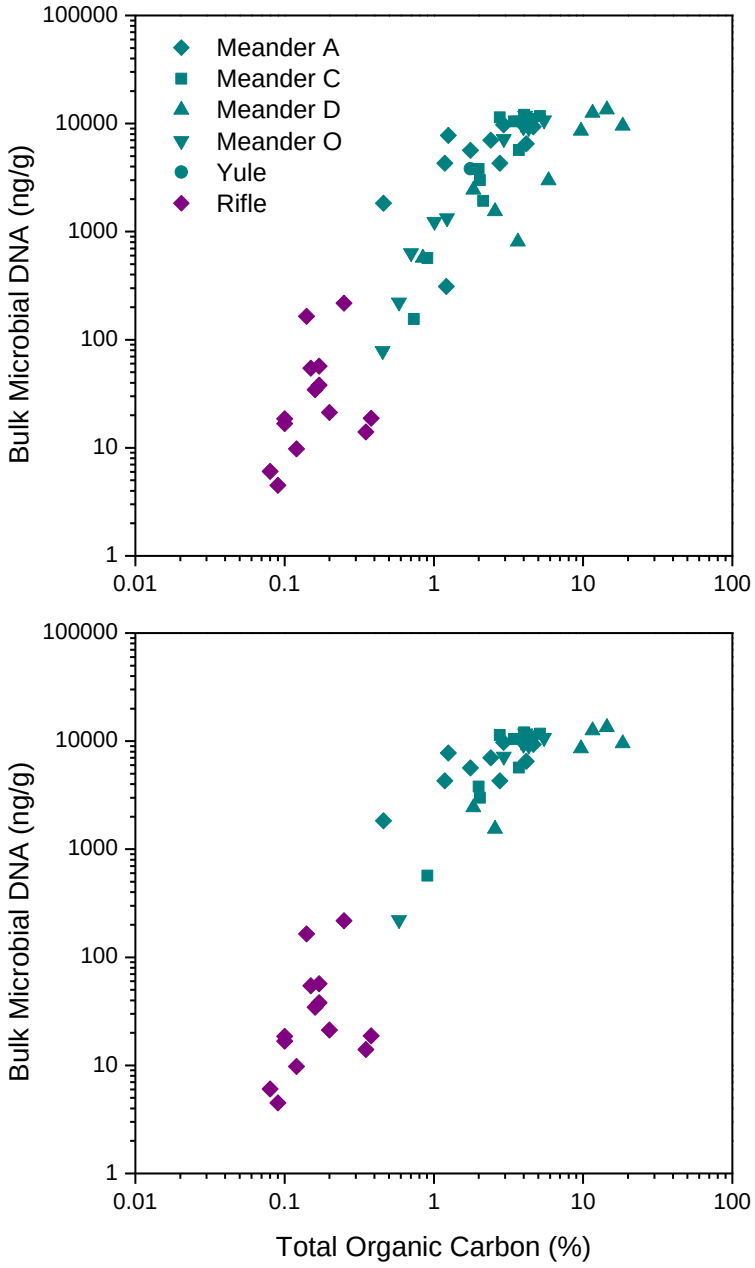

Figure 16. Bulk microbial DNA as a function of total organic carbon for (a) alluvial Rifle and all East River samples, (b) alluvial Rifle and shallow East River samples, with each meander distinguished by shape. The R-squared values of the linear relationships on log-transformed data were 0.84 and 0.87 for (a) and (b), respectively.

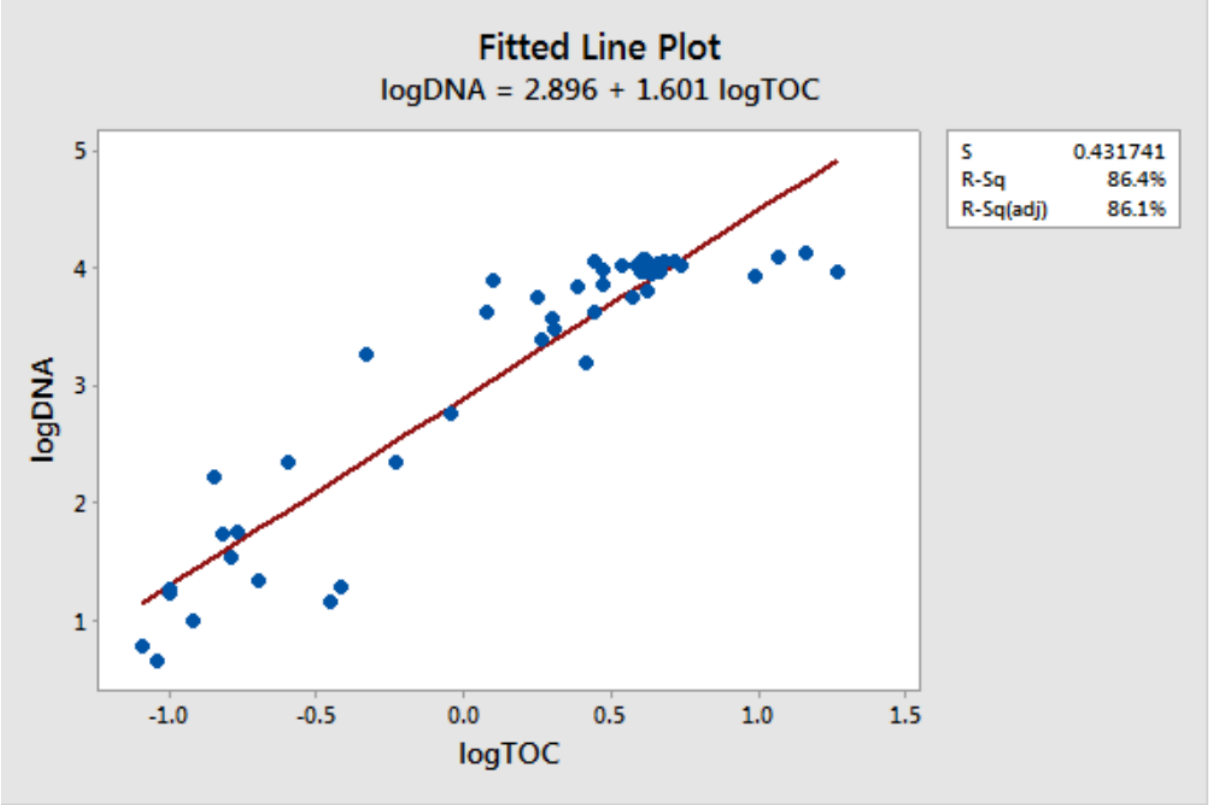

Figure 17. Linear regression of log-transformed and normalized TOC and bulk microbial DNA. The resulting R-squared value was 0.86.

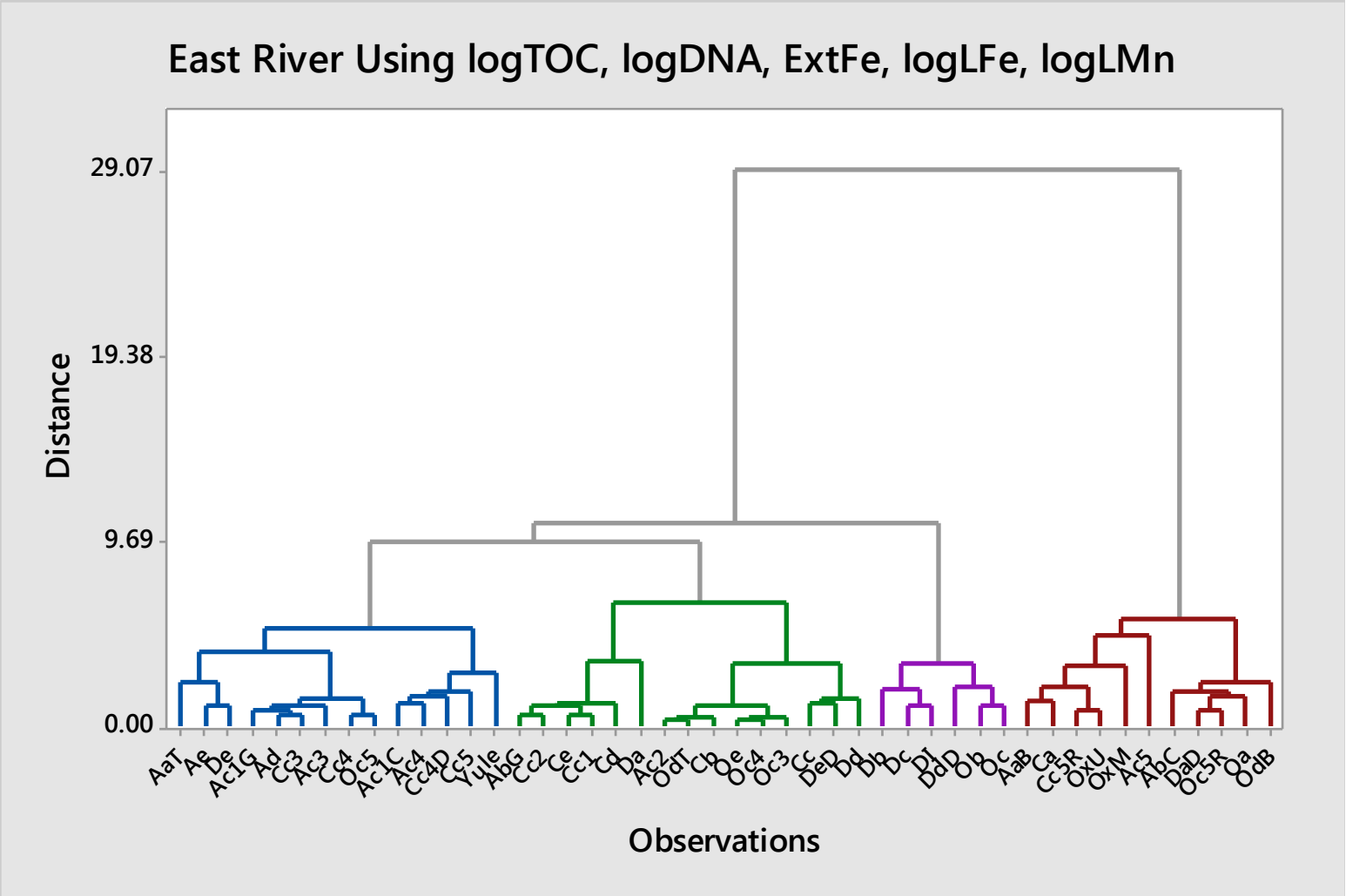

Figure 18. Dendrogram of statistical hierarchical clustering results using standardized average extractable iron and standardized log-transformed TOC, DNA, leached iron and leached manganese. Clustering was done using Ward linkages and Euclidean distances.

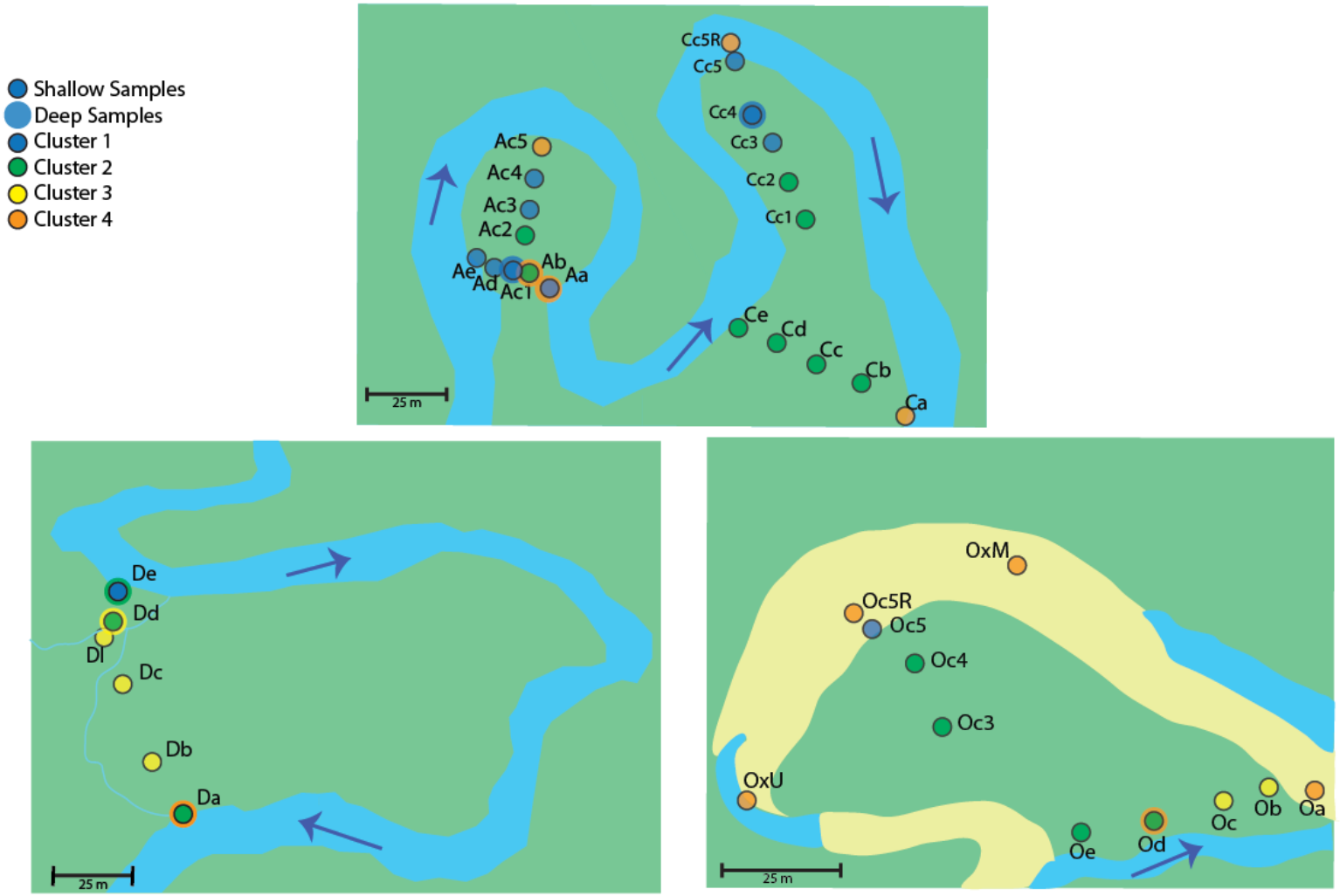

Figure 19. Sample-specific results of statistical hierarchical clustering analysis using standardized average extractable iron and standardized log-transformed TOC, DNA, leached iron and leached manganese. Cluster 1 mostly appeared on meander A and the toe of C, cluster 2 was mainly on meanders C and O, and cluster 3 was dominantly meander D. Cluster 4 samples were mainly along the riverbanks and oxbow bed.

APPENDIX B ADDITIONAL SOIL CHARACTERIZATION

B1 Methods

Methods associated with additional soil characterization investigate hydrologic and geochemical properties and distributions.

B1.1 Bulk Density and Moisture Content

Bulk density samples were placed in pie tins and dried in ovens at 110^{o}C or left covered on the counter until the mass was steady. This is generally according to ASTM Standard D2216-10 for evaluating moisture content (2010). The volume of the bulk density sampler was 302 cm^3 and bulk density and natural moisture content were calculated according to the following formulae:

$$\rho_b = \frac{M_{dry}}{V}$$

$$\theta = \frac{M_{wet} - M_{dry}}{V}\left(\frac{1\ cm^3}{1\ g}\right)$$

where ρ_b is bulk density, M_{dry} is the final mass of sediment, V is the volume of the bulk density sampler and M_{wet} is the initial mass. For stations with two bulk density samples rather than a bulk density and grab, each sample was sectioned into halves by mass and the bulk density procedure applied to only half of the volume.

B1.2 Size Characterization

Grain size was determined by hand-sieving dried bulk density samples. ASTM sieves 4, 10, 20, 50, 80, 100, 140 and 200 were used for initial grain size analyses. Aggregated soil was broken up using a mortar and pestle and mass of each sieve was recorded to 0.01 kg. It was then decided that separating into gravel, sands, silts and clays would be more appropriate for this study and the sieve suite was reduced to sizes 4, 50 and 200 only.

According to ASTM Standard D422-63 (2007), grains larger than the size 4 sieve were classified as gravel and those between size 4 and 50 sieves were considered sands (ASTM recommends the number 40 sieve for sands but using the number 50 sieve kept remaining samples consistent with initial grain sizes). Silts did not pass through the number 200 sieve and anything that did was considered clay-sized. There was some error involved in these measurements because of dust loss, precision of the scale, and soil aggregates.

B1.3 X-ray fluorescence (XRF) Spectrometry

XRF was applied to sediments and bedrock to approximate bulk elemental composition (inorganic). For sediment and soil samples a pellet method was applied to achieve a more accurately read flat, homogeneous surface. After drying and sieving (see Section 2.1), 5-7 g of dry sample was weighed. Using a mortar and pestle, sample was mixed with 3-4 drops of 10% polyvinyl solution until a sticky consistency resulted. The mixture was placed in a pellet die set and approximately 1000 lbs of pressure was applied for 5 minutes. The pellet was then removed from the die set and stored in a petri dish until analysis.

XRF was also applied to a river-exposed outcrop of Mancos shale adjacent to Seep 2 in June 2014. Stations were chosen based on accessibility and flat surfaces where more accurate readings were possible. A handheld XRF analyzer (Thermo Scientific Nitron XL3t) was used to analyze both outcrop and pellet samples. A system check and calibration check was conducted before each use. All samples were analyzed using the TestAllGeo setting for a 3 minute exposure.

B1.4 Fourier Transform Infrared Spectroscopy (FTIR)

Organic functional groups present in solid samples were characterized using Fourier Transform Infrared Spectroscopy (FTIR). This method analyzes vibrational spectra using the Fourier Transform to classify types of bonds in a sample (Stone et al., 2001). Spectra were collected with a Nicolet Nexus 470 FTIR (Thermo Scientific, USA) using an attenuated total reflectance crystal. Samples were first ground into a powder and large grains were removed.

Each scan used the absorption range of 4000 to 650 cm^{-1} at a 4 cm^{-1} resolution. Integration of 256 scans using Omnic software (Thermo Scientific, USA) produced a final

spectra for each sample. A background spectra was collected approximately every hour and the software subtracted this automatically from sample spectra to remove background influence. Background spectra were monitored and did not change substantially throughout the experiment. The absorption spectra were analyzed by identifying peaks based on tabulated wavenumbers from Stone et al. (2001) and Kloss et al. (2012).

B1.5 Ordinary Spatial Kriging of Total Organic Carbon and HCl Extractable Iron Data

Ordinary spatial kriging was applied to the TOC and HCl extractable iron data to get a better approximation of the spatial distribution. Note that the sample sizes were far less than usually used for this type of analysis and results should be interpreted as a general approximation; not a quantitative prediction. Variograms for HCl extractable manganese and leachable metals did not produce realistic results and therefore kriging was not applied to these datasets. For meander D there were not enough sample stations to perform an analysis. In addition, there was a large scale trend for meanders A and C. Normally this would be analyzed through the use of universal kriging which removes the effect of a spatially varying mean. However, in this case it was the large-scale trend that was of interest because there was insufficient data to recognize smaller scale trends.

The open source statistical software, R, was used to analyze TOC and extractable iron data. The domain was defined using the 'ripras' function which gives the Ripley-Rasson estimate of a domain given a set of spatial coordinates (Ripley & Rasson, 1977). This function works by first approximating a convex hull from the outermost points and then scaling up the resulting polygon. A polygonal domain created using this method encompasses all of the data points without including too much surrounding area where variability would be high.

Data was plotted using the last three digits of the coordinates. Variograms for each meander were chosen by adjusting cutoff and bin width until a maximized number of lag distances somewhat leveled off. These variogram fits did not meet the general rules of thumb and the resulting nugget, sill and range estimates are therefore not to be considered robust. Grid development began with a 100 by 100 grid over the entire rectangle encompassing the polygonal domain then only the cells within the Ripley-Rasson domain were selected. The ordinary kriging

function was applied to the resulting grid to predict TOC and HCl extractable iron concentrations throughout the domain.

B2 Results and Discussion

Characterization of additional hydrologic and geochemical properties resulted in more detailed understanding of the subsurface.

B2.1 Bulk Density and Moisture Content

Overall average moisture content including all samples was 44% but this included sample D-Inner with a moisture content of 80% and Yule with a moisture content of 0% (Figure B1). Similarly, bulk density varied from 0.27 to 2.51 g/cm^3 with an average of 1.21 g/cm^3. Moisture content strongly affected bulk density of the samples above 40 or 50%, causing bulk densities of less than 1 g/cm^3 (Figure B2). All samples from Meander D except for Da, DaD and De fell into this category and as a result had low bulk densities. Excluding these moisture-influenced samples, the bulk density of shoreline stations averaged slightly higher than inner samples (1.46 vs 1.25 g/cm^3). This may have been caused by rockier shorelines. Average moisture contents for river-adjacent and inner samples were fairly consistent, differing by only 10%. There was a linear trend between moisture content and TOC with an R^2 of 0.57 for shallow East River samples (Figure B3).

B2.2 Size Characterization

Size characterization was completed using dry sieving which likely introduced quite a bit of error. This is particularly true for fine materials which could be lost as dust or could aggregate and be reported as larger than their actual grain size. Overall, samples were dominantly sand with the exception of silty samples Aa and De (Figure B4). Average gravel content was 5% and most samples contained no gravel. Samples were on average 60% sand, 28% silt and 7% clay. Samples on the perimeter of meanders tended to have more gravel but also more silt and clay than samples inside meanders. This is probably due to varying size of material deposited on the river's edge throughout different seasons as water level changes. Though grain size was not tested for meander O, many of the samples near the cutoff neck contained more gravel than other

meanders, suggesting deposition during a high-flow event, perhaps before the oxbow was fully cut off.

B2.3 X-ray fluorescence (XRF) Spectrometry

Major elements in the soils were overall fairly consistent (Figure B5, Table D6). Potassium, magnesium and aluminum all had standard deviations of less than1% by weight. Only sample Oc5R had substantially less aluminum. Calcium was slightly more irregular and tended to be higher on the outer edges of meanders. The percentage of calcium was very low in meander D where the average was less than half that of the population. Silica was also variable but was only noticeably low in samples Db, Dc, Dd, DI, Ob and Oc5R. These samples generally had higher organic carbon concentrations (except for sample Oc5R) which reduced influence of the smaller mineral fraction.

Trace elements had lower weight percentages but were overall more variable with the exception of chromium, rubidium and strontium concentrations which were fairly consistent (Figure B6, Table D7). Lead varied somewhat in meanders A and C while meander D had inconsistent barium concentrations. Vanadium concentrations were somewhat lower in meander O. Uranium was quite variable but this was most likely just a reflection of low concentrations. Phosphorus was the most irregular of the trace elements and tended to be lower towards edges of meanders and in the oxbow riverbed. Phosphorus concentrations were also low in the center of meander C but high in the center of meander A. Samples Dd and Yule were particularly high in phosphorus, reflecting high native concentrations in the underlying Mancos shale. These samples showed, however, that high phosphorus concentrations generally got diluted out as sediment was redistributed throughout the watershed.

Iron was the dominant redox element in this system and was particularly variable in meander D where the maximum iron concentration was more than twice the minimum (Figure B7, Table D8). Iron was almost completely consistent along the center of meanders though was perhaps slightly higher at the meander neck. There was no consistent pattern across meander necks but there was variability. In particular, sample Dd had very high iron and also high phosphorus. Manganese concentrations were much lower and less irregular. The average concentration of manganese in meander D was half that of other meanders. Sulfur concentrations

varied considerably, especially in meanders D and O where the concentration went from near 0 in some samples to nearly 1%. The Mancos exposure from the dry meander bend was particularly high in sulfur. In meander D, sulfur concentrations were distinctly lower in samples which border the river.

The Mancos Shale outcrop was far more variable than sediment and soil samples. For major elements (Figure B8, Table D9) aluminum, potassium and silica were particularly high at stations Ma and Md while calcium was higher at stations with low silica. This may mark a difference between more feldspar-rich areas and calcium-rich areas. Overall, major elements in the outcrop were generally of lower weight percent than major elements in soils and sediments. Similarly, the overall amount of trace elements was low (Figure B8, Table D9). Stations Ma, Md and Mg which were also silica rich had much higher proportions of phosphorus than soil and sediment samples. Strontium and vanadium were also more prevalent elements for the outcrop while barium had relatively low concentrations. In terms of redox elements, it was generally sulfur that dominated in the outcrop rather than iron like in the soils and sediments (Figure B8, Table C9). Silica rich samples were slightly higher in iron and lower in sulfur than the calcium rich samples. Overall weight percent of redox elements in the outcrop was also much higher (up to twice as high) than for the soils and sediments.

Overall XRF results suggest that elements are more evenly spread during present deposition and formation than they were during the rock deposition. Outcrop XRF results suggest that weathered bedrock in the region is quite variable in composition and may contain both a feldspar-iron rich facies with high phosphorus as well as carbonate-sulfur rich facies. Variability may have been caused by vertical layering of rock types as stations were from different heights on the outcrop. Localized areas of limestone as well as calcite cementation have been reported in the Mancos Shale (Morrison et al., 2012). The two chemical compositions could also represent the calcareous Niobrara Member and the non-calcareous Juana Lopez member of the Mancos Shale (Tuttle et al., 2014). In addition, sulfur may not have shown up in the meander deposition either: a) because it was being used in microbial processes or b) it was oxidized to sulfate and was carried by the river water and not deposited, a similar trend to the mobile reduced iron. This corresponds somewhat to the exposed Mancos shale in the oxbow.

B2.4 Fourier Transform Infrared Spectroscopy (FTIR)

Fourier Transform Infrared Spectroscopy (FTIR) results indicated that certain signals were consistent for nearly all samples while others dominated in specific locations (Figure B9). Mineral and silicate signals dominate for all samples except Oc3 which did not show a signal at any point. This sample may have made improper contact with the crystal for analysis. A signal for cellulose was also evident in all samples at 895-900 cm^{-1} and 1160 cm^{-1} though only certain samples (mostly the marshy northern section of meander D and a few samples in meander O) responded at another wavenumber for cellulose which could also indicate CO polysaccharides. This could indicate that it was the polysaccharides causing the signal for the specific samples.

An aromatic C-H bond was evident in many near-bank samples on meanders A and C. It was also found in De and DeD as well as some samples in meander O, notably the oxbow bend. A signal for aliphatics, aromatic rings or lignin was seen in most samples except some interior stations. It was strongest in samples close to or in the banks, excluding OdB. The signal for double bonded carbon to O, OH or OO^{-}, or alternatively amides or double-bonded carbon rings was particularly strong in Ad, Db and DI. It was also found in Yule and many other samples but tended to be weaker towards the banks. In addition, a wide OH^{-} signal was found in Ad, Ac1C, Ac2, Cc4D, Cc3, Db and DI in particular though was also weakly in several more samples. Overall, strong signals in samples such as Db and DI were expected because of their high organic content. Surprisingly, several lower carbon samples such as Ac5, Cc4D, Oa and Oc5R also had certain strong signals. Results suggest that aromatics tended to occur closer to meander banks while double-bonded carbon organics dominated the interiors of meander where total organic carbon was higher. This chemical heterogeneity may also create heterogeneous microbial community distributions because different organisms are responsible for oxidation of different forms of organic matter (Lovley et al., 1991).

B2.5 Ordinary Spatial Kriging of Total Organic Carbon and HCl Extractable Iron Data

As explained in the methods section, results of the ordinary kriging analysis are only an approximation as there was insufficient data to reliably make predictions. General results, however, still showed an interesting large-scale trend (Figure B10). Meanders A, C and O all had low TOC nearest the toe of the meander. Meanders A and C had signals of high organic carbon

in the upstream portions of the meanders. Meander O had highest carbon closer to the center of the meander. The coarse material at the meander toes was presumably from more recent deposition of coarse material. The meander neck differences may be related to the activity of the meanders. Though meanders C and O were of similar shape, meander C had an active bank in the high carbon area whereas meander O's upstream bank was only touching water during the flood stage. This bank on meander O was high and collapsing, which may be attributed to having erosive forces cutting it at high flow and no longer receiving the fine grained deposition at low flow. On meanders A and C, during low flow, the river may be depositing fine grained materials and carbon at the neck before circling the meander. On the downstream side, erosion and coarse deposition seemed to dominate. Note that kriging of meander C did not show the same cross-sectional trend as the visual observation in Figure 7. The sample at station Ca may have had disproportionate influence on the kriging. Another interesting aspect of meander O was that the neck of the meander no longer had high TOC because the neck itself was near a steep bank and was experiencing erosion and potentially leaching of carbon. Instead, the highest carbon was found closest to the center of the meander and away from the influence of the river. Note that Jackson and Caldwell (1993) only found autocorrelation of soil organic matter at meter and smaller spatial scales on a tussocky field. However, an analysis of total carbon on meander O using 33 samples yielded a definitive spatial correlation across the meander at the East River site. This may be due to the less disturbed (by macrofauna) nature of the site and a greater consistency of grasses though shrubs were still present.

Kriging of HCl extractable iron produced approximate distributions of crystalline Fe(II) across meanders A, C and O (Figure B11). Meander A had very consistent iron across almost the entire meander except on the downstream bank where it was low. Meander C had highest iron across the main portion of the neck and extending towards the toe. The downstream bank and toe of the meander had lower extractable Fe. Meander O had an iron hotspot near the central-right area of the meander and extending to the upstream cutoff bank. Once again, the downstream bank was low, as was the dry meander bed. The toe of meander O was not as distinctly low in Fe as for the active meanders A and C.

B3 References for Appendix B

ASTM D422-63 (2007)e2. Standard test method for particle-size analysis of soils. ASTM International. West Conshohocken, PA.

ASTM D2216-10 (2010). Standard test methods for laboratory determination of water (moisture) content of soil and rock by mass. ASTM International. West Conshohocken, PA.

Kloss, S., Zehetner, F., Dellantonio, A., Hamid, R., Ottner, F., Liedtke, V., Schwanninger, M., Gerzabek, M.H., Soja, G. (2011). Characterization of slow pyrolysis biochars: Effects of feedstocks and pyrolysis temperature on biochar properties. *Journal of Environmental Quality, 41(4), 990-1000.*

Morrison, S.J., Goodknight, C.S., Tigar, A.D., Bush, R.P., Gil, A. (2012). Naturally occurring contamination in the Mancos Shale. *Environmental Science and Technology, 46, 1379-1387.*

Ripley, R.D., Rasson, J.P. (1977). Finding the Edge of a Poisson Forest. *Journal of Applied Probability, 14, 483-491.*

Stone, A.G., Traina, S.J., Hoitink, H.A.J. (2001). Particulate organic matter composition and pythium damping-off of cucumber. *Soil Science Society of America Journal, 65, 761-770.*

Tuttle, M.L.W., Fahy, J.W., Elliott, J.G., Grauch, R.I., Stillings, L.L. (2014). Contaminants from Cretaceous black shale: I. Natural weathering processes controlling contaminant cycling in Mancos Shale, southwestern United States, with emphasis on salinity and selenium. *Applied Geochemistry, 46, 57-71.*

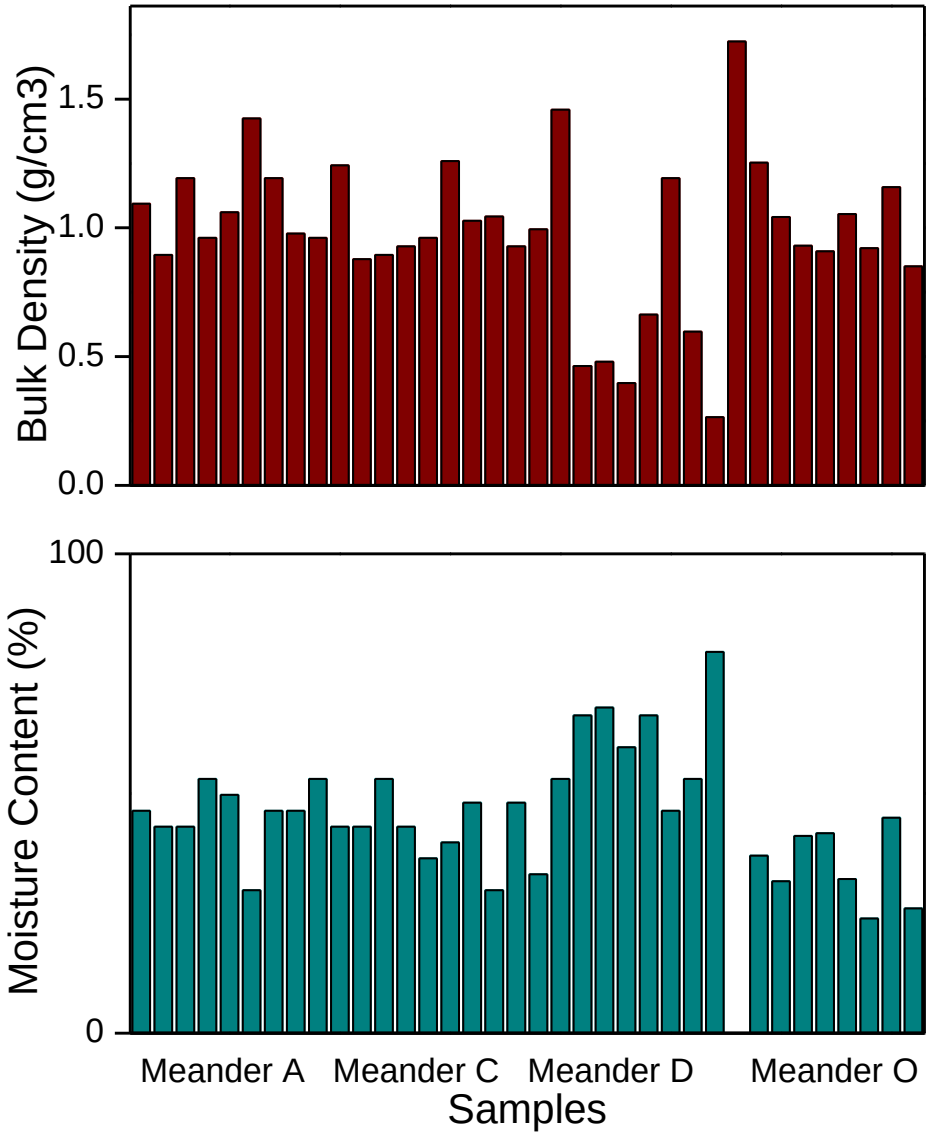

Figure B1. Bulk density of sediment in g per cubic centimeter and natural moisture content percentage by meander. Note that meander D had distinctly higher moisture content and low bulk density.

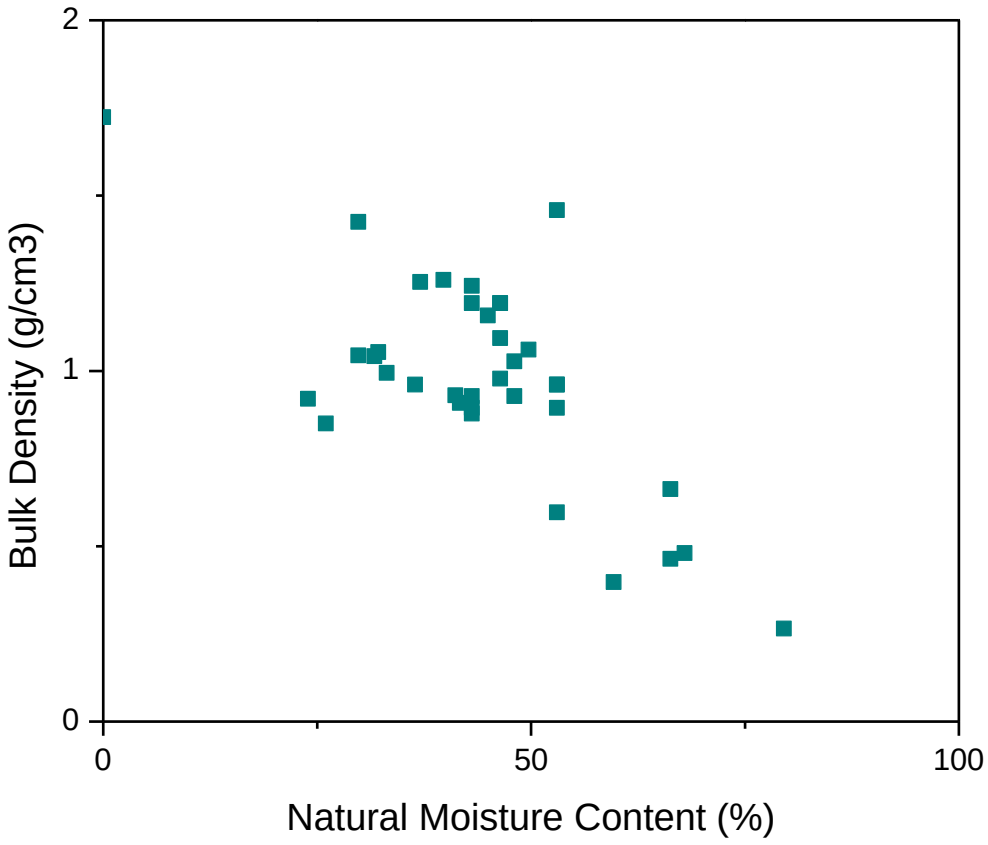

Figure B2. Bulk density of sediment as a function of natural moisture content. Moisture content had a strong influence at percentages above approximately 50%.

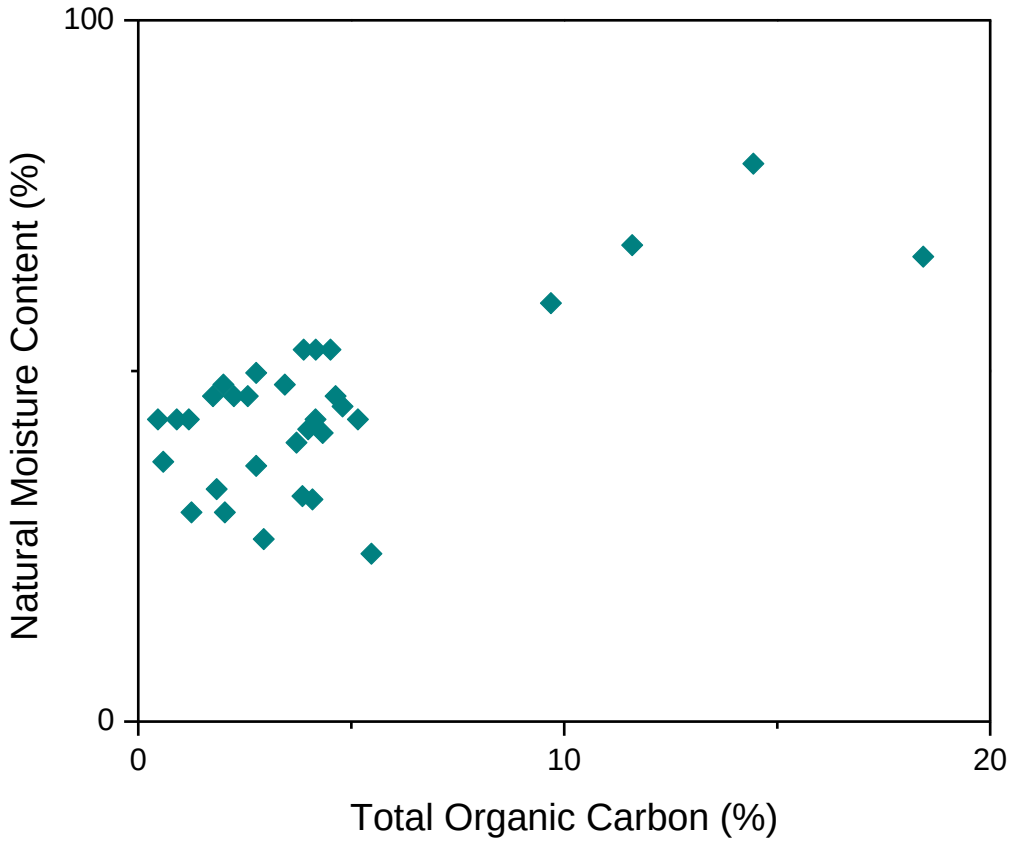

Figure B3. Natural moisture content as a function of total organic carbon. The high carbon samples in meander D were also those with exceptionally high moisture content.

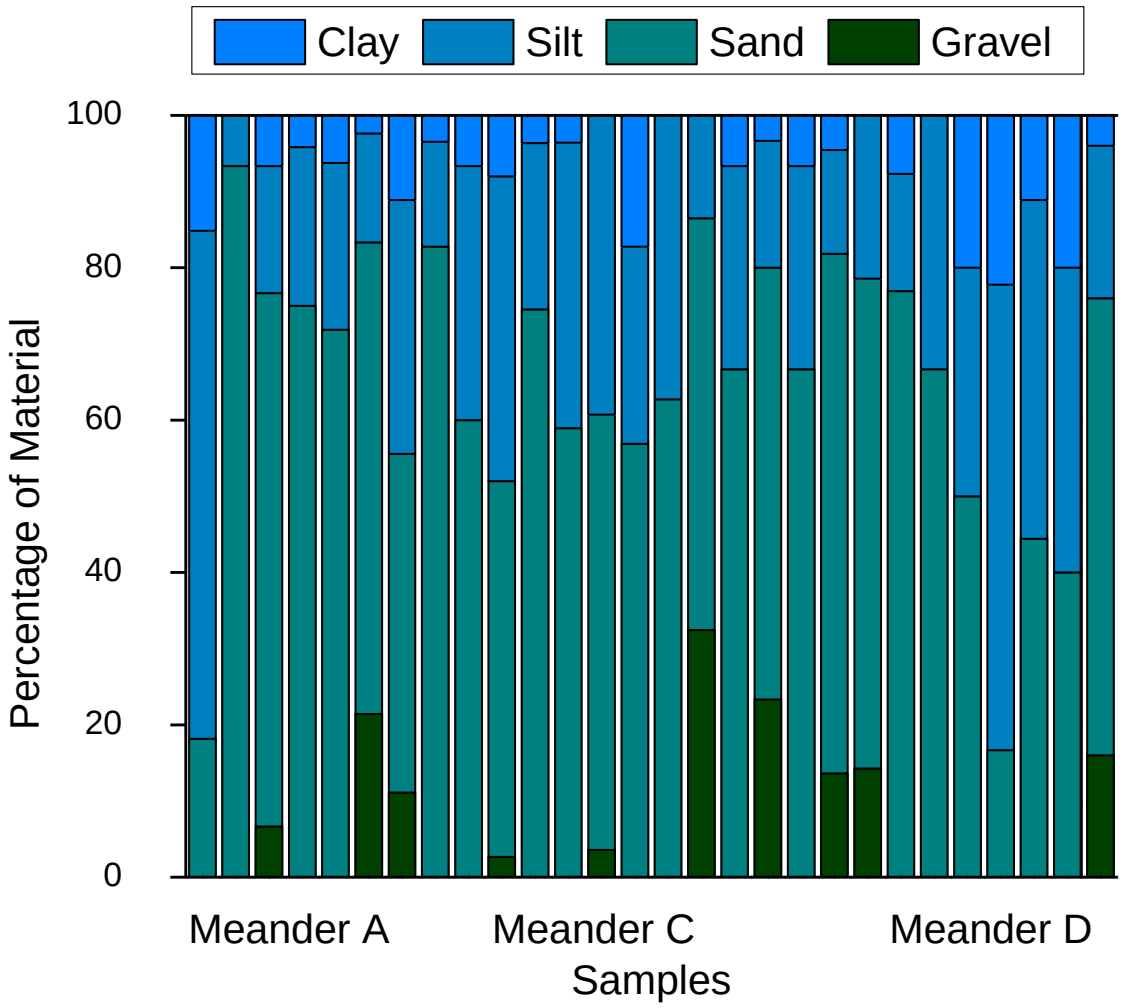

Figure B4. Grain size distributions of sediment by meander by dry sieving. Note that the concentration of fines is under-represented. Samples near the edges of the meanders tended to have both more fine and more coarse material.

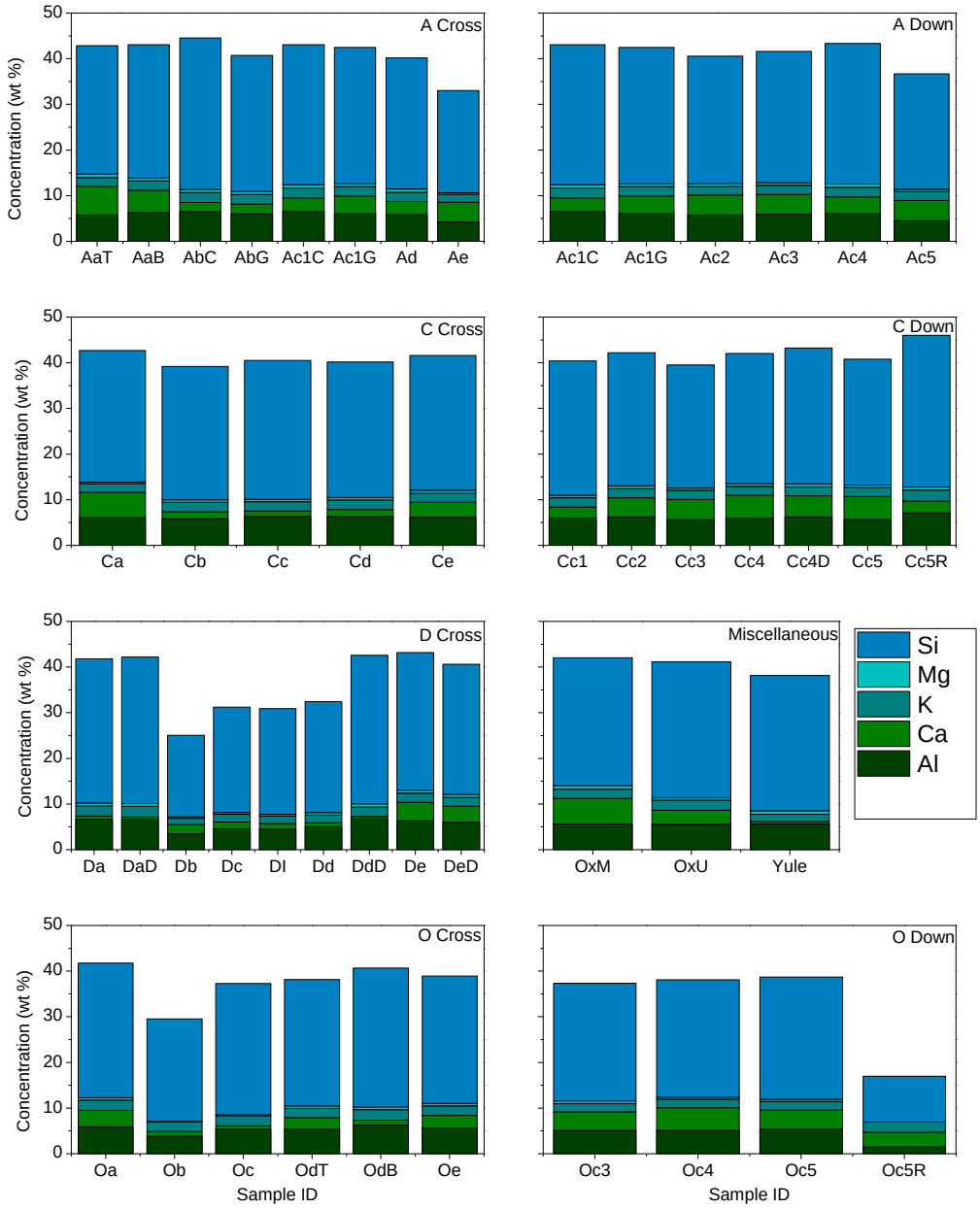

Figure B5. Major elemental content of soils from X-ray fluorescence (XRF) spectrometry.

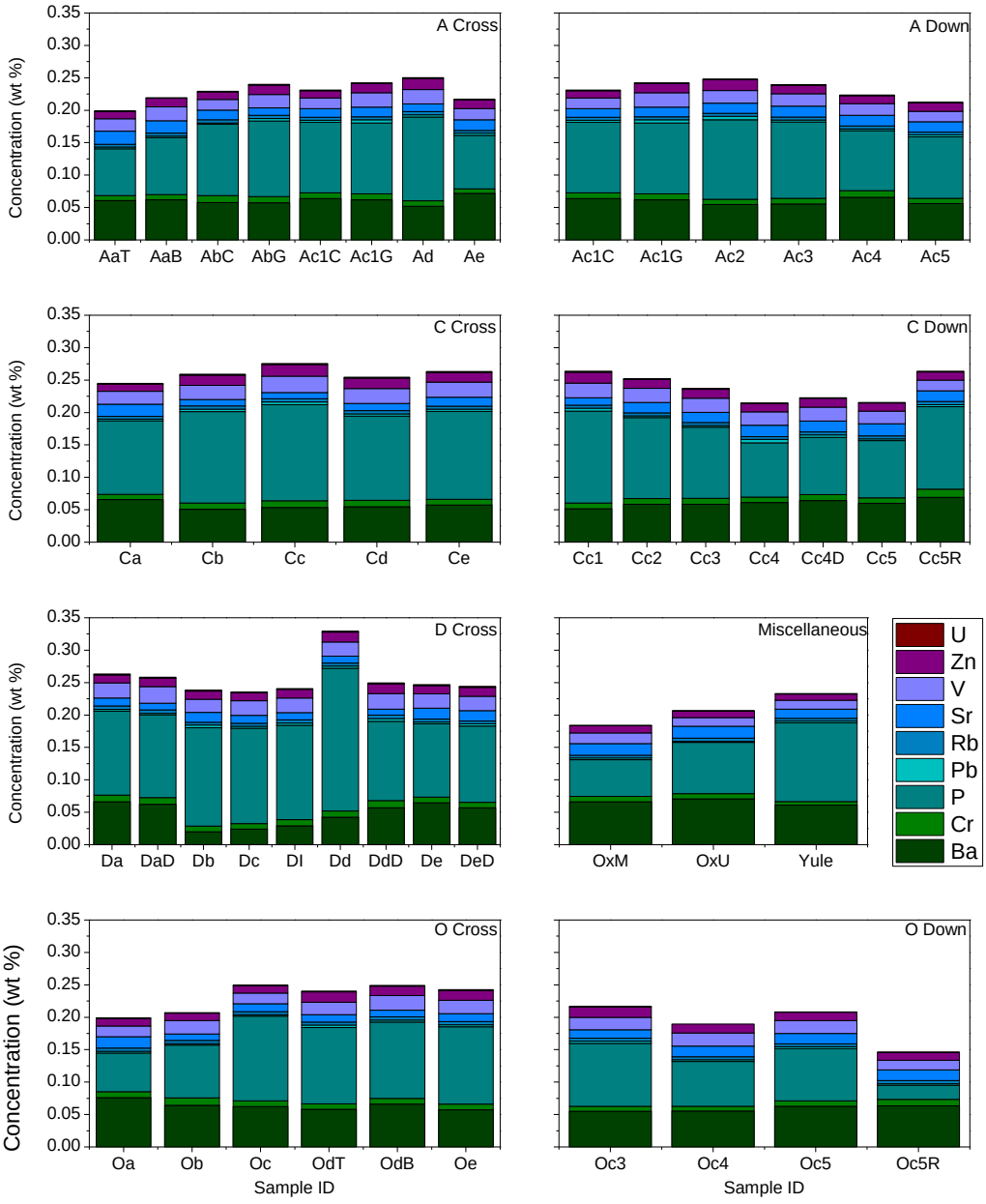

Figure B6. Trace elemental content of soils from X-ray fluorescence (XRF) spectrometry.

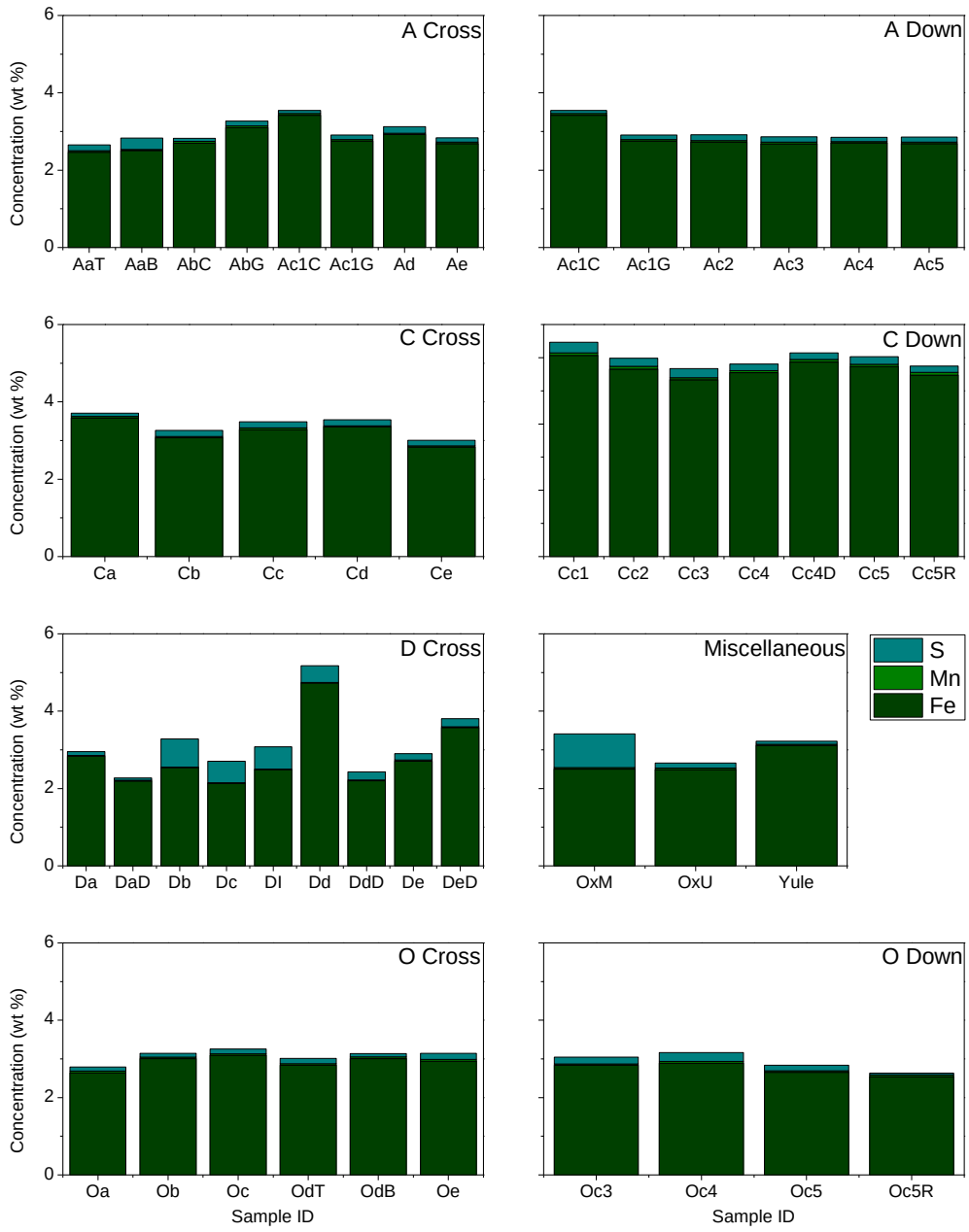

Figure B7. Redox elemental content of soils from X-ray fluorescence (XRF) spectrometry.

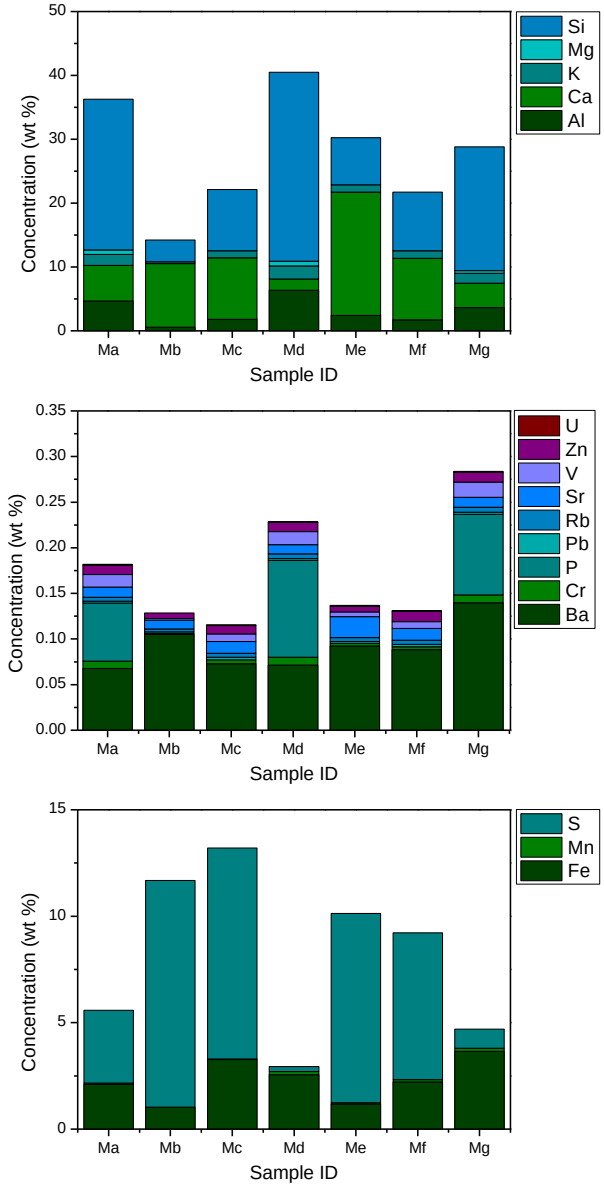

Figure B8. Major, trace and bulk elemental content of Mancos Shale outcrop from X-ray fluorescence (XRF) spectrometry.

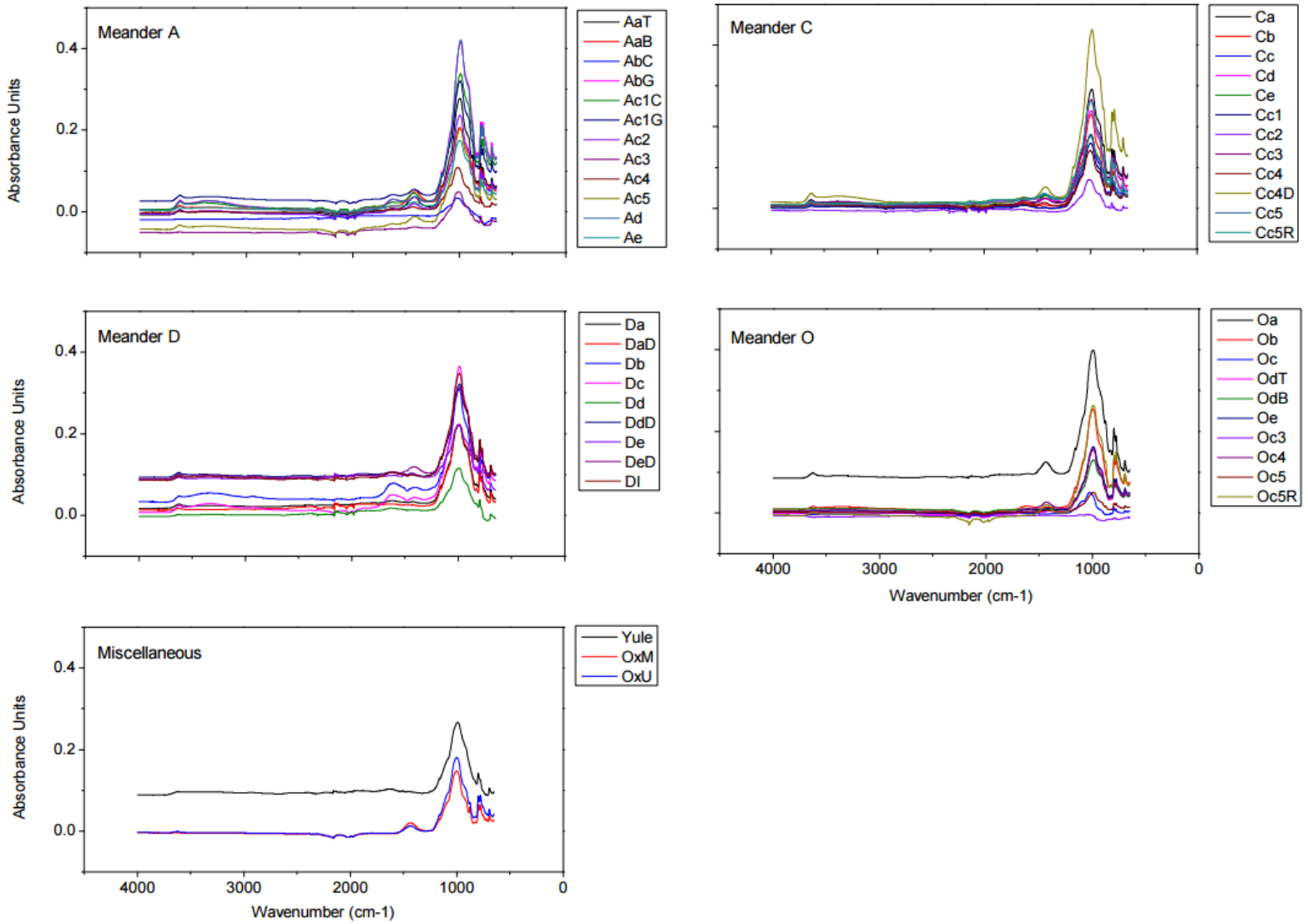

Figure B9. Absorbance peaks from Fourier Transform Infrared Spectroscopy (FTIR) Analysis. Peaks indicate types of organics.

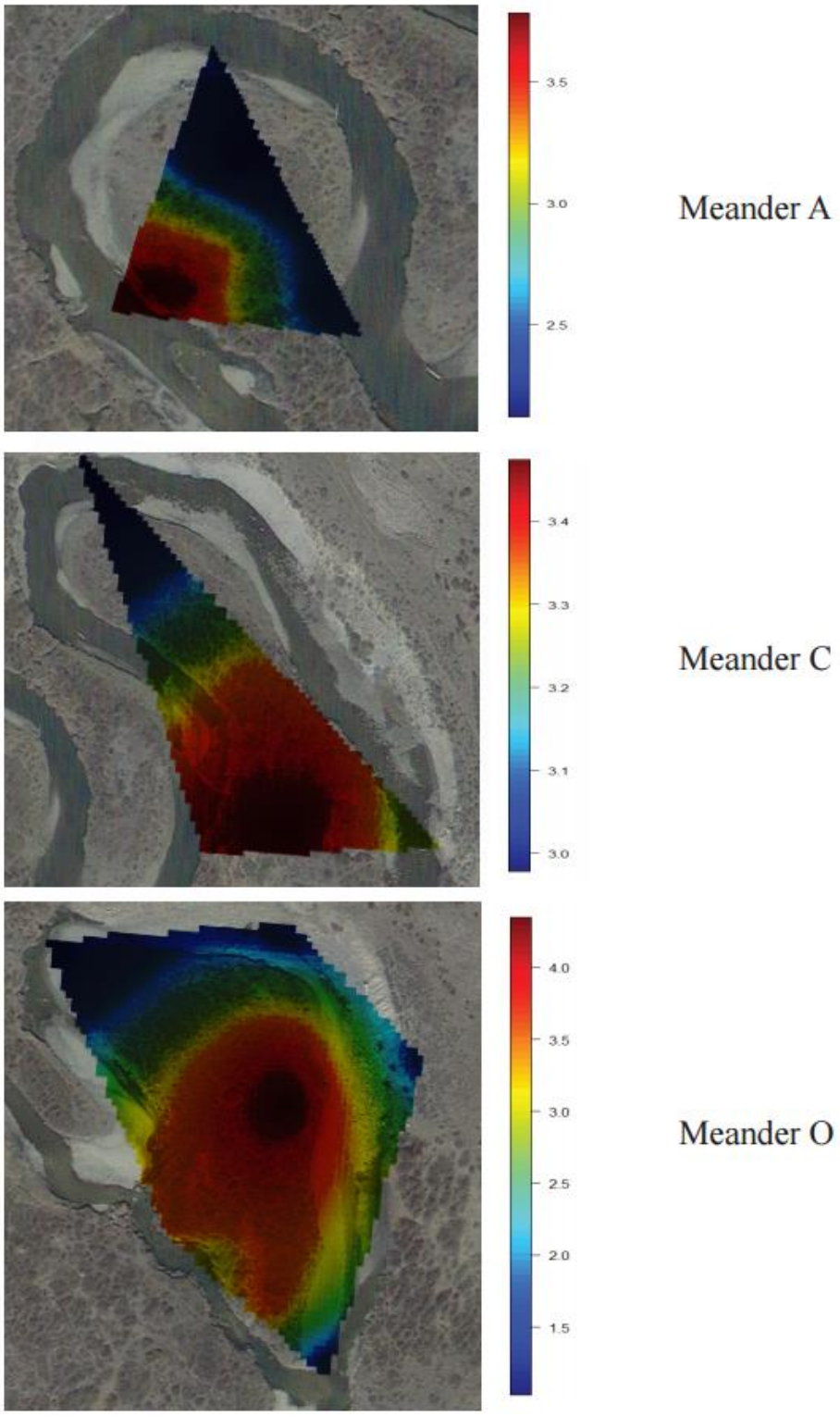

Figure B10. Ordinary kriging results for TOC in weight % carbon on meanders A, C and O.

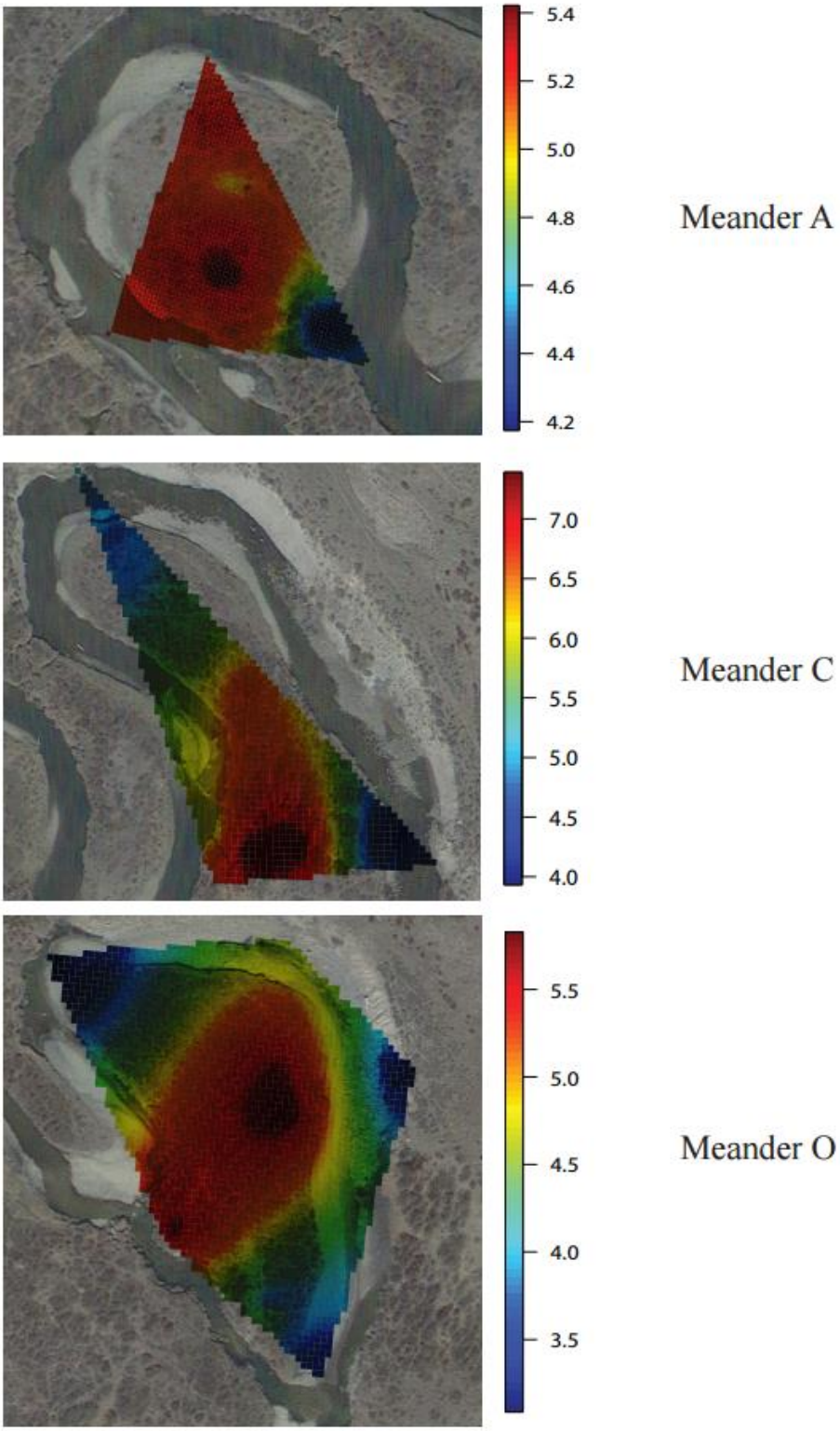

Figure B11. Ordinary kriging results for HCl extractable iron in g/kg on meanders A, C and O.

APPENDIX C WATER CHARACTERIZATION

C1 Introduction

A large-scale heterogeneity that may be critical in understanding fluvial microbial communities is the hyporheic zone, the sediment surrounding a riverbed that is influenced both by underlying groundwater and influx of surface water (Stanford, 1998). This scientifically stimulating region is a dynamic ecotone where spatial and temporal heterogeneity govern chemical and biological processes (Robertson & Wood, 2010). Not only is the hyporheic zone ecologically important as a habitat, it also plays a unique role in the nutrient cycling of adjacent groundwater and surface water systems (Brunke & Gonser, 1997). The interface is an area of transient storage with rapid changes of redox and high organics (Munz et al., 2011). This ideal habitat for microbes allows nutrients to be rapidly cycled or retained (Mullholland et al., 1997). Studying the hyporheic zone is important to floodplain geochemistry and microbiology. This study uses water samples from river water, groundwater seeps and the hyporheic zone to try to further understand this complex interface.

C2 Methods

The following methods describe how to characterize geochemical properties of surface water, groundwater and hyporheic water.

C2.1 Sample Collection and Laboratory Testing

Water samples were collected from the river, three groundwater seeps and three soil sampling stations which filled with water after digging (Cc3, Cc4 and Cc5). The filled holes were considered hyporheic samples as were samples collected using a hyporheic sampler inserted up to 70 cm into the soil (Aa, Ab, Ae, Ca, Ca3, Cb). Water sampling included samples for cations (new 15 mL centrifuge tubes, acidified with phosphoric acid), anions (new 50 mL HDPE bottles), ultraviolet absorbance (new 15 mL centrifuge tubes), and excitation-emission matrices (acid washed 125 mL amber bottles). All samples were collected through a 0.22 µm Sterivex filter (EMD Millipore Corporation, Billerica, MA, USA). Field measurement of pH, temperature, conductivity and dissolved oxygen were also taken using an HQ40d Portable ISE Multi-Parameter Meter connected to a PHC301 pH probe, an LDO101 luminescent/optical

dissolved oxygen probe and a CDC401 graphite, 4-pole conductivity probe from IntelliCAL (Hach Company, Loveland, CO).

Cations were determined using inductively coupled plasma atomic emission spectroscopy (ICP-AES) by the Department of Chemistry and Geochemistry at Colorado School of Mines (Golden, CO). Anions were analyzed using Ion Chromatography (IC) in the Aquatec Laboratories (Colorado School of Mines, Golden, CO).

C2.2 Ultraviolet Absorbance

Water samples were analyzed for specific ultraviolet absorbance at 254 nm (SUVA) using a DU 800 Spectrophotometer (Beckman Coulter, Brea, CA). Samples were run in triplicate in a 1 cm quartz cuvette and a blank was analyzed every 3 runs (every sample) to prevent drifting of the UV light. When irregular numbers were reported, an additional blank was analyzed to ensure that these numbers were accurate. The spectrophotometer used 254 nm wavelength UV light to evaluate aromatic carbon content. Results are presented as absorbance at 254 nm in cm^{-1} from the ratio of optical density and length (Saadi et al., 2006). SUVA absorbance could not be calculated as dissolved organic carbon content was unknown.

C2.3 Excitation-Emission Matrices

Samples were analyzed in a 1 cm quartz cell for excitation-emission matrices (EEMs) using an Aqualog Horiba Fluoromax 4 fluorometer (Horiba Ltd., Edison, NJ). Excitation wavelengths were analyzed from 240 to 600 nm and emission wavelengths from 240 to 800 nm to capture fulvic acids, humic acids and proteins. The emission increment was set to 4 pixels and the CCD gain medium. Three-dimensional absorbance was determined qualitatively. Several samples (Aa, Seep1B, Ca3) were oversaturated and were therefore analyzed under a ten times dilution. Emission matrices were corrected for a blank Milli-Q sample, inner filter effect and Rayleigh masking.

Emission matrices were evaluated qualitatively using wavelength ranges proposed by Leenheer and Croué (2003). This paper proposed that humic substances could be represented by peaks from ex. 330-350, em. 420-480 nm and ex. 250-260, em. 380-480 nm. In addition, peaks between ex. 300-350, em. 270-280 may represent proteins.

Matrices were also analyzed using a more general characterization used in Dahm et al. (2013). This method identified regions for aromatic proteins (ex. 220-250, em. 280-380), fulvic acid-like compounds (ex. 220-250, em. 380-580), microbial byproducts (ex. 250-470, em. 280-380), and humic acid-like compounds (ex. 250-470, em 380-580).

C2.4 DNA Extraction and Quantitative PCR Analysis

Groundwater samples were collected in Sterivex filter units (EMD Millipore Corporation, Billerica, MA, USA) and nucleic acids extracted with a PowerWater Sterivex DNA Isolation Kit (MO BIO Laboratories, Inc., Carlsbad, CA, USA) according to manufacturer's instructions. This kit was specifically designed to remove most qPCR inhibitors in environmental water samples (Green & Field, 2012). See Section 2.5 for quantitative PCR methods.

C3 Results and Discussion

The geochemical characteristics of the surface water, groundwater and hyporheic water are important because they both influence and are influenced by the solid phase properties.

C3.1 Sample Collection and Laboratory Testing

Table B1 summarizes the field results for pH, temperature, conductivity and dissolved oxygen for East River site water samples. Note that not all stations were analyzed for all chemical properties. Generally, conductivity was lowest in the river samples and highest in groundwater. As expected, the hyporheic zone's pH was between lower groundwater pH and higher river pH. This pH decrease with depth was expected as CO_2 from microbial respiration accumulates in the subsurface (Vinson et al., 2007). Temperatures averaged close to the same in the groundwater and hyporheic zone and lower in the river (note that most river samples were taken in May during a snowmelt-dominant system). Dissolved oxygen was very low in the hyporheic zone, slightly higher where groundwater was exposed and highest in river water. This suggests that the groundwater seeps did not come from a deep groundwater system.

Table C1. Average field water measurements

Parameter	Units	River	Groundwater	Hyporheic
Conductivity	uS/cm	214	407	335
pH	pH units	8.07	6.86	7.38
Temperature	Celsius	9.6	11.6	12.0
DO	mg/L	7.98	5.04	0.98

Sulfate concentrations were fairly consistent between stagnant water, river water and hyporheic water (Figure C1). However, there was a distinct difference between samples collected in the spring which had lower concentrations than samples collected in the fall. This may have been due to dilution through snowmelt during spring runoff. Sulfate concentrations in Seep 1 were fairly consistent through the seasons and substantially higher than other samples. In general, sulfate was higher in groundwater which was unexpected given the potential for sulfate reduction in deeper, more reduced waters (Kirk et al., 2009). The opposite trend of low sulfate concentrations in groundwater has also been recorded (Morrice et al., 2000). This could mean that groundwater seeps were not sulfate reducing at the East River site. It could also be a result of high sulfate concentrations being released from Mancos shale (Morrison et al., 2012). However, if the Mancos was dominating the system then high nitrates would also be expected in groundwater. Concentrations of nitrate and sulfate were approximately 3 orders of magnitude less than Mancos-influenced groundwaters studied by Morrison et al. (2012). In addition, groundwater seeps and stagnant oxbow water had lower concentrations of nitrate than the river as nitrate reduction may have been occurring in these environments (Vinson et al., 2007). Nitrate was lowest in the hyporheic zone with the exception of sample Cc5 near the river. This was likely due to nutrient cycling and microbial processes that were using available nitrate. Chlorine concentrations were slightly higher in the hyporheic zone followed by the groundwater but overall the trend was variable. Fluorine concentrations were similarly fluctuating with the highest concentrations in the groundwater seeps and lowest concentrations in the river.

Sodium concentrations were much higher in the fall than spring except Seep 3 where the concentration was very high (Figure C2). Potassium was variable, slightly higher in the hyporheic zone. Sulfur varied in groundwater but was otherwise consistent as were calcium and strontium. Magnesium was slightly higher in most groundwater samples. Lead and copper were

substantially higher in groundwater but zinc remained fairly consistent. Nickel was particularly low in the spring river water and slightly high in the groundwater samples. Iron was generally highest in groundwater but both iron and manganese were very low in Seep 2. Manganese was substantially higher in the hyporheic zone and fall groundwater than the river. Aluminum was quite variable but substantially higher in the fall groundwater samples. Seep 1B had lower general cation concentrations than all other samples but the metals concentrations tended to be some of the highest measured. Contrarily, Seep 3 had high general cations and high metals. It was also a sodium-potassium dominated water rather than a calcium dominated water like all other samples. Iron seemed to increase from the river inland on the Cc transect. This could be from reduction of Fe(III) to more soluble Fe(II). More reduced conditions also explain high iron in groundwater (Morrice et al., 2000). One would expect the same pattern in manganese because reduced Mn(II) is more soluble but the trend was not as consistent (Kirk et al., 2009). Overall it seemed groundwater had generally higher ions and, in particular, metals. The hyporheic zone reflected this progression from low to high ionic strength for only some of the parameters.

Another interesting observation appeared when plotting iron, aluminum and manganese against dissolved oxygen (Figure C3). There was a distinct gap in dissolved oxygen concentrations between samples. River water, as previously mentioned, had high dissolved oxygen. In addition, iron concentrations were highest, followed by aluminum then manganese with a few exceptions. Groundwater seeps from the fall sampling had the same chemical pattern but much lower dissolved oxygen. On the other hand, spring groundwater seeps had dissolved oxygen concentrations close to the river water. This suggests that the snowmelt was strongly influencing both groundwater and river water in the spring. It was also interesting that hyporheic zone samples from the holes in meander C all had low dissolved oxygen like fall groundwater. This, combined with high manganese concentrations, made the hyporheic samples very different than the other spring samples suggesting that snowmelt may not be playing as much of a role or may have a delayed role underneath meanders. Instead, the hyporheic water more closely resembled baseflow groundwater.

C3.2 Ultraviolet Absorbance

UV fluorescence was distinctly higher for groundwater except Seep 1 in the spring (Figure C4). Seep 3 was particularly high. This suggested higher organic concentrations in

groundwater which was consistent with DOC results from a study by Morrice et al. (2000). Stagnant water in the oxbow also had higher UV fluorescence, likely because the still water promoted decomposition and particulates. Spring river water was more fluorescent than the fall suggesting that the spring melt carried down organics that were deposited in the snow over the winter months. A similar conclusion was drawn in an investigation of DOC of streams before and after snowmelt (Baker et al., 2000). The hyporheic samples generally fell somewhere in between with perhaps decreasing fluorescence from the upstream to downstream edges of a meander (seen with samples Ae, Ab, Aa).

C3.3 Excitation-Emission Matrices

Excitation-emission matrices (EEMs) gave a qualitative approximation of humic and fulvic acids in a sample, as well as proteins and microbial biproducts. Humic acids can act as electron shuttles because they often have reducible functional groups. Electron-shuttling can increase microbial reduction by accessing small pore spaces (Parker et al., 2013).

After being diluted, samples Aa, Seep 1B and Ca3 still did not produce accurate results and were therefore not considered in the analysis. According to the general region characterization, fulvic acid- like compounds dominated most samples followed by humic acid-like compounds (Figure C5). Samples Oxbow Upstream, Oxbow Downstream, ~ OdRiver, Ca5, Ce, ~ Cc5 and Cc4 also had signals in the microbial biproducts region with a very strong signal in Cc4 particularly. This corresponded to several, though not all, of the samples with highest bulk microbial DNA. The oxbow water samples, Ca5, Ce and Yule also had signal in the aromatic protein-like region.

Using the peak analysis method, humic acids were dominant (there was no region for fulvic acids) and the samples which were classified as having microbial biproducts using the first analysis method were instead attributed to proteins.

To visualize the magnitude of fluorescence, the plots were also presented using the same scale on each (Figure C6). River and near-river samples tended to have low fluorescence, as did samples from meander A. Hyporheic samples from meander C were more variable. The stagnant Oxbow Upstream sample fluoresced quite strongly, as did Seep 2. Seep 1, like with UV analysis,

had substantially lower fluorescence than the other seep. The low metals and anions combined with high organic signal in Seep 2 may have indicated a snowmelt-fed groundwater system. This also made sense temporally as the seep was completely dry when revisited in the fall.

C3.4 DNA Extraction and Quantitative PCR Analysis

For the water samples, bulk microbial DNA varied between 0.05 and 2.5 ng/µl with an average of 0.82 ng/µl (Figure C7, Table D10). Though this information cannot be absolutely compared because different amounts of water may have passed through the filters, DNA was considerably more concentrated in the 'hyporheic samples' either collected with the hyporheic sampler or from holes which filled with water. Stagnant waters of the upstream and downstream oxbow as well as Seep 1 in the fall were also relatively high. Seep 3 had lower DNA concentrations but high particulate matter in this sample may have interfered with the extraction. Flowing river and groundwater samples contained much lower extractable DNA, consistently below 0.2 ng/µl.

Trends of *nirK* and *nirS* genes as a percent of 16S bacterial DNA were not as definitive (Figure C8). Flowing water seemed to have higher percentages of *nir* genes than more stagnant water. In hyporheic samples from dug holes the percent of *nir* genes decreased inland which may indicate a reduced activity of denitrifiers with distance from the river. Another microbial community may be dominating further inland, as was seen with soil DNA results (Section 3.4).

The percentage of *nirS* and *nirK* genes may also be related to pH of the waters (Figure C9). Low percentages of *nir* genes tended to have the widest variety of pH. As the genes became more predominant, pH stabilized to approximately 7.4 in most samples. This may have reflected a preferential habitat for denitrifying bacteria and was in agreement with Bergaust et al. (2010) who found that *nirS* was more prolific at pH 8 than at pH 6 though their study used soil pH. This trend was less obvious with temperature (Figure C10) as only a few samples could really be distinguished from the rest with the highest number of denitrifying bacteria at approximately 15^{o}C.

C4 References for Appendix C

Baker, M.A., Valett, H.M., Dahm, C.N. (2000). Organic carbon supply and metabolism in a shallow groundwater ecosystem. *Ecology, 81(11), 3133-3148.*

Bergaust, L., Mao, Y., Bakken, L.R., Frostegård, Å. (2010). Denitrification response patterns during the transition to anoxic respiration and posttranscriptional effects of suboptimal pH on nitrogen oxide reductase in *Paracoccus denitrificans. Applied and Environmental Microbiology, 76(19), 6387-6396.*

Brunke, M. and Gonser, T. (1997). The ecological significance of exchange processes between rivers and groundwater. *Freshwater Biology, 37, 1-33.*

Chen, J., LeBoeuf, E.J., Dai, S., Gu, B. (2003). Fluorescence spectroscopic studies of natural organic matter fractions. *Chemosphere, 50(5), 639-647.*

Dahm, K.G., Van Straaten, C.M., Munakata-Marr, J., Drewes, J.E. (2013). Identifying well contamination through the use of 3-D fluorescence spectroscopy to classify coalbed methane produced water. *Environmental Science and Technology, 47(1), 649-656.*

Green, H.C., Field, K.G. (2012). Sensitive detection of sample interference in environmental qPCR. *Water Research, 46, 3251-3260.*

Leenheer, J.A., Croué, J.P. (2003). Characterizing aquatic dissolved organic matter. *Environmental Science and Technology, 37, 19A-26A.*

Morrison, S.J., Goodknight, C.S., Tigar, A.D., Bush, R.P., Gil, A. (2012). Naturally occurring contamination in the Mancos Shale. *Environmental Science and Technology, 46, 1379-1387.*

Mullholland, P.J., Marzolf, E.R., Webster, J.R., Hart, D.R., Hendricks, S.P. (1997). Evidence that hyporheic zones increase heterotrophic metabolism and phosphorus uptake in forest streams. *Limnology and Oceanography., 42(3), 443-451.*

Munz, M., Krause, S., Tecklenburg, C., Binley, A. (2011). Reducing monitoring gaps at the aquifer-river interface by modelling groundwater-surface water exchange flow patterns. *Hydrological Processes, 25, 3547-3562.*

Parker, C.W., Wolf, J.A., Auler, A.S., Barton, H.A., Senko, J.M. (2013). Microbial reducibility of Fe(III) phases associated with the genesis of iron ore caves in the iron quadrangle, Minas Gerais, Brazil. *Minerals, 3, 395-411.*

Saadi, I., Borisover, M., Armon, R., Laor, Y. (2006). Monitoring of effluent DOM biodegradation using fluorescence, UV and DOC measurements. *Chemosphere, 63(3), 530-539.*

Stanford, J.A. (1998). Rivers in the landscape: introduction to the special issue on riparian and groundwater ecology. *Freshwater Biology, 40, 402-406.*

Vinson, D., Block, S., Crossey, L., Dahm, C. (2007). Biogeochemistry at the zone of intermittent saturation: Field-based study of the shallow alluvial aquifer, Rio Grande, New Mexico. *Geosphere, 3(5), 366-380.*

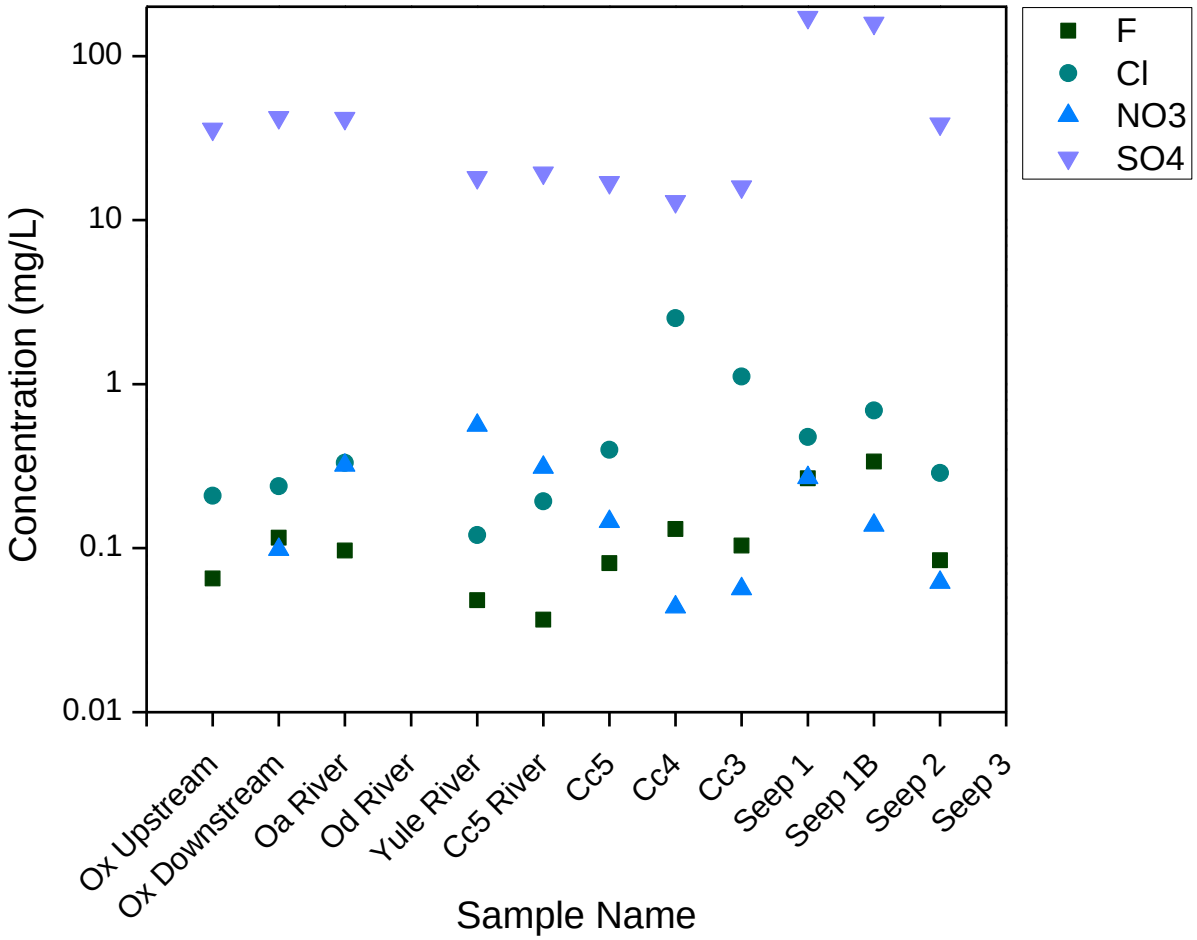

Figure C1. Anion concentrations in surface water, hyporheic water and groundwater. Sulfate had generally lower concentrations in the spring though was high in groundwater seeps. Nitrate was generally lowest in the hyporheic zone.

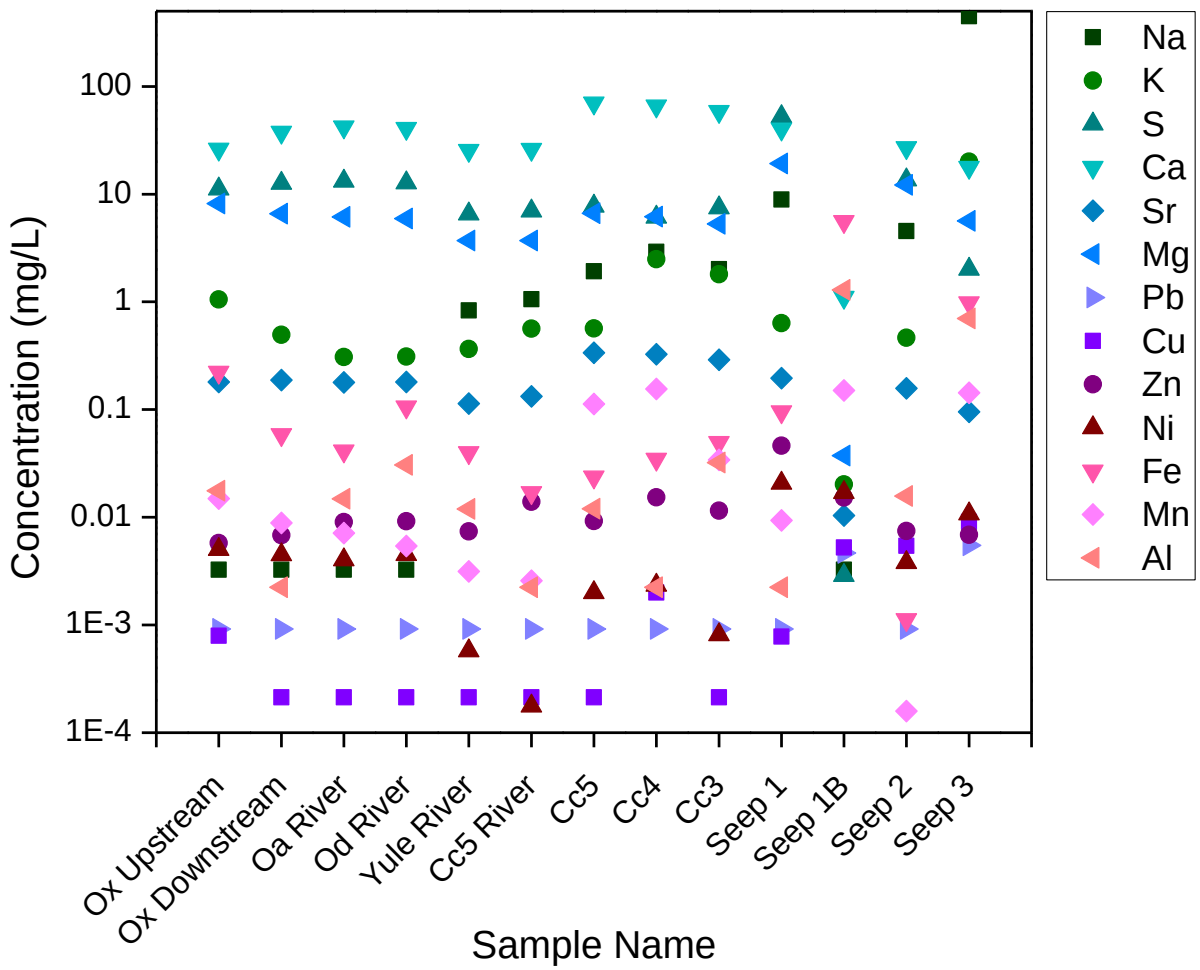

Figure C2. Cation concentrations in surface water, hyporheic water and groundwater. Manganese concentrations were high in the hyporheic zone and fall (baseflow) groundwater. Iron was also generally higher in groundwater seeps.

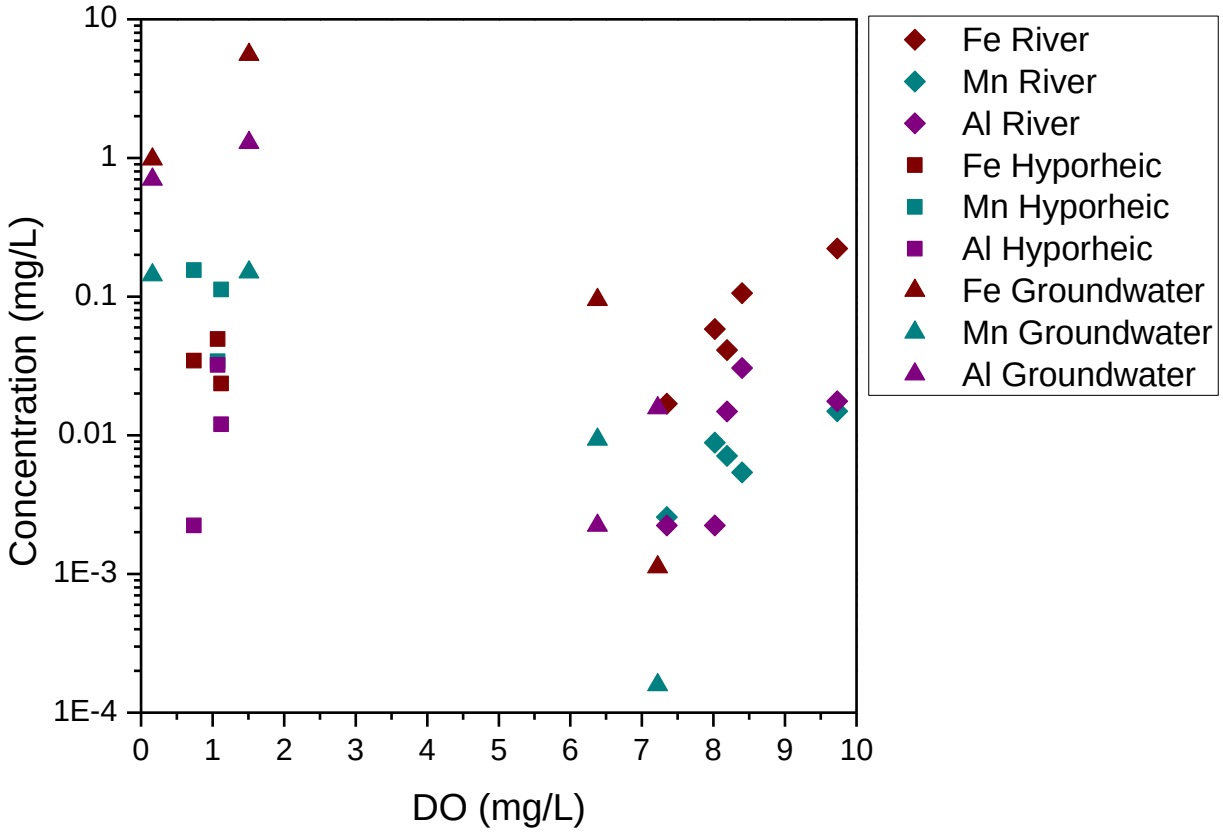

Figure C3. Select cations (iron, manganese and aluminum) plotted against dissolved oxygen for river water, hyporheic water and groundwater. Spring snowmelt-fed groundwater fell within the DO range of the river water whereas fall and spring hyporheic water had low dissolved oxygen.

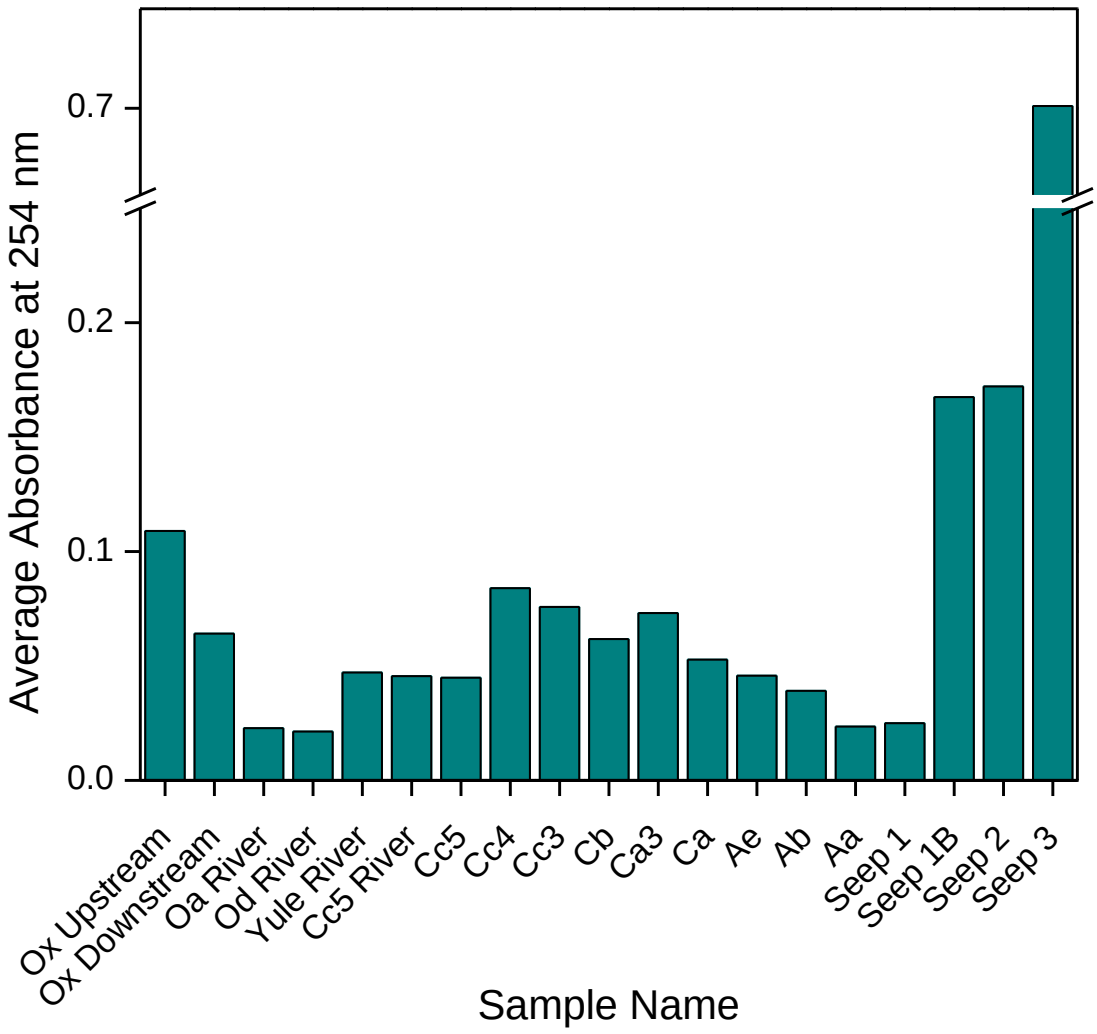

Figure C4. Ultraviolet (UV) absorbance for river water, hyporheic water and groundwater. The groundwater had distinctly higher fluorescence, and spring river water had higher fluorescence than fall suggesting that snowmelt was contributing organics to both these systems.

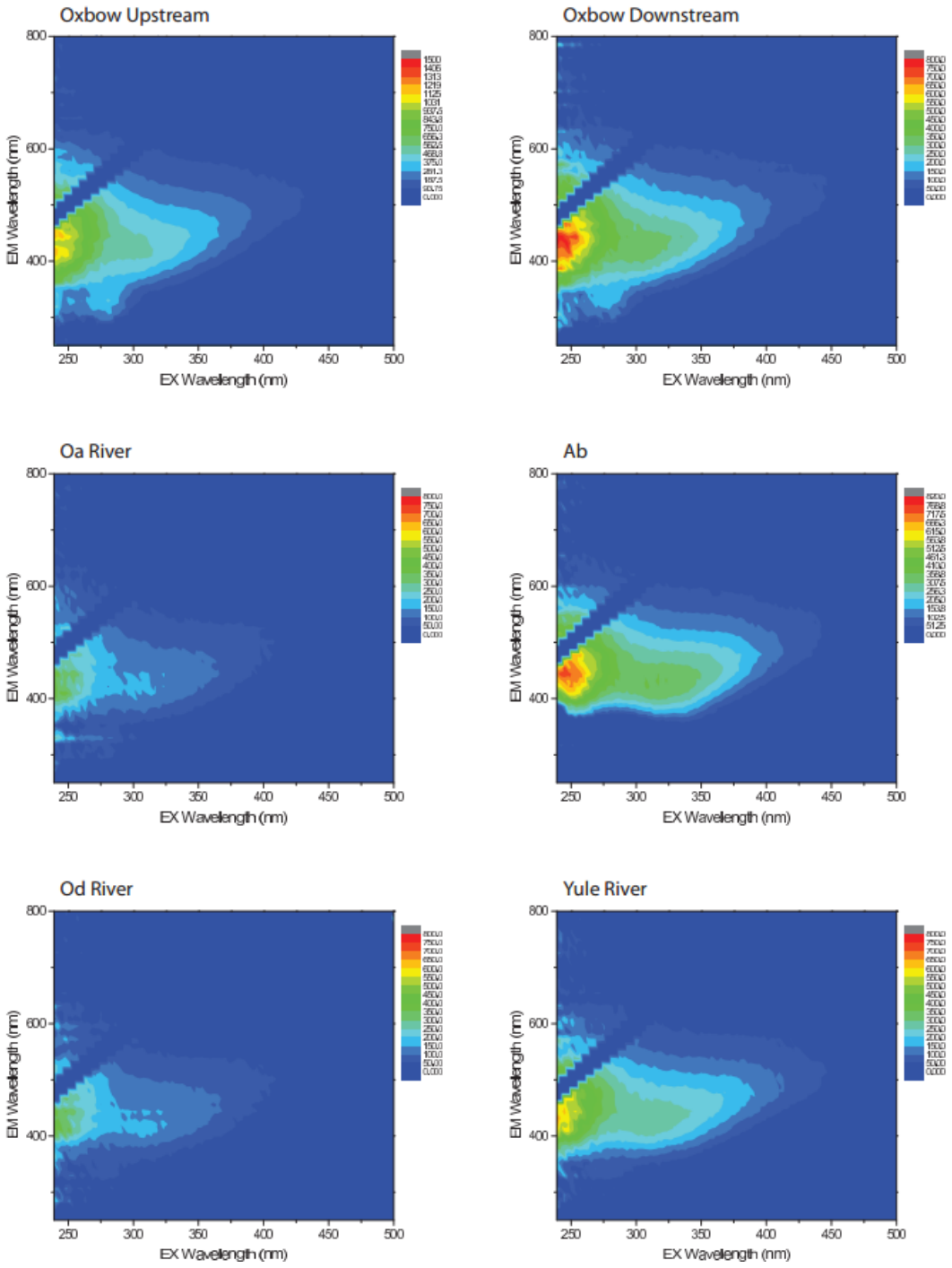

Figure C 5. Excitation-Emission Matrices for water samples. Areas on the far left indicate fulvic acids, the main tail humic acids and the spot in the lower portion seen in some samples represents microbial biproducts or proteins (3 pages).

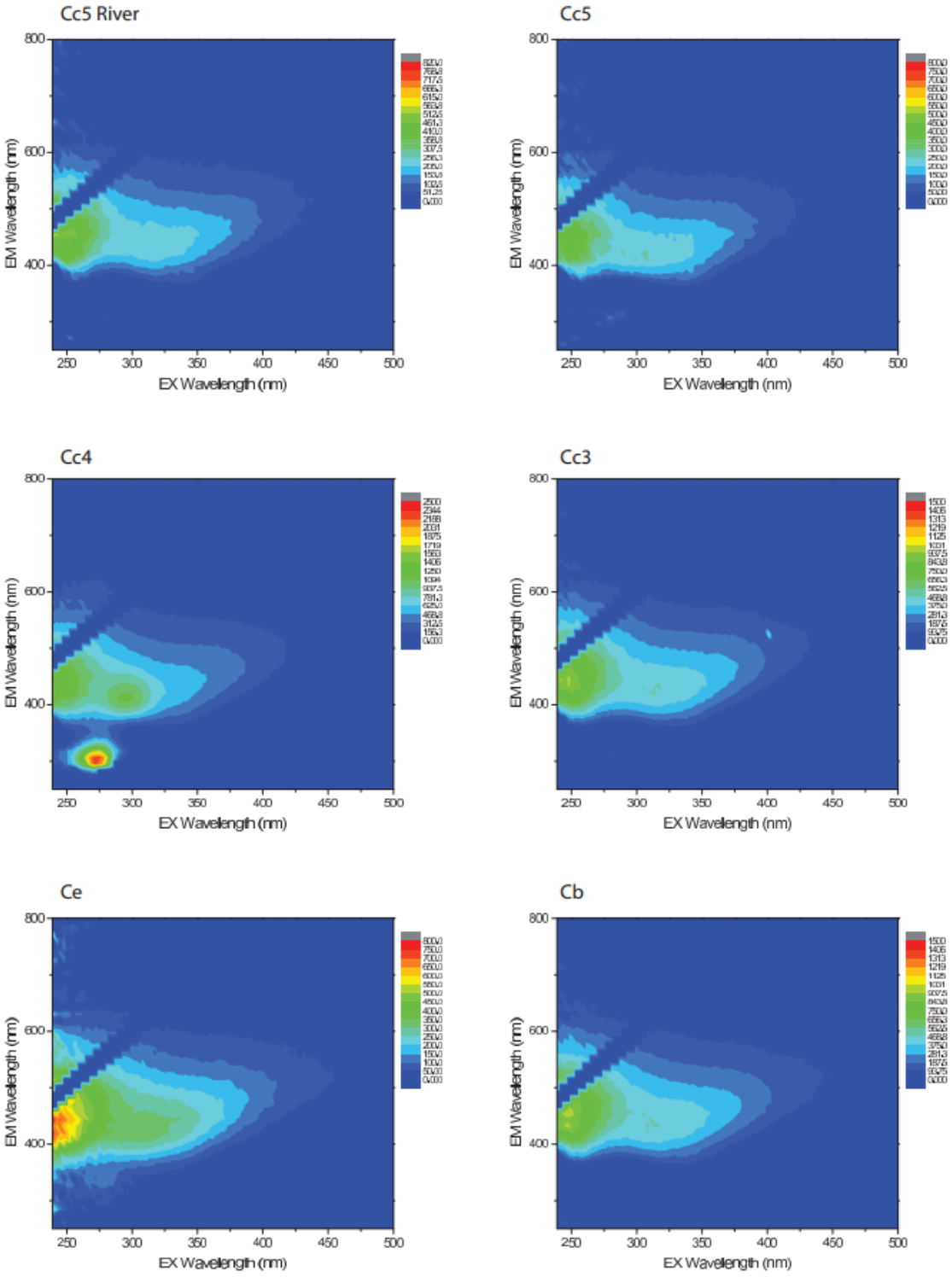

Figure C5 continued

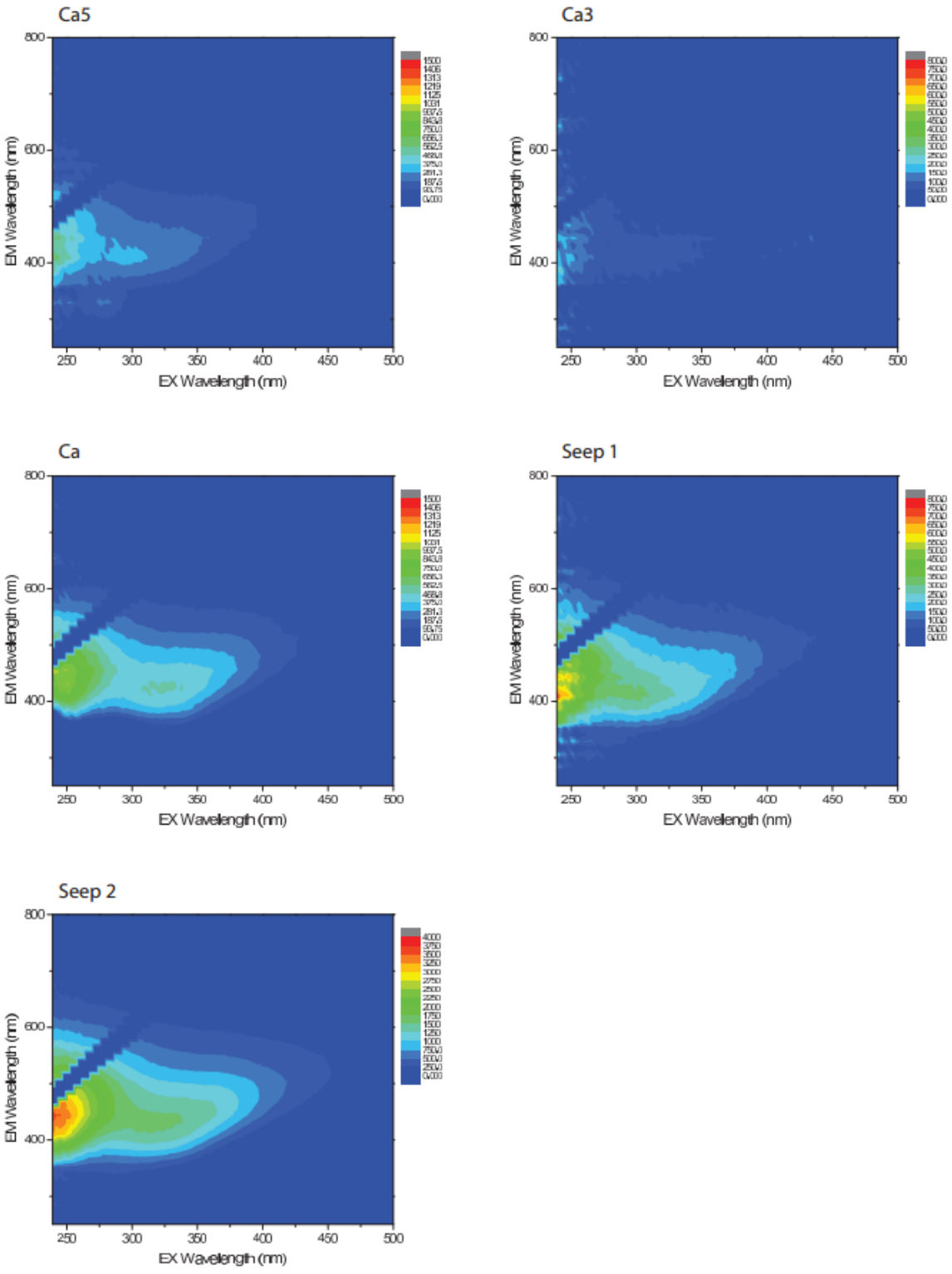

Figure C5 continued

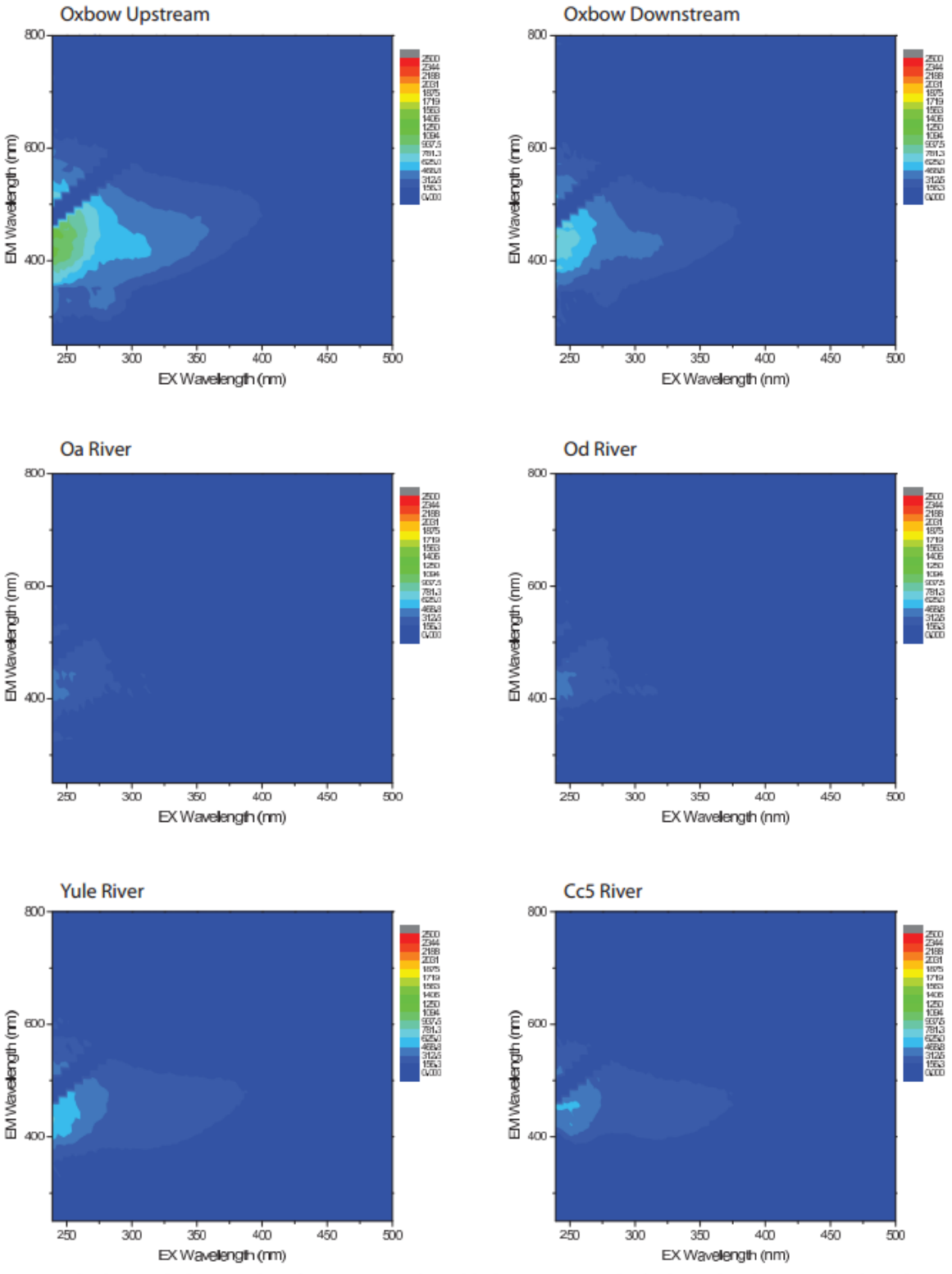

Figure C 6. Excitation-Emission Matrices for water samples with the same range in the legend. River samples had lower fluorescence while the stagnant water and groundwater seeps had generally higher fluorescence (3 pages).

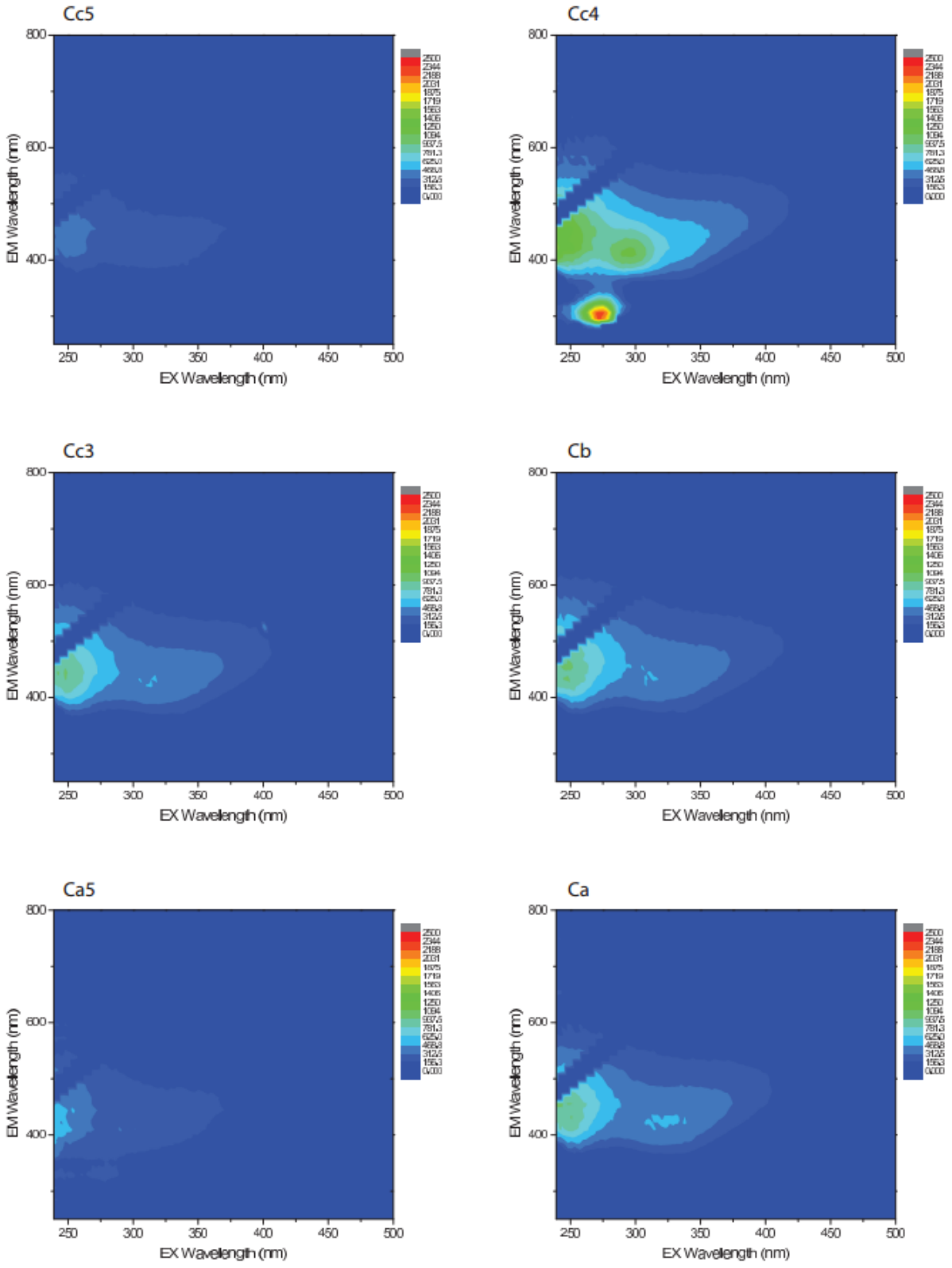

Figure C6 continued

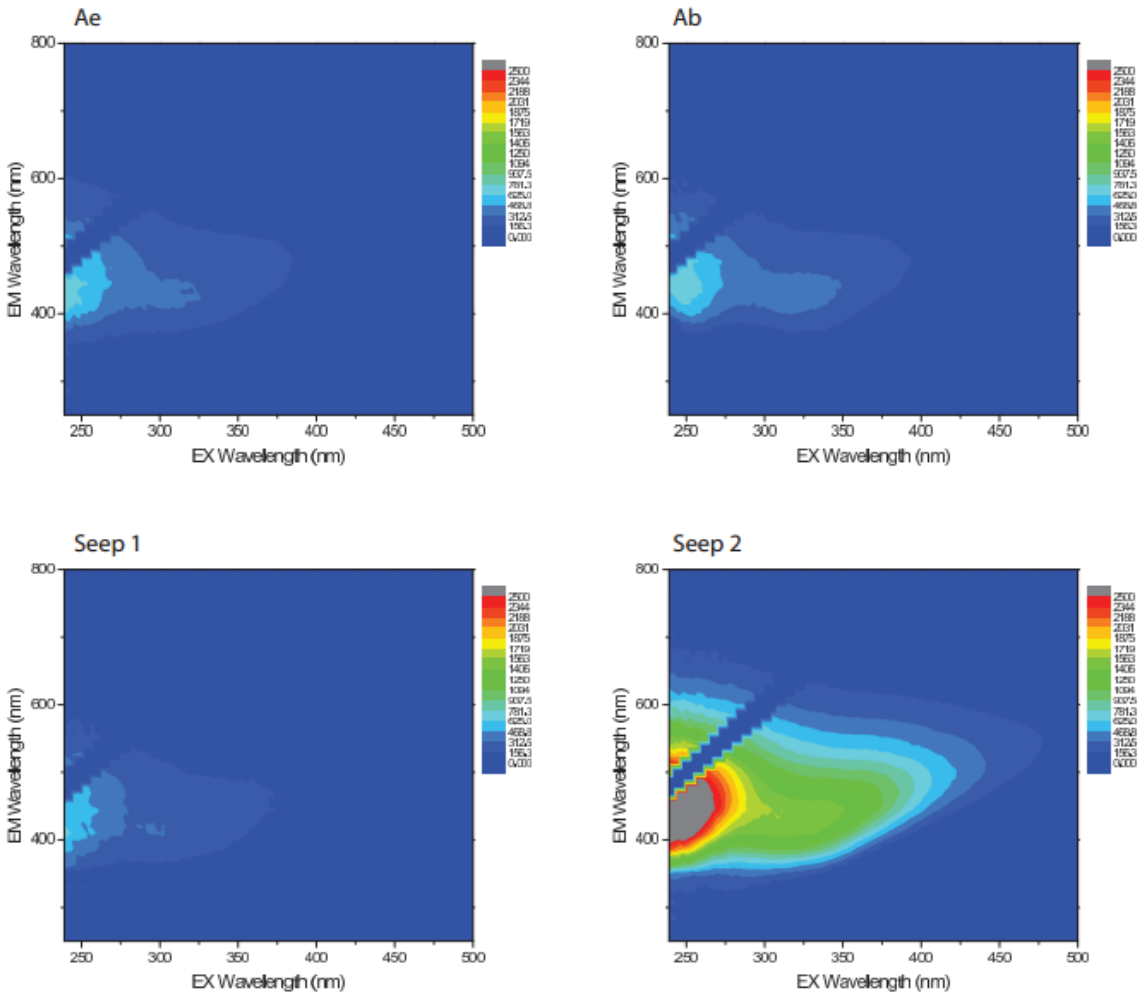

Figure C6 continued

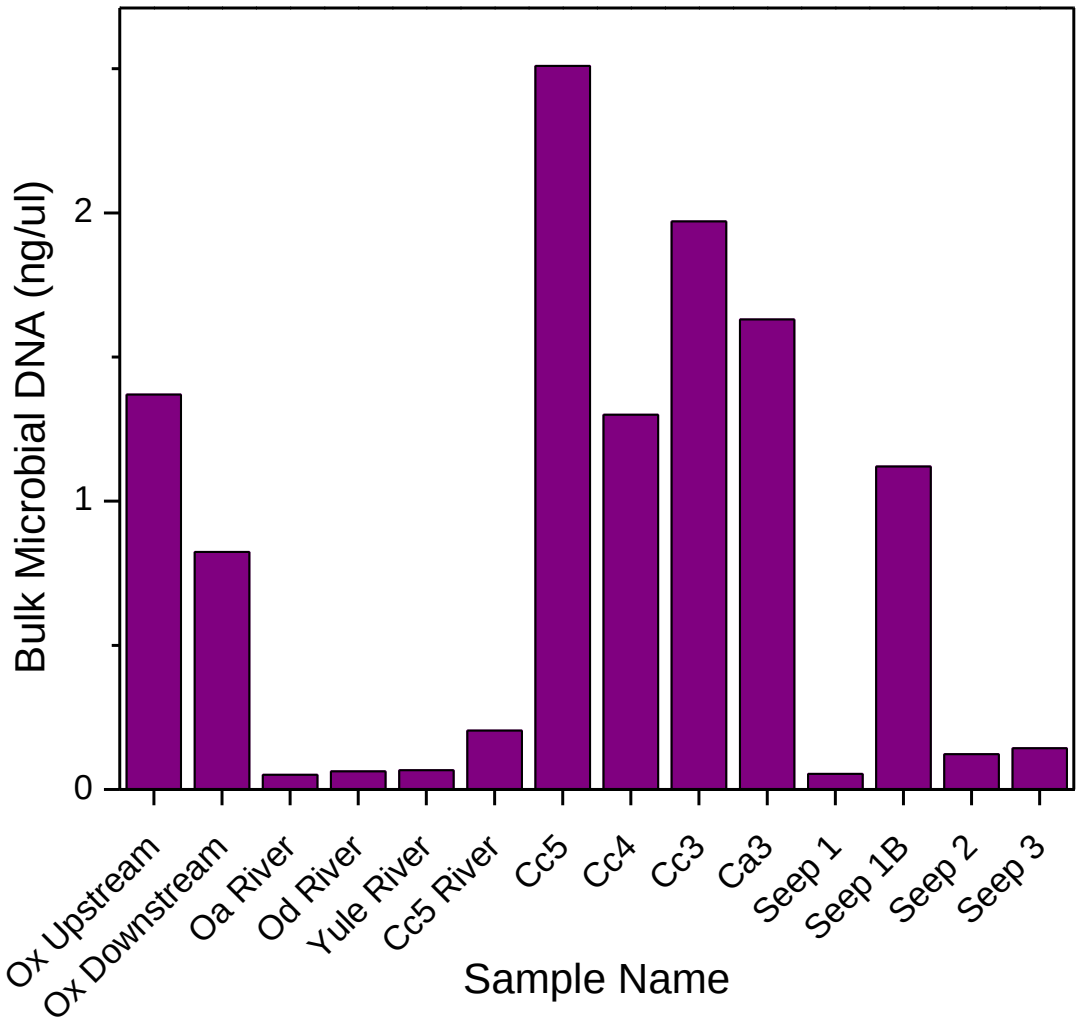

Figure C7. Bulk microbial DNA in river, hyporheic and groundwater samples. The hyporheic water and stagnant river water had distinctly higher bulk DNA though this depended on the amount passed through the filter.

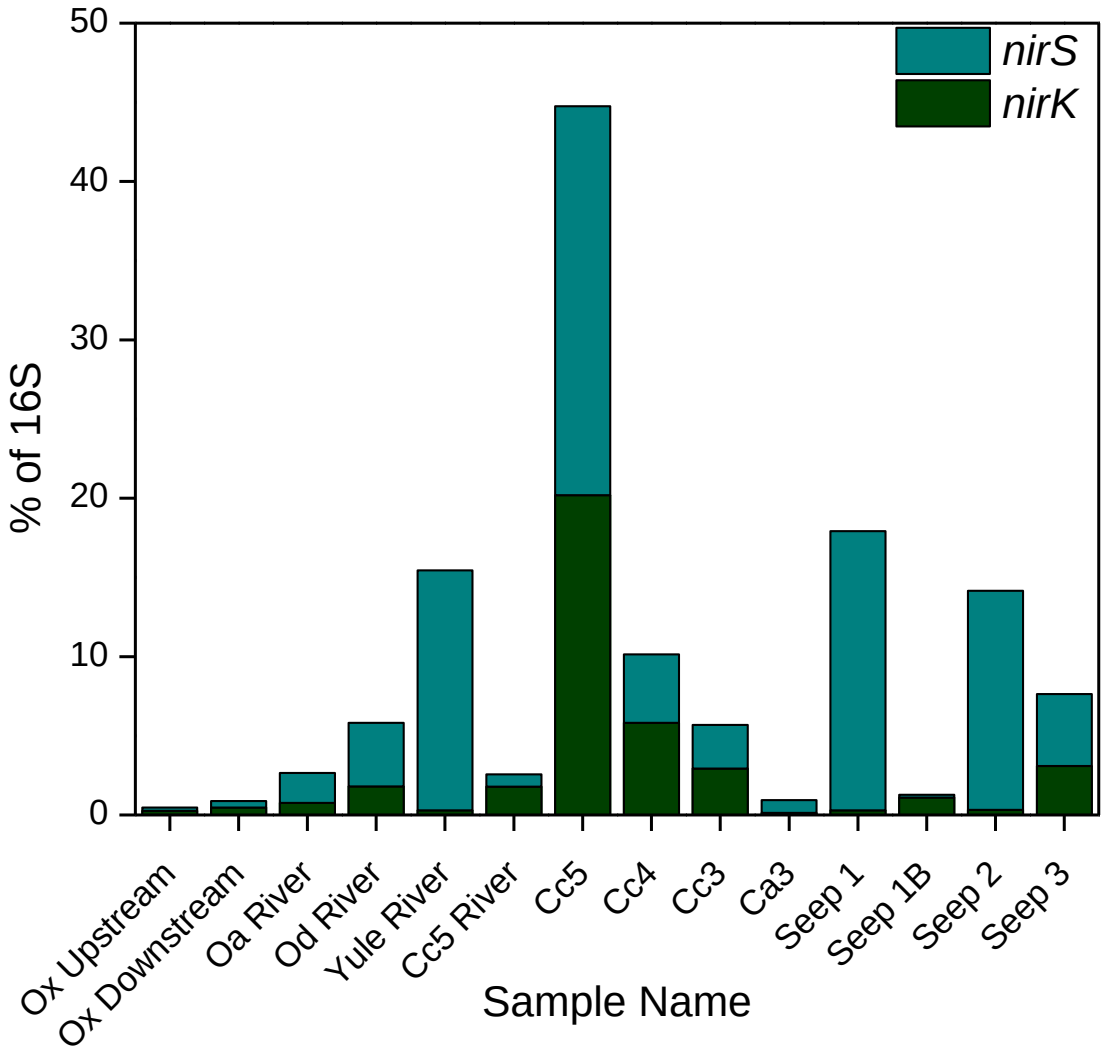

Figure C8. Percent of bacterial (16S) DNA represented by nirK and nirS denitrifying bacteria. Moving water (in the river, and flowing seeps) had higher denitrifying percentages. The percentage of denitrifying bacteria also decreased inland in the hyporheic water.

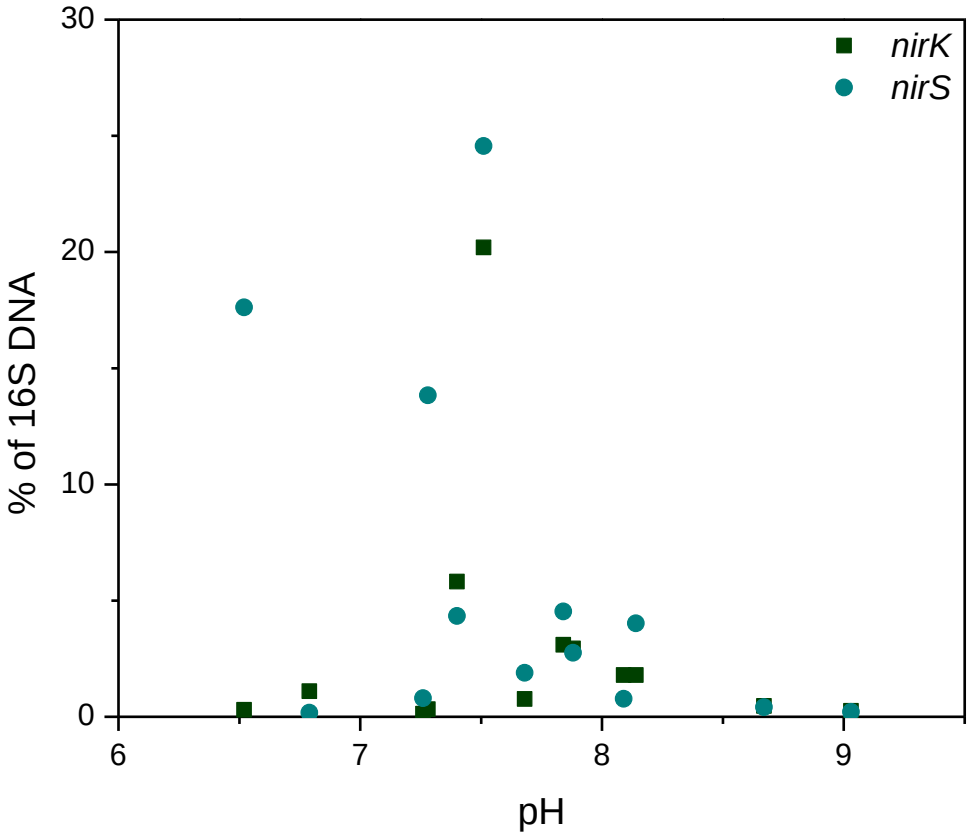

Figure C9. Percentage of bacterial (16S) DNA represented by nirK and nirS denitrifying bacteria as a function of pH. The denitrifying bacteria seemed to thrive best at a pH of approximately 7.4.

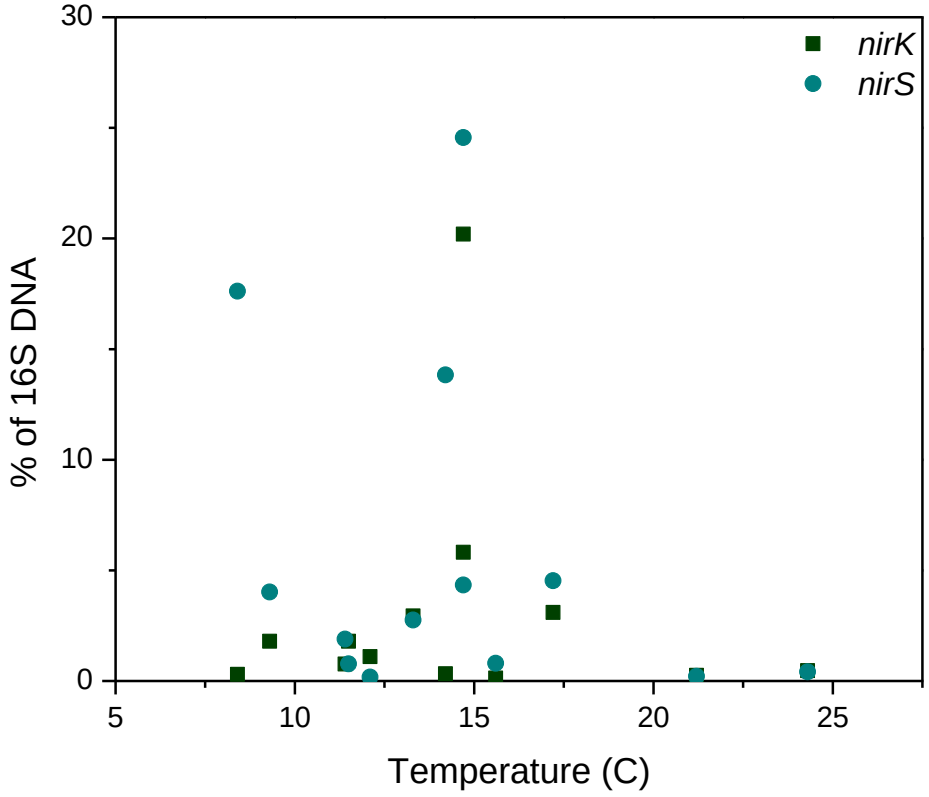

Figure C10. Percentage of bacterial (16S) DNA represented by nirK and nirS denitrifying bacteria as a function of water temperature. The denitrifying bacteria were most concentrated at approximately 15°C.

APPENDIX D ADDITIONAL PLOTS AND TABLES

Table D1. East River total organic carbon analysis (weight %)

Sample ID	*% Organic Carbon*	*% Inorganic Carbon*	*% Total Carbon*
AaT	1.76	1.49	3.25
AaB	1.21	1.14	2.35
AbC	0.46	0.37	0.83
AbG	2.93	0.42	3.35
Ac1G	2.41	0.86	3.27
Ac1C	1.19	0.56	1.75
Ac2	3.89	0.93	4.81
Ac3	2.77	1.07	3.84
Ac4	1.25	0.78	2.03
Ac5	2.25	1.08	3.33
Ad	4.63	0.64	5.27
Ae	4.17	1.03	5.19
Average A	2.41	0.86	3.27
Ca	0.91	1.13	2.03
Cb	5.16	0.14	5.30
Cc	4.51	0.04	4.55
Cd	4.03	0.15	4.18
Ce	3.44	0.72	4.16
Cc1	4.16	0.47	4.63
Cc2	2.77	1.00	3.77
Cc3	3.72	0.89	4.60
Cc4	2.00	1.26	3.26
Cc4D	2.15	1.10	3.25
Cc5	2.04	1.06	3.10
Cc5R	0.74	0.55	1.28
Average C	2.97	0.71	3.67
Da	1.84	0.02	1.86
DaD	0.85	0.00	0.85
Db	18.43	0.03	18.46
Dc	11.60	0.01	11.61
Dd	9.69	0.02	9.71
DdD	3.67	0.00	3.67
De	2.57	1.00	3.57
DeD	5.87	0.54	6.41
DI	14.44	0.01	14.45
Average D	7.66	0.18	7.84

Table D1 continued

Sample ID	*% Organic Carbon*	*% Inorganic Carbon*	*% Total Carbon*
Oa	0.59	0.78	1.36
Ob	4.09	0.05	4.14
Oc	4.33	0.02	4.35
OdT	3.99	0.24	4.23
OdB	1.23	0.19	1.41
Oe	3.86	0.58	4.43
Oc3	5.48	0.90	6.37
Oc4	4.80	1.12	5.92
Oc5	2.95	0.98	3.92
Oc5R	0.71	0.75	1.46
OxM	1.01	1.68	2.69
OxU	0.46	0.64	1.09
O1	n.a.	n.a.	5.01
O2	n.a.	n.a.	5.43
O3	n.a.	n.a.	8.25
O4	n.a.	n.a.	6.19
O5	n.a.	n.a.	5.82
O6	n.a.	n.a.	1.73
O7	n.a.	n.a.	3.32
O8	n.a.	n.a.	5.19
O9	n.a.	n.a.	2.53
O10	n.a.	n.a.	3.71
O11	n.a.	n.a.	4.95
O12	n.a.	n.a.	5.05
O13	n.a.	n.a.	5.90
O14	n.a.	n.a.	3.50
O15	n.a.	n.a.	3.78
O16	n.a.	n.a.	2.68
O17	n.a.	n.a.	2.43
O18	n.a.	n.a.	1.65
O19	n.a.	n.a.	4.42
O20	n.a.	n.a.	4.84
O21	n.a.	n.a.	5.19
O22	n.a.	n.a.	5.12
O23	n.a.	n.a.	5.47
Average O	2.79	0.66	4.10
Yule	1.76	0.00	1.76
Average All	3.67	0.62	4.34
Minimum	0.46	0.00	0.83
Maximum	18.43	1.68	18.46

Table D2. East River HCl extractable iron (mg/kg), hydroxylamine extractable iron (mg/kg) and relative percent difference (%)

Sample ID	***HCl Fe (mg/kg)***	***HA Fe (mg/kg)***	***RPD (%)***
AaT	2571	2686	4
AaB	1953	2219	13
AbC	2685	2869	7
AbG	5519	6307	13
Ac1G	5323	5616	5
Ac1C	3218	3250	1
Ac2	5980	5528	-8
Ac3	5539	5051	-9
Ac4	4612	4777	4
Ac5	5749	5292	-8
Ad	4912	5208	6
Ae	5347	4923	-8
Average A	4451	4477	2
Ca	3861	3878	0
Cb	6111	5550	-10
Cc	7400	6972	-6
Cd	7432	7083	-5
Ce	6084	5643	-8
Cc1	6510	6122	-6
Cc2	5763	5437	-6
Cc3	5447	4536	-18
Cc4	4981	4457	-11
Cc4D	3820	3508	-9
Cc5	4930	4037	-20
Cc5R	3061	3097	1
Average C	5450	5027	-8
Da	7047	7819	10
DaD	3968	3379	-16
Db	3079	2794	-10
Dc	3828	3441	-11
Dd	7310	7405	1
DdD	3762	3722	-1
De	4906	5550	12
DeD	7687	7584	-1
DI	4521	4478	-1
Average D	5123	5130	-2

Table D2 continued

Sample ID	*HCl Fe (mg/kg)*	*HA Fe (mg/kg)*	*RPD (%)*
Oa	3321	3840	14
Ob	4908	4759	-3
Oc	3379	2939	-14
OdT	5555	5358	-4
OdB	4352	4504	3
Oe	6077	5831	-4
Oc3	6291	5847	-7
Oc4	5902	5258	-12
Oc5	5047	4561	-10
Oc5R	4655	4368	-6
OxM	2836	2007	-34
OxU	2662	2253	-17
Average O	4582	4294	-8
Yule	1127	676	-50
Average All	4812	4629	-5
Minimum	1127	676	-50
Maximum	7687	7819	14

Table D3. East River HCl extractable manganese (mg/kg), hydroxylamine extractable manganese (mg/kg) and relative percent difference (%)

Sample ID	*HCl Mn (mg/kg)*	*HA Mn (mg/kg)*	*RPD (%)*
AaT	162	145	-11
AaB	52	55	6
AbC	146	161	10
AbG	208	248	17
Ac1G	191	211	10
Ac1C	179	163	-9
Ac2	205	188	-8
Ac3	187	185	-1
Ac4	177	184	4
Ac5	221	210	-5
Ad	198	226	13
Ae	184	176	-5
Average A	176	179	2
Ca	183	239	27
Cb	218	210	-3
Cc	287	273	-5
Cd	135	146	8
Ce	193	183	-5
Cc1	220	212	-4
Cc2	226	215	-5
Cc3	168	170	1
Cc4	137	134	-2
Cc4D	103	135	27
Cc5	170	186	9
Cc5R	179	171	-4
Average C	185	189	4
Da	69	80	15
DaD	45	35	-26
Db	13	12	-9
Dc	20	17	-14
Dd	23	24	2
DdD	15	15	-1
De	183	223	20
DeD	86	80	-7
DI	16	13	-17
Average D	52	55	-4

Table D3 continued

Sample ID	*HCl Mn (mg/kg)*	*HA Mn (mg/kg)*	*RPD (%)*
Oa	187	206	10
Ob	189	182	-4
Oc	217	179	-19
OdT	245	239	-2
OdB	79	84	7
Oe	294	290	-1
Oc3	225	202	-11
Oc4	166	158	-4
Oc5	186	160	-15
Oc5R	252	206	-20
OxM	94	75	-22
OxU	122	88	-32
Average O	188	173	-10
Yule	55	34	-47
Average All	155	153	-3
Minimum	13	12	-47
Maximum	294	290	27

Table D4. East River leachable iron (mg/kg) and leachable manganese (mg/kg) from a simulated precipitation leach test at pH 4.2 using 60:40 H2SO4:HNO3

Sample ID	*Leachable Fe (mg/kg)*	*Leachable Mn (mg/kg)*
AaT	1.19	1.58
AaB	1.36	0.39
AbC	1.59	0.24
AbG	1.70	0.29
Ac1G	1.40	0.53
Ac2	1.82	0.85
Ac3	0.75	0.64
Ac4	2.32	0.39
Ac5	1.27	1.15
Ad	1.58	0.49
Ae	1.59	1.73
Average A	1.51	0.75
Ca	1.42	0.51
Cb	2.58	0.76
Cc	3.52	0.84
Cd	2.00	0.29
Ce	1.82	0.51
Cc1	2.49	0.41
Cc2	2.58	0.31
Cc3	1.26	0.60
Cc4	2.32	0.70
Cc4D	3.83	0.33
Cc5	0.85	0.25
Cc5R	0.68	0.34
Average C	2.18	0.49
Da	9.25	0.22
DaD	1.07	0.14
Db	8.03	0.38
Dc	7.13	0.87
Dd	7.68	0.99
DdD	9.90	1.01
De	2.10	1.75
DeD	3.06	1.47
DI	12.83	1.24
Average D	6.78	0.90

Table D4 continued

Sample ID	*Leachable Fe (mg/kg)*	*Leachable Mn (mg/kg)*
Oa	0.52	0.15
Ob	5.12	1.11
Oc	5.75	1.39
OdT	2.40	0.79
OdB	2.74	0.08
Oe	3.44	1.08
Oc3	2.86	1.05
Oc4	3.26	0.98
Oc5	2.06	0.63
Oc5R	1.72	0.18
OxM	0.17	0.41
OxU	0.65	0.43
Average O	2.74	0.74
Yule	3.54	0.51
Average All	3.05	0.69
Minimum	0.17	0.08
Maximum	12.83	1.75

Table D5. East River bulk microbial DNA (ng/g) in soils and percentage of 16S DNA represented by nirK and nirS denitrifying genes

Sample ID	*Bulk Microbial DNA (ng/g)*	*NirK % of 16S*	*NirS % of 16S*
AaT	5645	0.8	3.9
AaB	311	0.3	4.6
AbC	1834	6.5	0.9
AbG	9743	0.0	0.1
Ac1C	4288	0.3	0.9
Ac1G	7019	0.0	0.2
Ac2	10107	0.1	0.5
Ac3	4287	0.1	0.7
Ac4	7791	0.1	1.0
Ac5	10	4.4	0.3
Ad	9341	0.0	0.1
Ae	6510	0.0	0.1
Average A	5574	1.1	1.1
Ca	569	0.4	4.2
Cb	11697	0.5	0.2
Cc	10965	0.2	0.2
Cd	11995	0.6	0.1
Ce	10433	0.2	0.2
Cc1	9344	0.3	0.4
Cc2	11377	0.0	0.3
Cc3	5669	0.3	0.0
Cc4	3794	0.0	0.1
Cc4D	1923	0.1	2.5
Cc5	2996	0.9	0.9
Cc5R	155	64.6	3.3
Average C	6743	5.7	1.0
Da	2435	1.0	0.5
DaD	572	7.1	6.7
Db	9518	0.0	0.0
Dc	12531	0.0	0.1
Dd	8545	0.0	0.0
DdD	808	2.0	0.8
De	1540	2.6	4.0
DeD	2971	0.5	0.7
DI	13481	0.0	0.0
Average D	5822	1.5	1.4

Table D5 continued

Sample ID	*Bulk Microbial DNA (ng/g)*	*NirK % of 16S*	*NirS % of 16S*
Oa	221	1.3	4.3
Ob	11844	1.0	0.2
Oc	9116	1.0	0.1
OdT	9260	0.8	0.5
OdB	1336	1.1	2.2
Oe	10657	1.4	0.9
Oc3	10727	0.9	1.0
Oc4	11302	0.1	0.1
Oc5	7188	0.7	0.8
Oc5R	633	2.1	1.3
OxM	1237	0.8	1.2
OxU	79	2.1	21.0
Average O	6133	1.1	2.8
Yule	3815	0.1	0.0
Average All	6035	2.3	1.6
Minimum	10	0.0	0.0
Maximum	13481	64.6	21.0

Table D6. East River major elemental concentration (weight %) in soil samples from XRF analysis

Sample ID	**Al**	**Ca**	**K**	**Mg**	**Si**
AaT	5.78	6.29	1.92	0.73	28.14
AaB	6.26	4.93	2.10	0.59	29.21
AbC	6.47	2.04	2.20	0.64	33.22
AbG	6.02	2.14	2.09	0.65	29.84
Ac1C	6.54	2.94	2.20	0.72	30.69
Ac1G	6.15	3.80	2.08	0.57	29.90
Ac2	5.76	4.36	1.93	0.53	27.99
Ac3	5.94	4.32	2.03	0.56	28.75
Ac4	6.15	3.55	2.15	0.72	30.78
Ac5	4.52	4.45	1.93	0.49	25.30
Ad	5.82	2.89	2.04	0.71	28.73
Ae	4.22	4.36	1.72	0.37	22.36
Average A	5.80	3.84	2.03	0.61	28.74
Ca	6.07	5.56	1.94	0.31	28.83
Cb	5.85	1.50	2.07	0.58	29.16
Cc	6.31	1.20	2.06	0.50	30.44
Cd	6.32	1.55	2.05	0.57	29.68
Ce	6.16	3.29	2.00	0.63	29.50
Cc1	5.98	2.41	2.03	0.53	29.44
Cc2	6.24	4.18	2.01	0.62	29.16
Cc3	5.64	4.42	1.99	0.50	26.99
Cc4	5.94	5.02	2.00	0.60	28.46
Cc4D	6.22	4.62	2.00	0.63	29.77
Cc5	5.67	5.06	2.00	0.50	27.55
Cc5R	7.09	2.65	2.40	0.63	33.27
Average C	6.12	3.45	2.05	0.55	29.35
Da	6.71	0.64	2.27	0.61	31.59
DaD	6.74	0.44	2.32	0.62	32.08
Db	3.49	2.02	1.39	0.29	17.85
Dc	4.58	1.49	1.66	0.40	23.08
Dd	5.00	0.89	1.70	0.52	24.30
DdD	6.72	0.52	2.08	0.72	32.53
De	6.32	4.05	2.03	0.67	30.13
DeD	6.00	3.55	1.93	0.66	28.49
DI	4.53	1.23	1.64	0.37	23.14
Average D	5.56	1.65	1.89	0.54	27.02

Table D6 continued

Sample ID	**Al**	**Ca**	**K**	**Mg**	**Si**
Oa	5.88	3.59	2.24	0.55	29.52
Ob	3.84	1.01	2.10	0.17	22.43
Oc	5.34	0.79	2.16	0.26	28.71
OdT	5.37	2.52	2.05	0.56	27.64
OdB	6.27	1.12	2.26	0.62	30.43
Oe	5.62	2.80	2.04	0.58	27.87
Oc3	5.10	4.05	1.83	0.59	25.75
Oc4	5.13	4.98	1.86	0.41	25.75
Oc5	5.35	4.19	1.95	0.46	26.75
Oc5R	1.47	3.29	2.18	0.00	10.06
OxM	5.62	5.63	2.00	0.75	28.03
OxU	5.56	3.14	2.16	0.51	29.81
Average O	5.05	3.09	2.07	0.46	26.06
Yule	5.62	0.52	1.61	0.75	29.68
Average All	5.64	3.04	2.01	0.54	27.89
Minimum	1.47	0.44	1.39	0.00	10.06
Maximum	7.09	6.29	2.40	0.75	33.27

Table D7. East River trace elemental concentration (weight %) in soil samples from XRF analysis

Sample ID	**Ba**	**Cr**	**P**	**Pb**	**Rb**	**Sr**	**V**	**Zn**	**U**
AaT	0.061	0.008	0.072	0.003	0.004	0.020	0.019	0.011	0.001
AaB	0.062	0.008	0.088	0.002	0.005	0.019	0.021	0.013	0.001
AbC	0.058	0.011	0.110	0.002	0.005	0.015	0.017	0.011	0.001
AbG	0.057	0.010	0.117	0.004	0.005	0.012	0.020	0.015	0.001
Ac1C	0.064	0.009	0.109	0.003	0.005	0.013	0.016	0.011	0.001
Ac1G	0.062	0.009	0.109	0.005	0.005	0.015	0.022	0.014	0.001
Ac2	0.055	0.008	0.123	0.005	0.004	0.016	0.019	0.017	0.001
Ac3	0.056	0.009	0.118	0.003	0.004	0.017	0.019	0.013	0.001
Ac4	0.066	0.010	0.093	0.002	0.005	0.017	0.018	0.012	0.001
Ac5	0.056	0.008	0.095	0.003	0.004	0.016	0.016	0.013	0.001
Ad	0.052	0.009	0.129	0.004	0.005	0.012	0.022	0.017	0.001
Ae	0.072	0.007	0.083	0.003	0.004	0.016	0.017	0.013	0.001
Average A	0.060	0.009	0.104	0.003	0.005	0.016	0.019	0.013	0.001
Ca	0.066	0.008	0.114	0.003	0.004	0.019	0.020	0.011	0.001
Cb	0.051	0.009	0.141	0.004	0.005	0.010	0.022	0.016	0.002
Cc	0.054	0.010	0.149	0.004	0.005	0.010	0.025	0.018	0.001
Cd	0.055	0.010	0.130	0.004	0.005	0.011	0.023	0.016	0.001
Ce	0.057	0.009	0.135	0.004	0.005	0.013	0.023	0.015	0.001
Cc1	0.052	0.009	0.142	0.004	0.005	0.011	0.023	0.017	0.001
Cc2	0.058	0.009	0.125	0.003	0.005	0.016	0.022	0.014	0.001
Cc3	0.058	0.009	0.110	0.003	0.005	0.015	0.022	0.014	0.001
Cc4	0.061	0.008	0.083	0.005	0.004	0.017	0.021	0.013	0.001
Cc4D	0.064	0.009	0.088	0.004	0.004	0.017	0.022	0.014	0.001
Cc5	0.060	0.008	0.088	0.003	0.005	0.019	0.019	0.013	0.001
Cc5R	0.069	0.013	0.127	0.003	0.005	0.016	0.017	0.013	0.001
Average C	0.059	0.009	0.119	0.004	0.005	0.015	0.022	0.014	0.001
Da	0.066	0.010	0.129	0.003	0.005	0.012	0.023	0.012	0.001
DaD	0.062	0.010	0.128	0.002	0.006	0.010	0.026	0.013	0.002
Db	0.020	0.009	0.152	0.004	0.004	0.015	0.021	0.012	0.002
Dc	0.024	0.008	0.147	0.003	0.005	0.012	0.023	0.012	0.001
Dd	0.043	0.009	0.220	0.004	0.005	0.011	0.022	0.015	0.001
DdD	0.057	0.011	0.122	0.004	0.005	0.009	0.024	0.015	0.002
De	0.064	0.009	0.113	0.003	0.005	0.017	0.022	0.013	0.001
DeD	0.057	0.008	0.118	0.003	0.004	0.016	0.022	0.014	0.001
DI	0.029	0.010	0.146	0.003	0.005	0.011	0.022	0.013	0.001
Average D	0.047	0.009	0.142	0.003	0.005	0.013	0.023	0.013	0.001

Table D7 continued

Sample ID	**Ba**	**Cr**	**P**	**Pb**	**Rb**	**Sr**	**V**	**Zn**	**U**
Oa	0.076	0.009	0.060	0.003	0.005	0.017	0.016	0.012	0.001
Ob	0.064	0.011	0.081	0.002	0.005	0.010	0.021	0.011	0.001
Oc	0.062	0.009	0.131	0.002	0.005	0.012	0.016	0.011	0.001
OdT	0.058	0.008	0.118	0.004	0.005	0.012	0.019	0.016	0.001
OdB	0.066	0.009	0.118	0.003	0.005	0.010	0.023	0.014	0.001
Oe	0.057	0.009	0.119	0.003	0.005	0.012	0.021	0.015	0.002
Oc3	0.055	0.008	0.097	0.003	0.005	0.013	0.019	0.016	0.001
Oc4	0.055	0.007	0.069	0.003	0.004	0.016	0.021	0.014	0.000
Oc5	0.063	0.008	0.081	0.003	0.004	0.016	0.020	0.013	0.001
Oc5R	0.063	0.010	0.022	0.003	0.005	0.017	0.015	0.012	0.001
OxM	0.066	0.009	0.056	0.002	0.005	0.018	0.016	0.011	0.001
OxU	0.071	0.008	0.079	0.002	0.005	0.018	0.013	0.010	0.001
Average O	0.063	0.009	0.086	0.003	0.005	0.014	0.018	0.013	0.001
Yule	0.061	0.005	0.121	0.003	0.004	0.014	0.014	0.009	0.001
Average All	0.058	0.009	0.111	0.003	0.005	0.014	0.020	0.013	0.001
Minimum	0.020	0.005	0.022	0.002	0.004	0.009	0.013	0.009	0.000
Maximum	0.076	0.013	0.220	0.005	0.006	0.020	0.026	0.018	0.002

Table D8. East River redox elemental concentration (weight %) in soil samples from XRF analysis

Sample ID	**Fe**	**Mn**	**S**
AaT	2.46	0.04	0.15
AaB	2.51	0.02	0.29
AbC	2.70	0.04	0.08
AbG	3.10	0.05	0.13
Ac1C	3.42	0.04	0.08
Ac1G	2.75	0.04	0.12
Ac2	2.73	0.04	0.15
Ac3	2.68	0.04	0.14
Ac4	2.71	0.04	0.11
Ac5	2.69	0.04	0.13
Ad	2.92	0.04	0.17
Ae	2.69	0.04	0.11
Average A	2.77	0.04	0.14
Ca	3.58	0.04	0.08
Cb	3.07	0.03	0.16
Cc	3.28	0.05	0.16
Cd	3.35	0.03	0.15
Ce	2.83	0.03	0.14
Cc1	3.03	0.04	0.16
Cc2	2.83	0.04	0.12
Cc3	2.67	0.03	0.14
Cc4	2.77	0.03	0.10
Cc4D	2.94	0.04	0.10
Cc5	2.87	0.03	0.11
Cc5R	2.73	0.04	0.09
Average C	3.00	0.04	0.13
Da	2.84	0.02	0.10
DaD	2.19	0.02	0.06
Db	2.54	0.01	0.73
Dc	2.14	0.01	0.55
Dd	4.73	0.02	0.43
DdD	2.20	0.02	0.21
De	2.71	0.03	0.16
DeD	3.57	0.02	0.21
DI	2.49	0.01	0.57
Average D	2.82	0.02	0.34

Table D8 continued

Sample ID	Fe	Mn	S
Oa	2.64	0.05	0.10
Ob	3.01	0.04	0.10
Oc	3.09	0.04	0.13
OdT	2.84	0.03	0.14
OdB	3.01	0.04	0.08
Oe	2.94	0.04	0.16
Oc3	2.83	0.04	0.18
Oc4	2.89	0.04	0.23
Oc5	2.66	0.04	0.15
Oc5R	2.54	0.04	0.05
OxM	2.50	0.04	0.87
OxU	2.49	0.04	0.13
Average O	2.79	0.04	0.19
Yule	3.11	0.04	0.08
Average All	2.86	0.03	0.19
Minimum	2.14	0.01	0.05
Maximum	4.73	0.05	0.87

Table D 9. East River major, trace and redox elemental concentration (weight %) in Mancos Shale outcrop from XRF analysis

Sample ID	**Ma**	**Mb**	**Mc**	**Md**	**Me**	**Mf**	**Mg**
Major Elements							
Al	4.67	0.56	1.81	6.34	2.42	1.71	3.65
Ca	5.56	9.97	9.64	1.79	19.30	9.65	3.81
K	1.75	0.27	1.10	2.04	1.14	1.19	1.54
Mg	0.69	0.00	0.00	0.73	0.00	0.00	0.41
Si	23.58	3.41	9.60	29.59	7.39	9.17	19.40
Trace Elements							
Ba	0.068	0.105	0.073	0.071	0.092	0.088	0.140
Cr	0.008	0.001	0.004	0.009	0.003	0.003	0.009
P	0.063	0.000	0.000	0.106	0.000	0.000	0.088
Pb	0.002	0.002	0.003	0.002	0.002	0.003	0.002
Rb	0.004	0.003	0.004	0.005	0.004	0.005	0.005
Sr	0.011	0.010	0.013	0.010	0.023	0.013	0.011
V	0.014	0.002	0.008	0.015	0.005	0.008	0.017
Zn	0.010	0.006	0.009	0.010	0.006	0.011	0.011
U	0.001	0.000	0.001	0.001	0.001	0.001	0.001
Redox Elements							
Fe	2.10	1.03	3.27	2.55	1.18	2.22	3.65
Mn	0.06	0.00	0.03	0.15	0.05	0.11	0.14
S	3.42	10.65	9.90	0.23	8.89	6.89	0.90

Table D 10. East River bulk microbial DNA (ng/g) in water and percentage of 16S DNA represented by *nirK* and *nirS* denitrifying genes

Sample ID	***Bulk Microbial DNA (ng/µl of extract)***	***nirK % of 16S***	***nirS % of 16S***
Ox Upstream	1.37	0.3	0.2
Ox Downstream	0.82	0.5	0.4
Oa River	0.05	0.8	1.9
Od River	0.06	1.8	4.0
Yule River	0.07	0.3	15.2
Cc5 River	0.20	1.8	0.8
Cc5 River	2.51	20.2	24.6
Cc4	1.30	5.8	4.3
Cc3	1.97	2.9	2.8
Ca3	1.63	0.1	0.8
Seep 1	0.05	0.3	17.6
Seep 1B	1.12	1.1	0.2
Seep 2	0.12	0.3	13.8
Seep 3	0.14	3.1	4.5

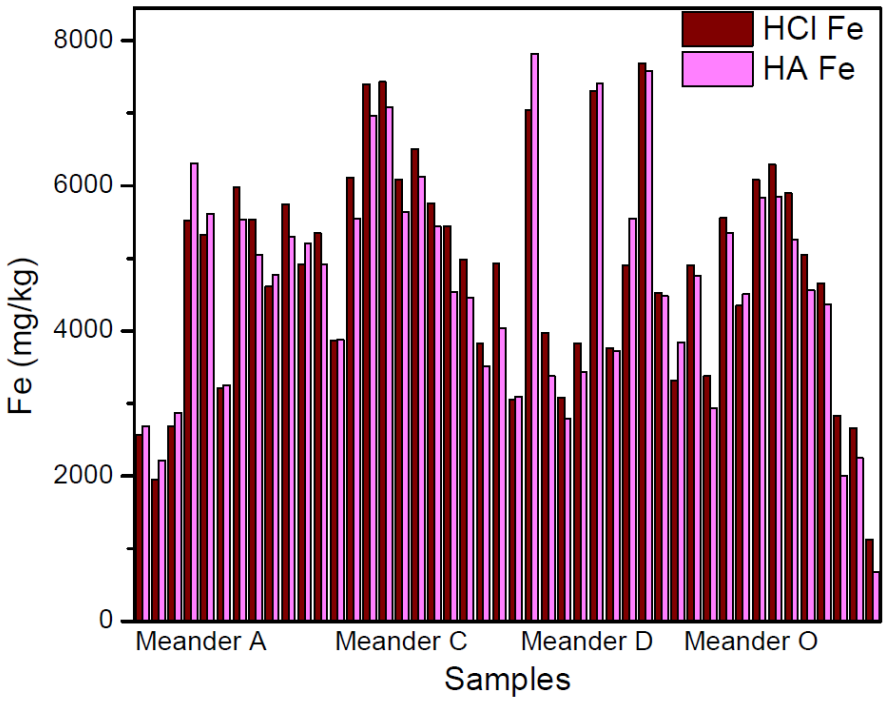

Figure D1. Iron extracted from soils with 0.5N HCl and 0.25N hydroxylamine in 0.5N HCl (HA).

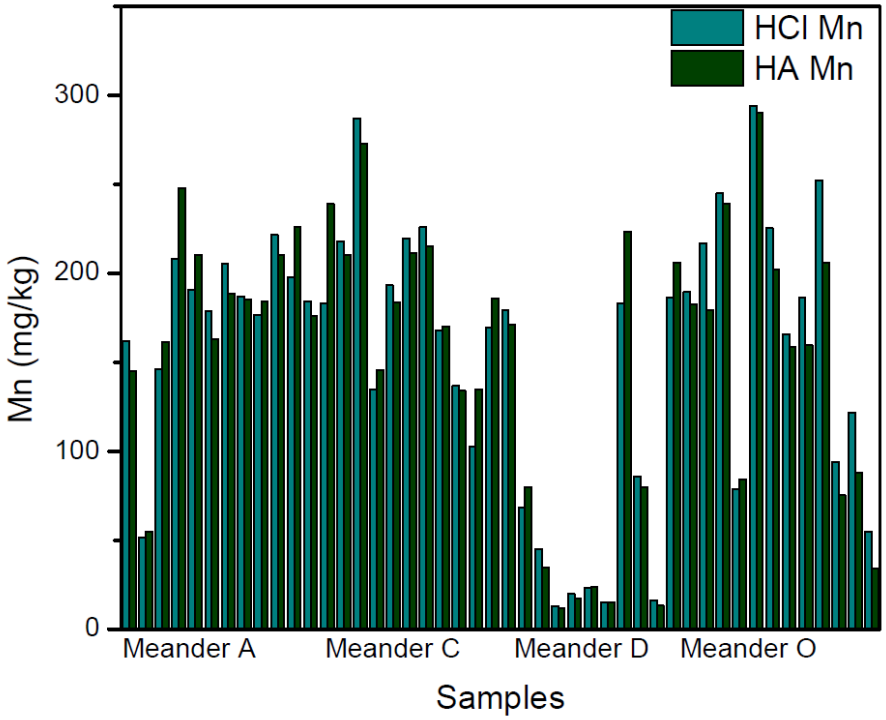

Figure D2. Manganese extracted from soils with 0.5N HCl and 0.25N hydroxylamine in 0.5N HCl (HA).

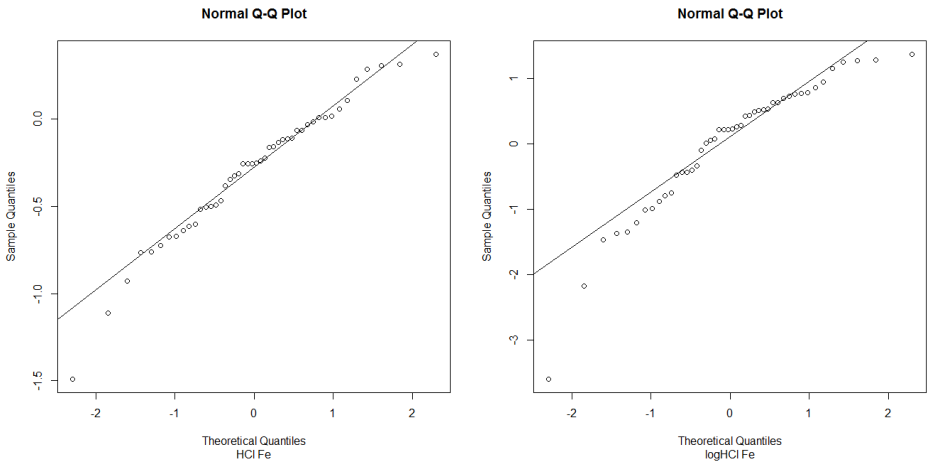

Figure D3. Q-Q plots for HCl extractable Fe and log-transformed HCl extractable Fe.

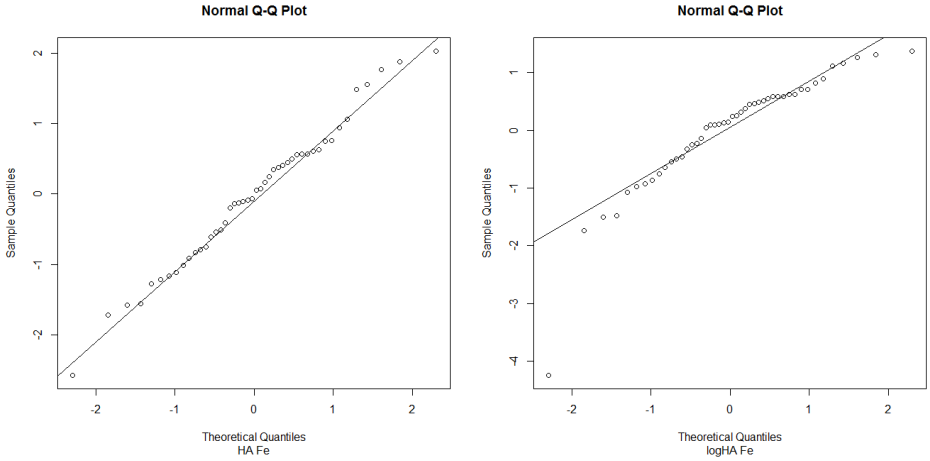

Figure D4. Q-Q plots for HA extractable Fe and log-transformed HA extractable Fe.

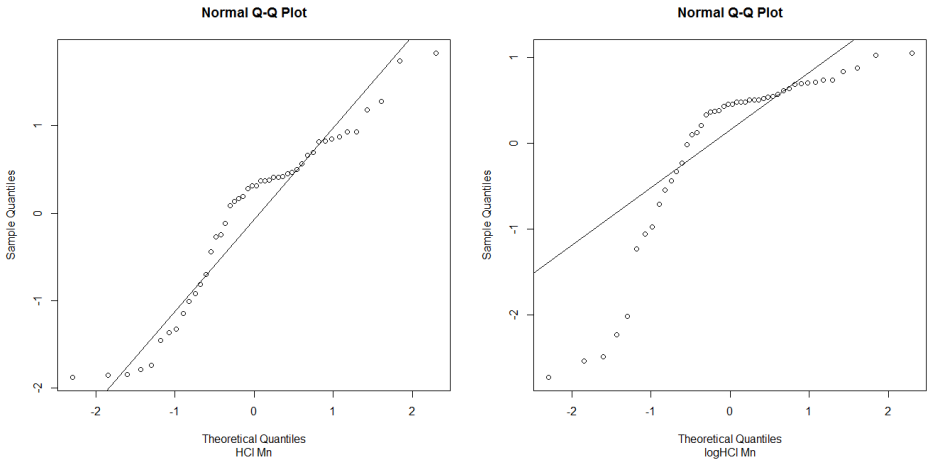

Figure D5. Q-Q plots for HCl extractable Mn and log-transformed HCl extractable Mn.

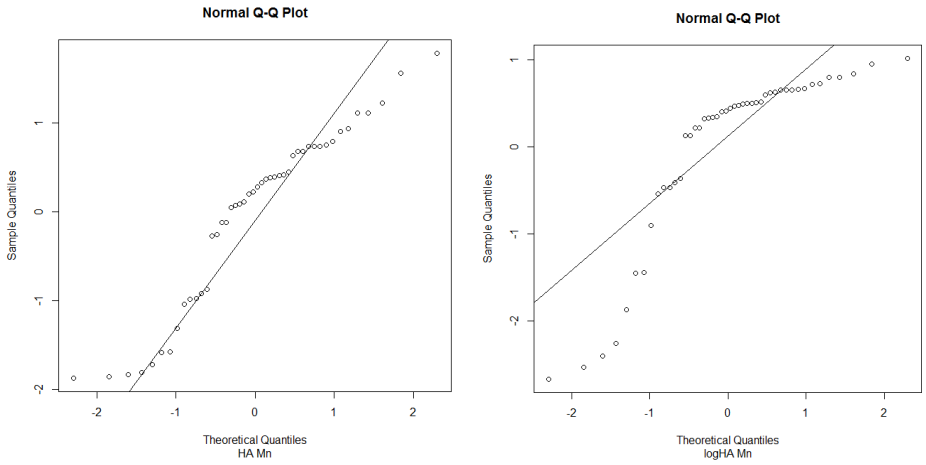

Figure D6. Q-Q plots for HA extractable Mn and log-transformed HA extractable Mn.

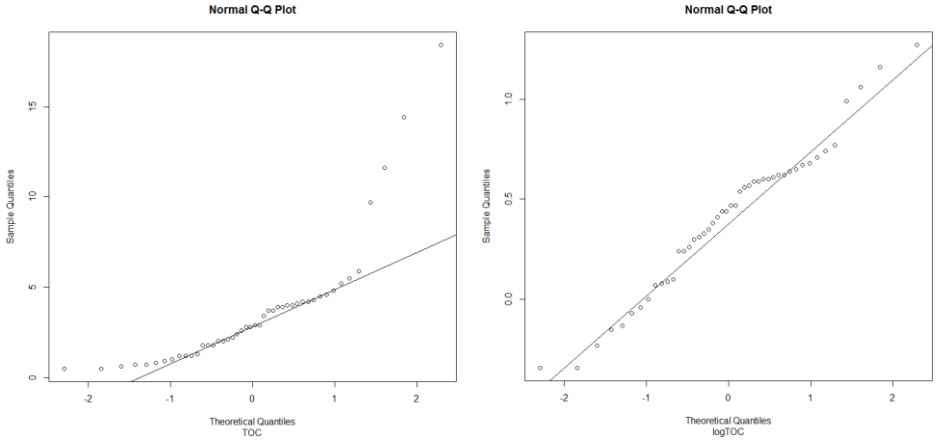

Figure D7. Q-Q plots for TOC and log-transformed TOC.

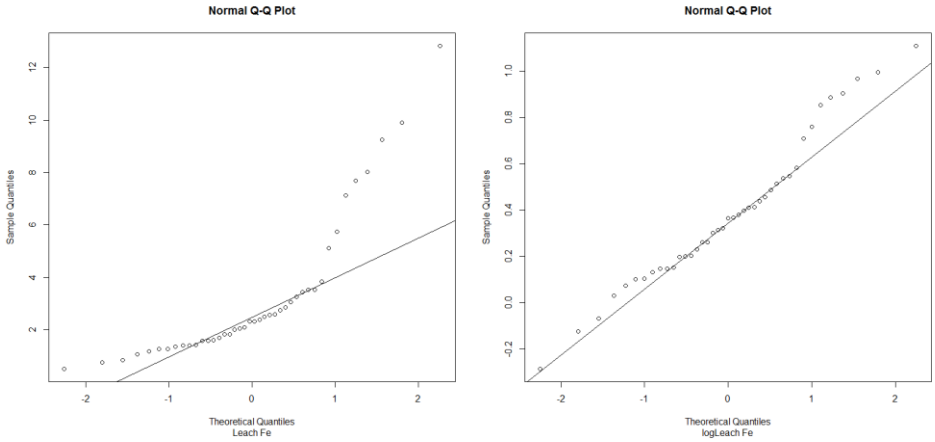

Figure D8. Q-Q plots for leach Fe and log-transformed leach Fe.

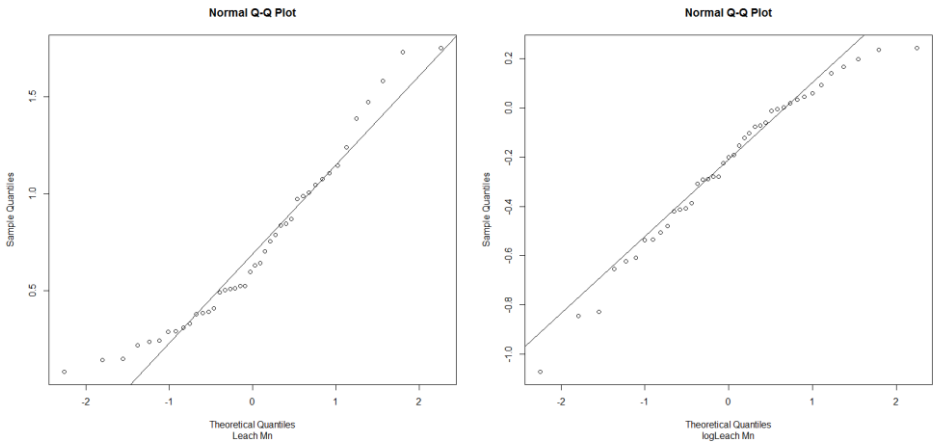

Figure D9. Q-Q plots for leach Mn and log-transformed leach Mn.

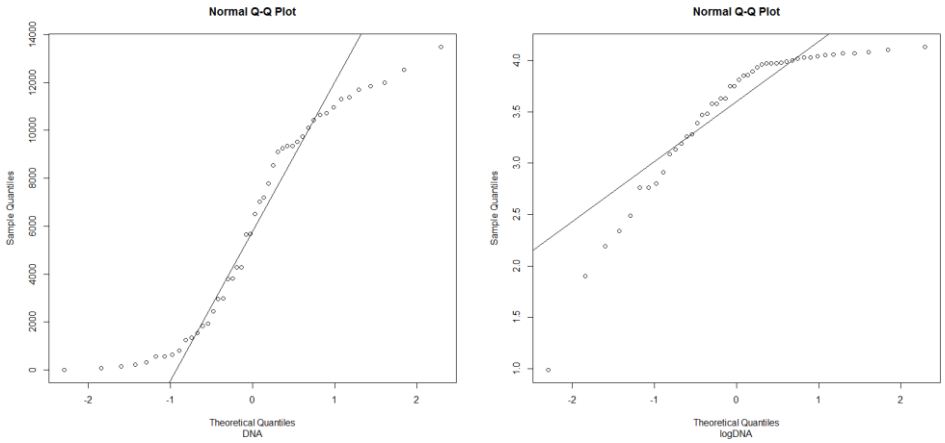

Figure D10. Q-Q plots for DNA and log-transformed DNA.

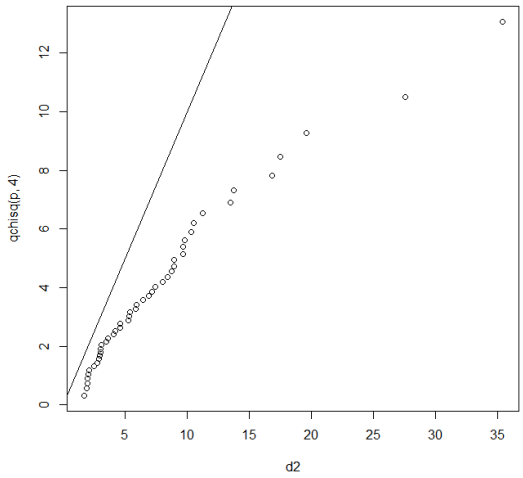

Figure D11. Multivariate Q-Q plot with logTOC, logDNA, HCl extractable Fe, HA extractable Fe, HCl extractable Mn, HA extractable Mn, log-leach Fe and log-leach Mn.

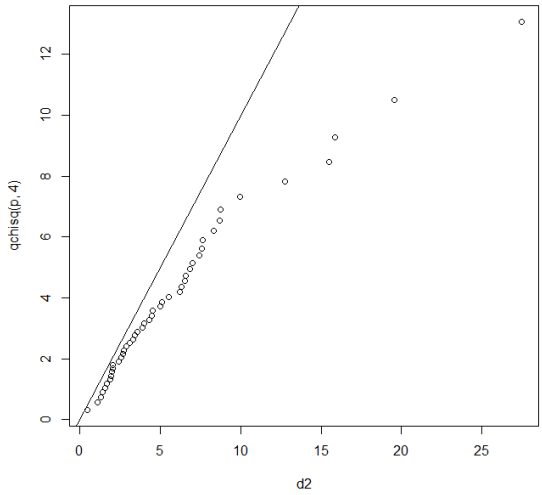

Figure D12. Multivariate Q-Q plot with logTOC, logDNA, HCl extractable Fe, HCl extractable Mn, log-leach Fe and log-leach Mn.

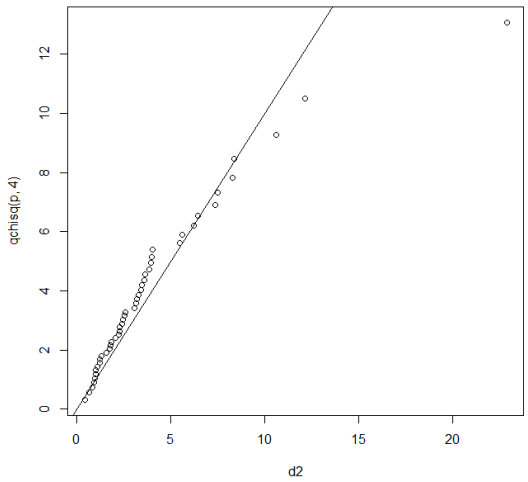

Figure D13. Multivariate Q-Q plot with logTOC, logDNA, log-leach Fe and log-leach Mn.

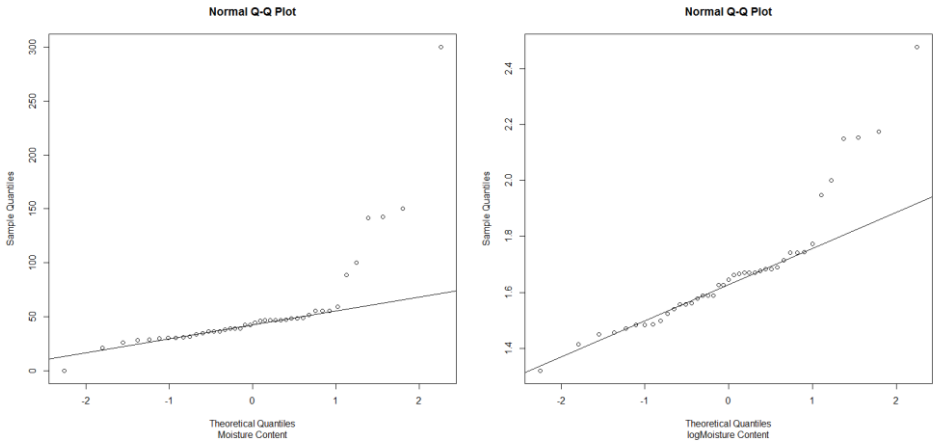

Figure D14. Q-Q plots for moisture content and log-transformed moisture content.

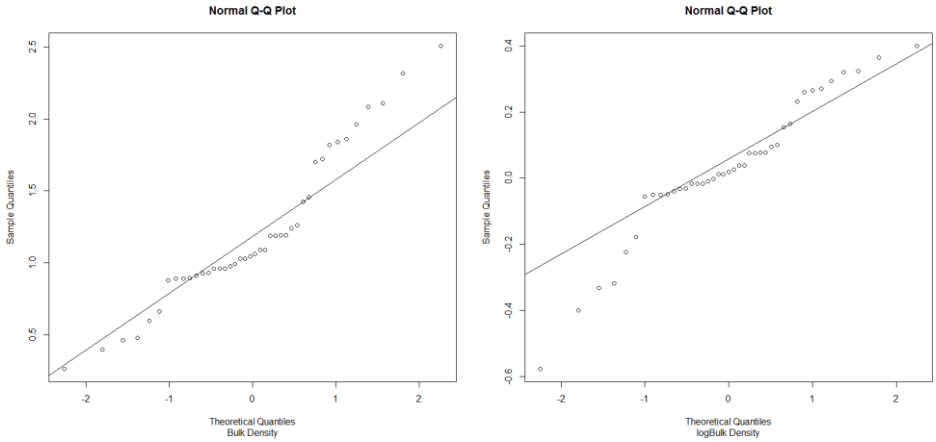

Figure D15. Q-Q plots for bulk density and log-transformed bulk density.